MANY-BODY APPROACH IS THE QUANTUM DOT

by

PATRICK MERLOT

THESIS

for the degree of

MASTER OF SCIENCE

(Master in Computational Physics)

Faculty of Mathematics and Natural Sciences
Department of Physics
University of Oslo

August 2009

Det matematisk-naturvitenskapelige fakultet
Universitetet i Oslo

Contents

Chapter 1

Introduction

1.0.1 [Subject and Definitions]

Following their recent successes in describing and predicting properties of materials, electronic structure calculations using numerical computation have become increasingly important in the fields of physics and chemistry over the past decade, especially with the development of supercomputers. From the basic constituants of a system of particles and their interactions, a computational approach enables to derive the electronic structure and the properties of the system.

A system of particles that is currently considered with attention is the quantum dot: it is an artificial system consisting of several interacting electrons confined to small regions between layers of semiconductors. The whole system can be seen as a nanoscopic box of semiconductor with exceptional electrical and optical properties. Applications based on quantum dots are developped in numerous fields of medicine and modern electronics.

1.0.2 [Overview + Motivation + contribution]

This thesis describes a computional study of a quantum dot in two dimensions. It presents the methods used in numerical simulations and some many-body techniques with various levels of sophistication: Hartree-Fock method, perturbation theory, variational Monte-Carlo and large scale diagonalisation (e.g. full configuration interaction) techniques. It focuses on the restricted Hartree-Fock method, one of the fastest and cheapest techniques but also one of the less accurate. The aim of the study is to assess the pertinence of this method to study quantum dots in two-dimensions confined by a spherical potential and squeezed by an external magnetic field. Results from Hartree-Fock can be used alone, or used as inputs to other ab-initio methods like perturbation theory (PT), variational Monte-Carlo (VMC) or full configuration interaction (FCI). Similar Hartree-Fock studies were performed by Johnson and Reina in 1992 [25] and Pfannkuche in 1993 [45]. In addition here the results from Hartree-Fock are compared to the results obtained with other techniques developped by my colleagues: Rune Albrigtsen with variational Monte-Carlo [2] and Simen Kvaal with configuration interaction method with and without effective interaction [33].

"While exact diagonalization provides an unrestricted solution of the problem, it

is computationally expensive and is unlikely to be possible for more than about 10 electrons. In contrast, the Hartree-Fock method is potentially applicable to more electrons, but there are doubts about its accuracy. Its usefulness would be greatly enhanced if its reliability was properly understood.“ [45]

As for [45] which compute the open-shell HF, my closed shell HF highlights the inaccuracy of HF compared to an ”exact treatment“ when using FCI, but compared to open shell system, it does not give many insigth on the electronic structure responsible for this inaccuracy of the correlation effects.

In [25], Johnson derived an analytical expression for the exact and HF approximation for ground state energy of a N-particle QD. They managed it by approximating the electron interactions by a cut-off to first order of the coulomb interaction. So our model was not fully comparable, but we finally come up with the same conclusion regarding the behaviour of the HF algorithm.

1.0.3 [My contribution, guide to the reader]

what I have done? be able to discuss my contribution to the problem compared to what's existing

paper on the limit of Hartree-Fock
short description of the results:

- A Hartree-Fock simulator has been developped in 2D.
- what are the limitations of HF according to the strength of the confinement wrt other methods?
  - accuracy wrt to the size of the system?
  - accuracy wrt to strength of the confinement?
  - simulation duration (compare the limits of each method for a given system, and compare the size of the biggest system achievable by each method-> other method like DFT might be of interest to study huge system in a reasonnable amount of time)?
  - Are HF results accurate enough for the confinement (B field) in use today in laboratories for confining electrons in a quantum dot?
  - HOW fast HF converges wrt other ab initio methods? It is possible to explicitely give the convergence rate?
- what are the improvements when using the HF basis set as input of VMC or CI?

1.0.4 [structure of the thesis]

This thesis is organized as follows. Chapter 2 presents briefly the history of quantum dots, describes their phenomenological aspects and legitimates the quest for more accurate models and their numerical simulations. Chapter 3 describes the phenomenological aspects and properties of quantum dots as well as some techniques in use today for manipulating those artificial systems.

Chapter 4 reviews some models of QD leading to the theoretical approximation used in this thesis. Some particular cases solvable analytically are developped and used as references when checking the stability and accuracy of the simulator. When it comes to the treatment of the QD model for numerical simulation, chapter 5 introduces some possible many-body techniques, and more particularly the Hartree-Fock theory as one of them. Its resulting iterative procedure is worked out within the goal of our implementation.

Chapter 6 describes the computational implementation of the Hartree-Fock techniques applied to the QD model and perturbation theory up to third order both as an improvement of the Hartree-Fock energy or as an independant technique. Results are provided in chapter 7 for closed shell systems, compared to other *ab initio* many-body techniques and a numerical analysis provides information on the convergence, stability behaviour and on the efficiency of Hartree-Fock.

Concluding remarks and suggestions for futur work are given in the conclusion 8.

Chapter 2

History and Motivations

In our current understanding of nanotechnology, quantum dots are the most functional and reproducible nanostructures available to researchers. Common shapes include pyramids, cylinders, lens shapes, and spheres. Different synthesis routes create different kinds of quantum dots. They are very small by nature, the smallest objects that we can synthesize on the nanoscale. From this fact, they are assimilated to dots, though one quantum dot can be made out of roughly thousands of atoms. All the atoms pool their electrons to "sing with one voice", that is, the electrons are shared and coordinated as if there was only one atomic nuclei attraction at the centre. That property enables numerous revolutionary schemes for electronic devices and quantum dots are often referred to as artificial atoms.

The total diameter of a quantum dot varies between 2-10 nm depending on its application, corresponding to 10-50 atoms in diameter and a total of $100 - 100,000$ atoms within the quantum dot volume [46] with an equivalent number of electrons. Almost all electrons are tightly bound to the nuclei of those atoms, however the number of “free electrons” in the dot can be very small: between one and a few hundreds [1]. The reason why 'quantum' prefixes the name is because the dots exhibit quantum confinement properties in all three dimensions. This means that electrons within the dot can't freely move around in any direction leading to quantization as we will show in 3. The only thing that behaves like this in nature is the atom. Commpared to an atom, a quantum dot is at least ten times bigger and above all tunable. This has a lot of important consequences for researchers. For example they exhibit quantized energy levels like an atom. For a given energy of excitation, for instance, a quantum dot will only emit specific spectra of light. Quantum theory predicts that if their diameter is decreased there will be a corresponding increase in frequency (e.g. in energy) of the emitted light as depicted in figure 2.1, and this property is now used in many applications.

This element of control over quantum dots' emission properties has huge implications for both electronic devices and medical applications. Due to their excellent confinement properties not seen in nanowires or quantum wells, quantum dots are extremely efficient at emitting light. They have been the source of some of the world's most powerful lasers produced to date, though the practicality of a quantum dot laser is still being improved. In medical studies, quantum dots are already in practice as

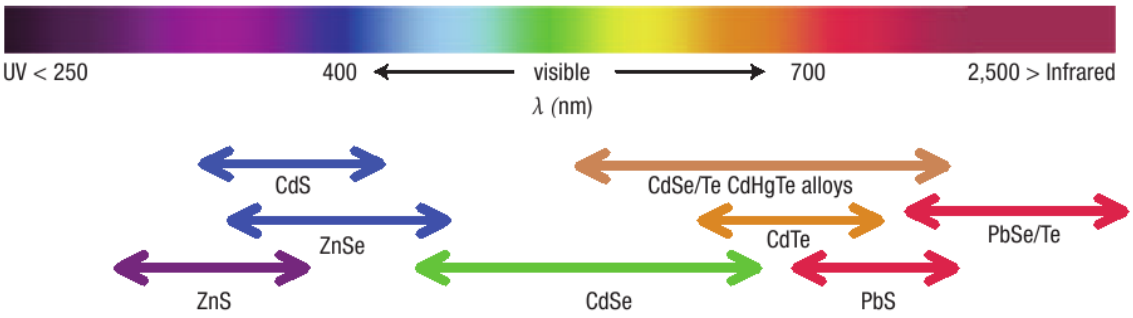

Figure 2.1: Emission spectra of quantum dots built from different materials. (Image courtesy of ?????)

tags that can be inserted into patients. These tags can be seen under most medical scanning technologies and can help pinpoint biological processes as they occur.

2.1 History of Quantum Dots

In the late 50's began the first studies of artificial quantum systems, mostly theoretical due to the lack of funds. In the 60's, epitaxial depositions was developed and with it, the possibility to build ultra-clean composite layers of semiconductor material sandwiched between two other layers of another semiconductor. The first optical properties were discovered and the two-dimensional character of the sample has been observed. At the beginning of the 80's, rapid progress in technology were made with accurate lithography technics (the first quasi one-dimensional quantum wire was done with these progress) [19].

Colloïdal quantum dots were discovered in 1981, during the development of materials for the photo-cleavage of water. Bulk cadmium sulfide (CdS) is known to be an ideal electrode material; however it experiences photocorrosion upon irradiation. It was believed that colloidal particles of cadmium sulfide, coated with a protective agent (i.e. RuO_2), would be more resistant to corrosion. Therefore, a synthesis method was developed to produce colloidal CdS through aqueous precipitation. The resulting particles displayed unique properties not found in the bulk, including fluorescent emission. These properties were determined to be the result of quantum size effects [26], and were found to be tunable by altering the size of the particle [50]. This provided a method for selecting excitation and emission wavelengths and particle band gaps.

In the middle of the 80's, the first quantum dot was developed based on etching technique [Reed et al.;1986]. As a consequence, a complete quantization of the electron free motion was possible.

At the end of the 80's and in the 90's, the methods evolved: lithography and etching are still in use, but electron or ion-lithography have replaced light-lithography and so increased precision [19].

Lent predicted in 1993 the need for building quantum cellular automata (QCA)

cells of 2 nm in order to work at room temperature, where quantum cellular automata refers to any models of quantum computation.

"Ultimately, temperature effects are the principal problem to be overcome in physically realizing the QCA computing paradigm. The critical energy is the energy difference between the ground state and the first excited state of the array. If this is sufficiently large compared with k_BT, the system will be reliably in the ground state after a characteristic relaxation time. Fortunately, this energy difference increases quadratically as the cell dimensions shrink. If the cell size could be made a few Ångstroms, the energy differences would be comparable to atomic energy levels (i.e. several electron-Volts!)".

"As technology advances to smaller and smaller dimensions on the few-nanometer scale, the temperature of operation will be allowed to increase. Perhaps our envisioned QCA will find its first room temperature implementation in molecular electronics." [36]

Interest in the use of quantum dots in biomedicine began in 1998. Coupling the quantum dots directly to biorecognition molecules (e.g. antibodies, proteins), the particles could be targeted to particular parts of the cell, producing a fluorescent indicator [7, 8].

Early this year (Jan. 2009), the four-quantum dot cell dreamed by Lent to build his "quantum cellular automata" as a replacement for classical computation using *CMOS* technology has now been achieved with the fabrication and control of a 1 nm-scale assembly of four coupled silicon dangling bond (In condensed matter physics, a dangling bond occurs when an atom is missing a neighbor to which it would be able to bind. Such dangling bonds are defects that disrupt the flow of electrons and that are able to collect the electrons). Indeed single atom quantum dots make possible a new level of control over individual electrons, a development that suddenly brings quantum dot-based devices within reach [16]. **Composed of a single atom of silicon and measuring less than one nanometre in diameter, these are the smallest quantum dots ever created**. Until now, quantum dots have been useable only at impractically low temperatures, but the new atom-sized quantum dots perform at room temperature. And because they operate at room temperature and exist on the familiar silicon crystals used in today's computers, researchers expect these single atom quantum dots to transform theoretical plans into real devices. Figure (2.2) shows how atom-sized QD can be manipulated at room temperature. The single atom quantum dots have also demonstrated another advantage: significant control over individual electrons by using very little energy. This low energy control is seen as the key to quantum dot application in entirely new forms of silicon-based electronic devices, such as ultra low power computers.

2.2 Some applications of QD

Exceptional electrical and optical properties make quantum dots **attractive components for integration into electronic devices**. One significant asset of quantum dots over traditional optoelectronic materials is that they exist in the solid state.

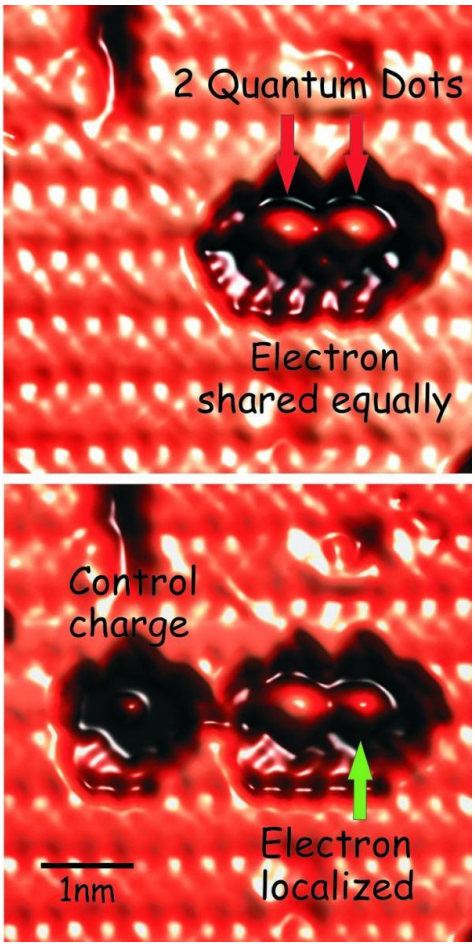

Figure 2.2: Two coupled atomic quantum dots are shown in this room temperature scanning tunneling microscopy image. In the top frame the dots share one electron. The electron moves freely between the dots just like an electron in a chemical bond within a molecule. The lower frame demonstrates control over that single electron and the potential to do computations in a new way. The electric field from the control charge pushes the electron to prefer staying on only one of the quantum dots. (Image courtesy of University of Alberta/Prof. Robert A. Wolkow)

Solids tend to be more compact, easly cooled, and allow for direct charge injection. Additionally, quantum dots can interconvert light and electricity in a tunable manner dependant on crystal size, allowing for easy wavelength selection. This is a significant improvement over silicon-based materials, which require modification of their chemical composition (i.e. doping) to alter optical properties [58]. Thus researchers have experimented with quantum dots in lasers, LEDS, photovoltaics and also for new generations of transistors, prototypes of spin devices, logic gates with quantum computers as a final aim. Most of these applications are still in early development; however the benefits of quantum dot components are evident, soon leading to a complete revolution of the way of building electronic components at atomic scale.

Also one of the fastest moving and most exciting interfaces of nanotechnology is the use of (colloïdal) **quantum dots in biology**. Again their unique optical properties make them appealing as *in vitro* and *in vivo* fluorophores in a variety of biological investigations, in which traditional fluorescent labels based on organic molecules fall short of providing long-term stability and simultaneous detection of multiple signals [40]. The ability to make quantum dots water soluble and target them to specific biomolecules has led to promising applications in cellular labelling, thus improving diagnostic methods (ex. tracking cancer cells *in vivo* during metastasis [14, 22, 56]) and in developing better drug delivery systems to improve disease therapy [29]. It is even currently studied as neuroelectronic interface for converting optical energy into electrical signal responding to the need for prosthetic devices that can repair or replace nerve function [64]. However there are still many open questions about the toxicity of inorganic QD. The size and charge of most nanoparticles preclude their efficient clearance from the body as intact nanoparticles. Without such clearance or their biodegradation into biologically benign components, toxicity is potentially amplified and radiological imaging is hindered. Some neutral organic coatings prevents adsoption of serum proteins (which otherwise increased the total diameter by $> 15nm$ and prevent renal clearance). A final hydrodynamic diameter $< 5.5nm$ resulted in rapid and efficient urinary excretion and elimination of quantum dots from the body [52].

These achievements, even in their premises, have laid the **foundations for theoretical investigations** to enable advances in the understanding of the fundamental structure, stability and aqueous assembly of nanoparticle architectures. A physical systems consisting of between $10s - 1000s$ of atoms is already too complex to be studied otherwise than using numerical methods for a reliable description. The concept of artificial atom can even be generalized to artificial molecules.

Moreover QDs appears as good tools for studying atomic spectra of many-body systems on a theoretical point of view using computational techniques. Thanks to the possibility to build our own artificial atoms without considering the complexity of the nucleus, it becomes simpler to confront numerical and experimental results.

2.3 Clarifications about computational studies

The usefulness of numerical simulation is more and more recognized and today it is used in many domains of research and development: mechanics, fluid mechanics, solid state physics, astrophysics, nuclear physics, climatology, quantum mechanics, biology, chemistry... More than being limited to scientific subjects numerical simulation is also used in human sciences (demography, sociology) as well as in finance or economy.

In physics, beside the importance for our basic understanding of quantal systems, the capability to develop and study stable numerical quantum mechanical systems with many degrees of freedom is of great importance, as analytic solutions are rare or impossible to obtain.

Some definitions:

A numerical simulation reproduces the fundamental behaviour of a complex system in order to study its properties and predict its evolution. It is based on the implementation of theoretical models, ie it is an adaptation of mathematical models to numerical tools. Data mining and virtual reality are different from numerical simulation and should not be mistaken with it.

A numerical simulation is performed in several steps:

The model describes the system analysed by listing its essential parameters and by writing the physical laws that rule its behaviour (and link the parameters) as mathematical equations.

The simulation itself is the translation of the equations into computer language, associated with the discretization of the physical domain to make it finite (select a time step, a finite number of points, an acceptable level of accuracy, etc)

Computational techniques The resolution of the equations leads to the determination of the numerical values of all the parameters of the system in every points, ie the state of the system is known. Various computational techniques can be used to solve the equations, they can be grouped into two main approaches: the deterministic and the statistical (or probabilistic) methods.

In the first approach, an algorithm will solve predictably the equations. For example the object (or the domain) is discretized and the parameters of each element are linked to its neighbours through algebraic equations. It is up to the computer to solve the system that links all the equations. A deterministic method will always produce the same output when given the same input, and the underlying machine will always go through the same sequence of states (which is why it is called "deterministic"). The Hartree-Fock method used in this thesis belongs to this category as well as the Finite element method or the large scale diagonalisation.

The second approach, which groups the âĂIJMonte-CarloâĂİ methods, is particularly suited to phenomena characterized by a sequence of steps in which each element of the object can be affected by different âĂIJa prioriâĂİ possible events. From step to step, the evolution of the sample will be determined through a random

draw (the name of the method comes from this idea)

Validation of the results: the theoretical model and its translation into computer programming must be validated by comparing with experimental data, or by testing a very simple case for which an analytical solution can be found.

Numerical simulations once validated, can explore more cases or unused configurations that were not tested by experiments, sometimes predicting unexpected behaviours, leading to a greater knowledge of the physical behaviour of the system. Therefore numerical simulation is the third form of study of phenomena, after theory and experiment.

Chapter 3

Physics of Quantum Dots: the artificial atoms

As described previously, a quantum dot is a semiconductor whose charge-carriers are confined in all three spatial dimensions, so much confined that quantum effects become visible in many ways: fluorescent effect, quantized conductance, quantized energy spectrum, etc.

The physics behind it involves the (electronic) structure of the material (here mainly semiconductors) and some basic quantum mechanical effects such as size quantization, quantum tunneling or Coulomb blockade.

This chapter reviews the basic quantum mechanical effects that explain the properties of quantum dots. First it explains what size quantization is and how it happens for a confined particle. Then it presents the properties of semiconductors and the specific features of semiconductors quantum dots, and how it enables the size quantization to occur at larger scale. It then explains the consequences of size quantization on the optical and electronic properties of quantum dots. Finally, it presents the quantum dots in a magnetic field.

3.1 Size quantization

Before applying quantum theory to quantum dots, we will explain how quantization arises and why it is not always noticeable in everyday life.

The particle in a box We consider the well-known example of a particle in a one-dimensional box of size a trapped by an infinite (potential) barrier (see figure 3.1a). The potential $V(x)$ is given below:

$$\begin{aligned} V(x) &= 0, \qquad for\ 0 < x < a \\ V(x) &= \infty, \qquad for\ x \leq 0, x \geq a \end{aligned} \tag{3.1}$$

How do these boundary conditions affect the particle? Due to the wave-particle

duality we can write the time-independent Schrödinger equation for this system:

$$\frac{d^2\Psi(x)}{dx^2} = \frac{2m}{\hbar^2}\left[V(x) - E\right]\Psi(x) \tag{3.2}$$

If we write the solutions of the Schrödinger equation under the form $\Psi(x) = Asin(kx) + Bcos(kx)$, we can find the constants A and B by using the boundary conditions: at the boundaries of the box Ψ is null ie $\Psi(0) = \Psi(a) = 0$

$$\begin{aligned} \Psi(0) &= 0 + B = 0 \\ \Psi(a) &= Asin(ka) = 0 \end{aligned} \tag{3.3}$$

This can only be satisfied by $B = 0$ and if either $A = 0$ or if $ka = n\pi$. Setting $A = 0$ would mean that the wave function is always zero, which is unacceptable, we conclude that:

$$\Psi_n(x) = Asin(\frac{n\pi x}{a}), \qquad for\ n = 1, 2, 3, 4, \ldots \tag{3.4}$$

The constant A can be determined by normalization, by saying that $\Psi_n(x)^*\Psi_n(x)dx$ is the probability density, ie the probability of finding the particle in the interval of width dx centered on x. The probability density at any given point is shown in figure 3.1c. Because the probability of finding the particle somewhere in the entire interval $[0, a]$ is one,

$$\int_0^a \Psi_n(x)^*\Psi_n(x) = 1$$

From that we obtain the normalized eigenfunctions plotted in figure 3.1b

$$\Psi_n(x) = \sqrt{\frac{2}{a}}\, sin\left(\frac{n\pi x}{a}\right) \tag{3.5}$$

Now that we have the eigenfunctions, we can re-introduce them into the Schrödinger equation to find the eigenvalues (i.e. eigen-energies of the system):

$$E_n\Psi_n(x) = -\frac{\hbar^2}{2m}\frac{d^2\Psi_n(x)}{dx^2} \tag{3.6}$$

$$= \frac{\hbar^2}{2m}\left(\frac{n\pi}{a}\right)^2\sqrt{\frac{2}{a}}\, sin\left(\frac{n\pi x}{a}\right) \tag{3.7}$$

It leads to the following expression for the eigenvalues, which are also the possible energies of the system:

$$E_n = \frac{\hbar^2}{2m}\left(\frac{n\pi}{a}\right)^2 = \frac{\hbar^2 n^2}{8ma^2}, \qquad for\ n = 1, 2, 3, \ldots \tag{3.8}$$

Compared to a free particle, we see that the energy for a particle in a box is discrete: this is called quantization and the integer n is a quantum number. Another important result of the calculation is that the lowest energy allowed is greater than zero. The particle has a non zero minimum energy compared to a free particle, known as a zero point energy.

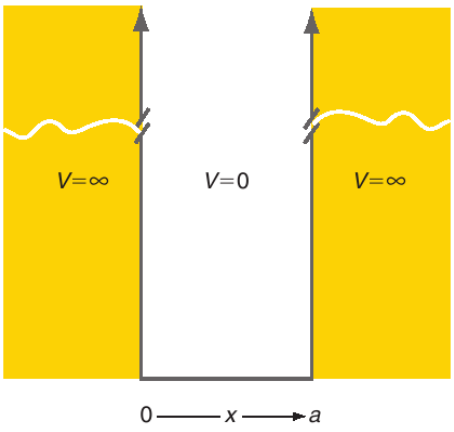

(a) The potential

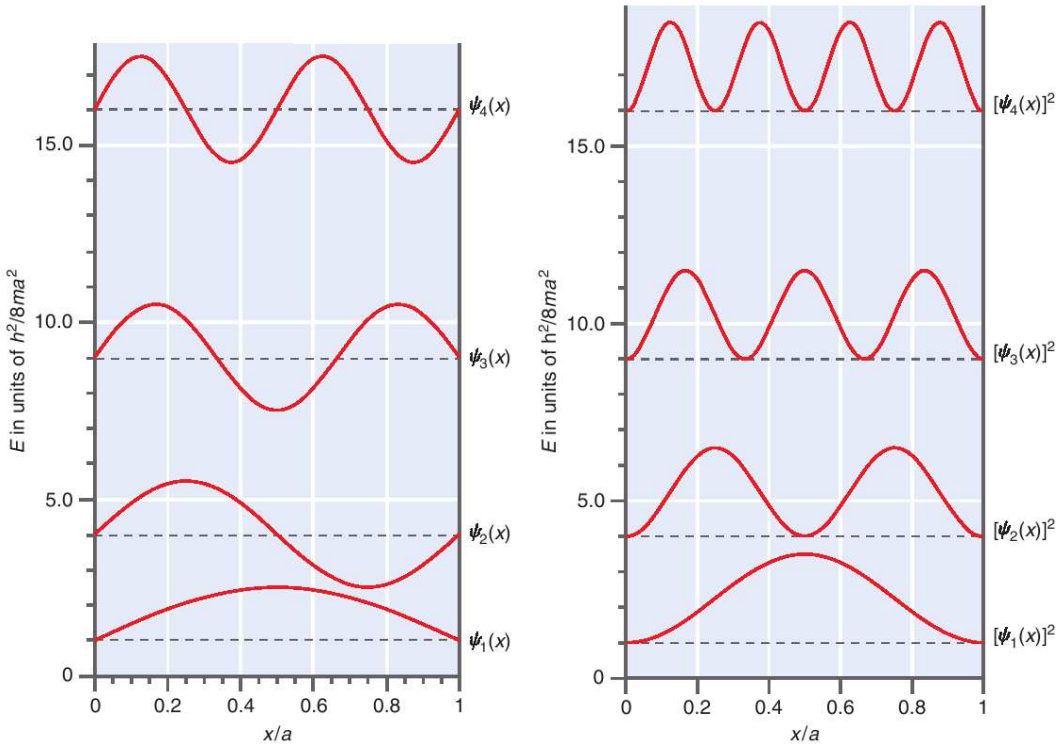

(b) First eigenfunctions **(c)** Probability densities

Figure 3.1: (a) The potential described by equation (3.1). As the particle is confined to the range $0 \leq x \leq a$, we say that it is confined to a one-dimensional box.
(b) The first few eigenfunctions for the particle in a box are shown together with the corresponding energy eigenvalues. The energy scale is shown on the right with the zero for each level indicated by the dashed line.
(c) The square of the magnitude of the wavefunction, or probability density, is shown as a function of distance together with the corresponding energy eigenvalues. The energy scale is shown on the left. The square of the wave function amplitude is shown on the right with the zero for each level indicated by the dashed line.

Therefore quantization is simply a result of the confinement of the particle and provides new properties to the particle. By making the box size a tend to infinity, the confinement condition is removed and the discrete energy spectrum becomes continous in this limit. More generally, it means that any particle trapped with some boundaries will experience quantization effect, like the particles trapped in the quantum dots.

One way to see quantization effects is to look for observables. The total energy is one example of an observable that can be calculated once the eigenfunctions of the time-independent Schrödinger equation are known. Another observable that comes directly from solving this equation is the probability density, which is the quantum mechanical analogue of position.

Observation of size quantization depending on temperature What is the limit size of the confinement so that such quantization effects are observable at our scale? We consider for example that the particle is an electron trapped in a box. The answer will come from the very small constants we have from the Schrödinger equation: the reduced Planck constant $\hbar = h/\pi = 1.05 \times 10^{-34}\ J.s\ (kg.m^2.s^{-1})$ and the mass of the electron $m = 9.11 \times 10^{-16}\ kg$. To be noticeable, the energy should be much greater than the thermal energy which is in the order of magnitude of k_BT, where $k_B = 1.38 \times 10^{-34}\ J.K^{-1}$ is the Boltzmann constant and T the temperature, otherwise thermal fluctuations will disturb the motion of electrons and will smear out the quantization effects.

At room temperature (i.e. 20℃ $\simeq 293K$), $k_BT \simeq 4.045 \times 10^{-21}\ J$. The gap between the first two energy levels should be greater than this value:

$$\begin{aligned} \Delta E = E_2 - E_1 = \frac{3\hbar^2}{8ma^2} = \frac{4.54 \times 10^{-54}}{a^2} \gtrsim k_BT \\ \Rightarrow a \lesssim 1.06 \times 10^{-11} m = 0.0106\ nm \end{aligned} \tag{3.9}$$

At dilution refrigerator temperatures (i.e. $\sim 100\ mK$), $k_BT \simeq 1.380 \times 10^{-35}\ J$. The gap between the first two energy levels doesn't need to be so big this time:

$$\begin{aligned} \Delta E = E_2 - E_1 = \frac{3\hbar^2}{8ma^2} = \frac{4.54 \times 10^{-54}}{a^2} \gtrsim k_BT \\ \Rightarrow a \lesssim 5.734 \times 10^{-10} m = 0.573\ nm \end{aligned} \tag{3.10}$$

We notice here that it is impossible to observe quantum effect with such a "free electron" at room temperature, since the box should be roughly the size of an atom, but it could be done at very low temperature.

We could therefore deduce the same for quantum dots, that are made of one or several electrons confined in a semiconductor. From what we saw above it is not possible to create a quantum dot small enough to observe size quantization at room temperature. However we will see in the following section that the mass of the charge carriers, which influences the limit size of the confinement, is not the same when the material is a semiconductor.

3.2 Quantum dots made of semiconductors

A semiconductor is a material that has a resistivity value between that of a conductor and an insulator. The conductivity of a semiconductor material can be varied under an external electrical field.

Most semiconductors on the market are made of silicon (Si). Dozens of other materials are used like germanium (Ge) or gallium arsenide (GaAs). Semiconductor materials are the basic constituants of modern electronic devices (radio, computers, telephones, and many others). Semiconductor devices include the transistor, solar cells, many kinds of diodes including the light-emitting diode, the silicon controlled rectifier, and digital and analog integrated circuits. Solar photovoltaic panels are large semiconductor devices that directly convert light energy into electrical energy.

Energy bands in semiconductors In a metallic conductor, current is carried by the flow of electrons, but in semiconductors, current can be carried either by the flow of electrons or by the flow of positively-charged "holes" in the electron structure of the material. As shown in the previous section 3.1 electrons trapped in matter will experience discretized energies. However compared to the particle in a box, electrons in semiconductors as in other solids will not have narrow discrete energy levels but tickher allowed bands of energy separated by forbidden gaps between them. Therefore electrons trapped in matter can have energies only within certain **energy bands**; the lowest energy is the **ground state**, corresponding to electrons tightly bound to the atomic nuclei of the material, and the highest energy is the free electron energy, which is the energy required for an electron to escape entirely from the material. The energy bands each correspond to a large number of discrete quantum states of the electrons. Most of the states with low energy (closer to the nucleus) are full, up to a particular band called the **valence band**. Semiconductors and insulators are different from metals because the valence band in the semiconductor materials is very nearly full under usual operating conditions, thus causing more electrons to be available in the **conduction band**, which is the band immediately above the valence band as shown in figure 3.2. The ease with which electrons in a semiconductor can be excited from the valence band to the conduction band depends on the band gap between the bands, and it is the size of this energy bandgap that serves as an arbitrary dividing line between semiconductors and insulators.

In the picture of delocalized states, for example in one dimension that is in a wire, for every energy band there is a state with electrons flowing in one direction and one state for the electrons flowing in the other. For a net current to flow, electrons must occupy more states corresponding to the flow in one direction than they occupy states for the flow in the other direction, and for this they need energy. For a metal this can be a very small energy. In the semiconductor the next higher states lie above the band gap. However, as the temperature of a semiconductor rises above absolute zero, there is more energy in the semiconductor to spend on lattice vibration and on lifting some electrons into an energy states of the conduction band. The current-carrying electrons in the conduction band are known as "**free electrons**", although they are often simply called "electrons" if context allows this usage to be clear.

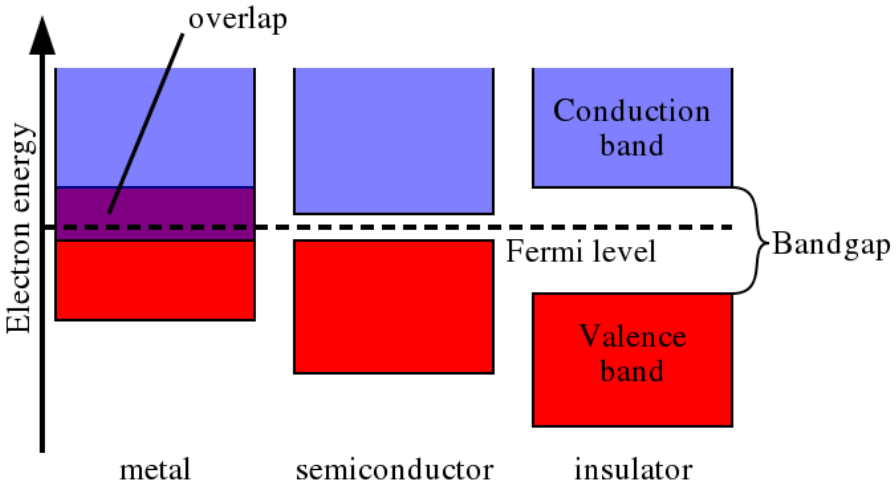

Figure 3.2: Simplfied diagram of the electronic band structure of metals, semiconductors and insulators. (Image courtesy of P. Kuiper)

Electrons excited to the conduction band leave behind electron holes, or unoccupied states in the valence band. Both the conduction band electrons and the valence band holes (**excitons**) contribute to electrical conductivity. The holes themselves don't actually move, but a neighboring electron can move to fill the hole, leaving a hole at the place it has just come from, and in this way the holes appear to move, and the holes behave as if they were actual positively charged particles.

One covalent bond between neighboring atoms in the solid is ten times stronger than the binding of the single electron to the atom, so freeing the electron does not imply destruction of the crystal structure.

In semiconductors, the dielectric constant is generally large, and as a result, screening tends to reduce the Coulomb interaction between electrons and holes. The result is a Mott-Wannier exciton, which has a radius much larger than the lattice spacing. As a result, the effect of the lattice potential can be incorporated into the **effective masses** of the electron and hole (see table 3.1 for typical values), and because of the lower masses and the screened Coulomb interaction, the binding energy is usually much less than a hydrogen atom, typically the order of 0.1 eV (Wannier excitons are found in semiconductor crystals with small energy gaps and high dielectric constant).

In quantum mechanics, the positions of electrons and holes are described as wavefunctions or probability distributions. The exciton has a certain size, determined by the combined probability distribution functions, and if this size exceeds the particle diameter, quantum confinement occurs. The size limit for quantum confinement can be approximated from the modified version of the De Broglie wavelength equation considering its effective mass m^*:

$$\lambda_B = \frac{h}{p} = \frac{\hbar}{m^* \omega} \tag{3.11}$$

where λ_B is the de Broglie wavelength (the wavelength associated to a particle with

Semiconductor material	ϵ_r	m_e^*	m_h^*
(Free electron mass $m_e = 9.11 \times 10^{-16}\ kg$)			
(Dielectric constant of vaccuum $\epsilon_0 \simeq 8.854 \times 10^{-12}\ A^2 s^4 kg^{-1} m^{-3}$)			
Silicon (Si) (4.2 K)	11.7	1.08 m_e	0.56 m_e
Germanium (Ge)	16.4	0.55 m_e	0.37 m_e
Gallium arsenide (GaAs)	$11.1 - 12.4$	0.067 m_e	0.45 m_e
Indium antimonide (InSb)	15.9 (at 77K)	0.013 m_e	0.6 m_e
Zinc oxide (ZnO)	–	0.19 m_e	1.21 m_e
Zinc selenide (ZnSe)	–	0.17 m_e	1.44 m_e
Cadmium sulfide (CdS)	–	–	–
Cadmium telluride (CdTe)	–	–	–

Table 3.1: Relative dielectric constant (ϵ_r) measured at 290K [63] and effective mass of charge-carriers for some common semiconductors [17], m_e^* and m_h^* respectively for the electron and hole effective mass

momentum p), $\hbar$ the reduced Planck constant and ω the angular frequency of the particle.

Nanocrystals contain much fewer atoms than the bulk, therefore charge screening effects are reduced. The effective mass declines and the de Broglie wavelength can become extremely large, up to several nanometers and make the nanocrystal excited with much less energy than an atom. For cadmium sulfide (CdS) and cadmium telluride (CdTe), these wavelengths are 5.5 nm and 7.5 nm [64]. For particles that are confined within sizes smaller than this wavelength, the excitons "feel" restricted. Thus the nanocrystal will display a band gap and associated (optical and electrical) quantum effects inversely proportional to its size.

Energy spectrum of semiconductor quantum dots An additional feature to the transition from bulk crystals to nanocrystals is a radical change in the energy spectrum of the free carriers. It changes when the diameter d of the crystal becomes comparable to the de Broglie wavelength of electrons in the crystal. Motion in the direction accross the nanocrystal can be assumed bounded, and the energy spectrum in this direction becomes discrete (Figure 3.3).

Bulk semiconductor materials are characterized by bands of allowed potential energy values. For an electron to be excited, it must absorb an energy higher than the band gap. Any value greater than the band gap will produce an excited state.

When we examine a system consisting of only two atoms, the molecular orbitals formed create discrete potential energy states (Figure **??**). Electrons will only be excited if the energy absorbed corresponds to specific discrete quantities. Other values are not permitted and will not produce excited states.

Quantum Dots are an intermediate between discrete and continuous energy levels (Figure **??**). As the number of atoms in the particle is reduced, the energy bands split and shrink but not to the point of being exactly discrete. Thus electrons in quantum dots may be excited by energies in discrete intervals.

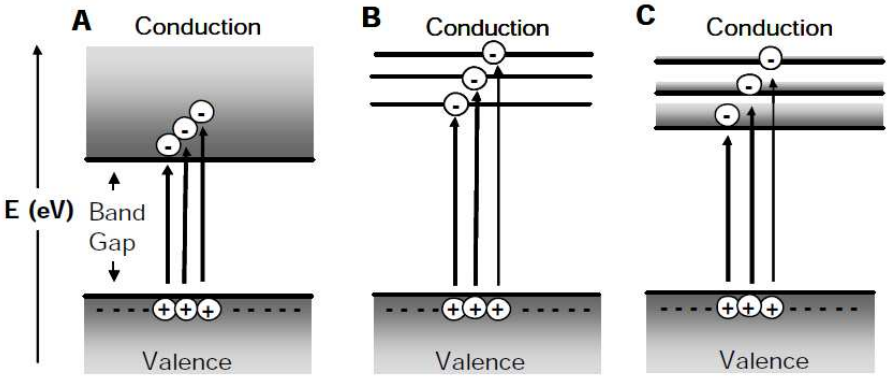

Figure 3.3: Possible energy states as a function of the particle size.
(**A**) **Bulk materials** have continuous energy bands and absorb energy at a value greater than the band gap. (**B**) **Molecular materials** possess discrete energy lelvels and only absorb energy wuth certain values. Moreover the band gap is greater than that of a bulk materail as a result of shrinking and splitting of the energy bands. (**C**) **Quantum dots** lie between the extremes (A,B). They possess discrete energy bands and absorb energy in discrete intervals. The band gap is greater than that of a molecular material. (Image courtesy of J. Winter [64])

3.3 Optical properties

A lot of applications rely on the optical properties of quantum dots which result from quantum confinement.

The electrical and optical energy of the band gap are equivalent through the following conversion:

$$\Delta E = \hbar\omega = \frac{2\pi hc}{\lambda} \tag{3.12}$$

where ΔE is the band gap difference (figure **??**), $\hbar$ is the reduced Planck's constant, c is the speed of light, λ and ω respectively the wavelength and the angular frequency of the incident light. Thus the energy difference of the band gap is inversely proportional to the wavelength of the incident light. Nanoparticles will only absorb light of weavelengths shorter than that determined by the band gap value.

For example, CdS (bulk) has a band gap of 2.42 eV, which corresponds to a wavelength of 512 nm. So CdS (bulk) begins to absorb light at 512 nm and absorbs continuously into the UV (e.g. shorter wavelengths/higher energies). As particle size declines, the band gap increases and the absorbance starts at shorter wavelengths (Figure 3.4).

The influence of particle size on optical properties is not limited to absorbance. Particle fluorescence is also a function of the band gap. After an electron is excited, some of its energy is lost to atomic vibrations, satisfying the second law of thermodynamics. Typically, this energy is converted to heat. When the electron decays into the ground state, it will emit light, at a longer wavelength because of this energy loss (Figure 3.5a). As the band gap decreases, a smaller amount of energy is dissipated through fluorescent emission to return to the ground state, and the wavelength of emitted light will shift to the red (Figure 3.5b). Because the band gap is inversely

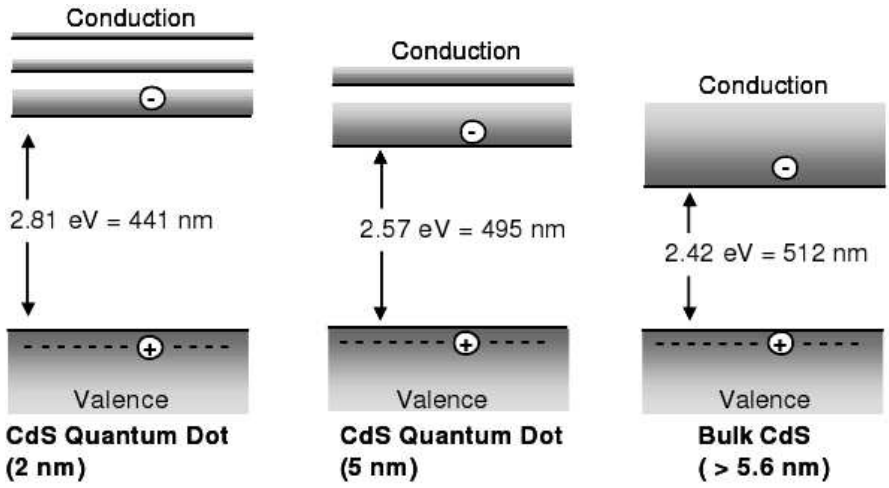

Figure 3.4: Band gap energy and optical absorption as a function of the crystal size.
The band gap (eV) increases with decreasing nanoparticle size. Band gap is inversely related to the start in absorbance (λ) through the relationship $E = hc/\lambda$. Therefore smaller particles begin to absorb at shorter wavelengths [59] (Image courtesy of J. Winter [64]).

proportional to nanocrystal size, larger nanocrystals display red-shifted emission. Additionally, the energy lost to heat decreases in a size-dependent manner.

3.4 Electronic properties/Manipulation of quantum dots

Electron-transfer between materials Quantum confinement also affects the electrical properties of nanocrystals. Since gap energies are size dependent, electrical properties that depend on this difference will display size dependence as well. One such property is electron transfer. Electrons with no additional energy added prefer to move to lower energy states within a given material. Because there are no energy states in the band gap, the electron will decay until it reaches the lowest state in the conduction band, and then return to the valence band through another mechanism (i.e. electron-hole recombination, non-radiative energy loss, etc). However, if the electron encounters a material with lower available energy states (i.e. lower conduction band); it can transfer its electron to that material (Figure 3.6). This process is dependent on the band gap. As the band gap increases, excited electrons occupy higher energy levels, and can decay to a greater number of lower state values. As a result of size-tunable band gaps within the quantum dot, electron transfer can be optimized to many materials.

Single electron transport in quantum dots: Single-electron tunneling and Coulomb blockade Electron transport through a quantum dot is studied by connecting the quantum dot to surrounding reservoirs (Figure 3.7). The fact that the charge on the electron island is quantized in units of the elementary charge e regulates transport through the quantum dot in the Coulomb blockade regime. Here the transport

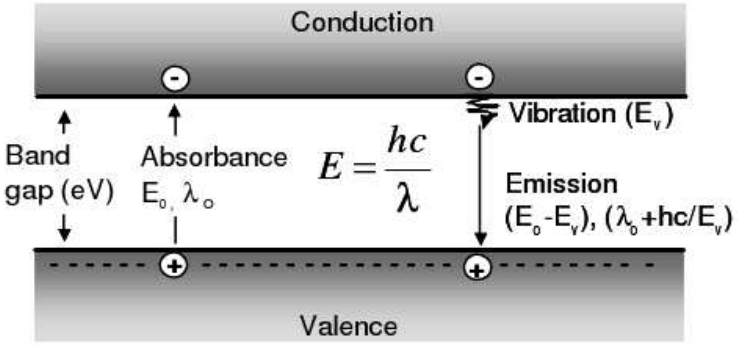

(a) Fluorescence and red-shift of λ due to energy loss.

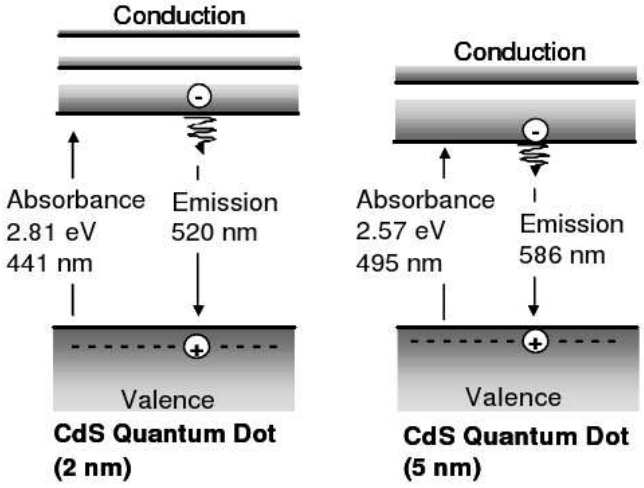

(b) Red-shifted emission due to crystal size.

Figure 3.5: Fluorescent emission and particle band gap, functions of the crystal size.
(a) Photon absorption creates an excited electron. This electron loses some energy to heat; then decays to ground, emitting a photon. The emitted photon has a longer wavelength than the absorbed photon because of the energy lost to heat.
(b) As the band gap decreases, the particle will absorb at longer wavelengths. This will produce a red-shift in particle fluorescent emission. (Image courtesy of J. Winter [64])

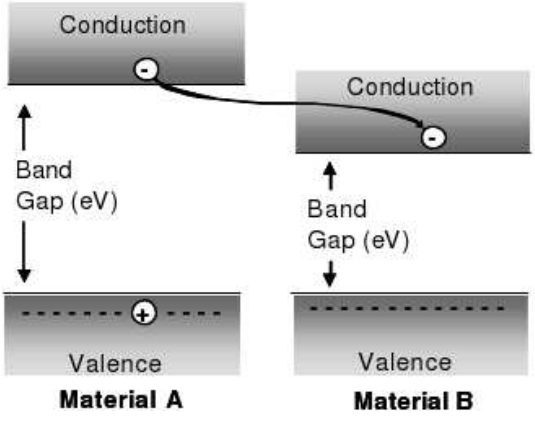

Figure 3.6: Electron transfer between materials with different band gaps.
If an excited electron in one material (A) encounters a second material (B) with a lower band gap energy, it can transfer its electron to that material. (Image courtesy of J. Winter [64])

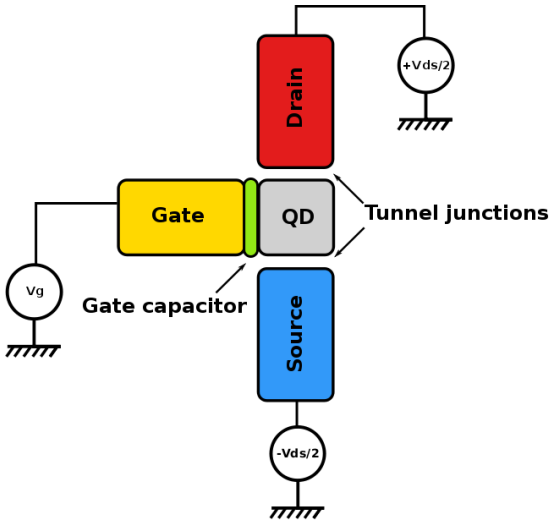

Figure 3.7: Schematic of a Single Electron Transistor (SET).
Setup for transport measurements on a lateral quantum dot. Because of the small size of the island or quantum dot (QD) in the middle of the two tunnel junctions the capacitance becomes very high and we see coulomb blockade effect.

between the reservoirs and the dot occurs **via tunnel barriers**, which are thick enough so that the transport is dominated by resonances due to quantum confinement in the dot. This requires a small transmission coefficient through the barriers, and thus the tunnel resistance has to be larger than the quantum resistance h/e^2. If the dot is fully decoupled from its environment, it confines a well defined number N of electrons. For weak coupling, deviations due to tunneling through the barriers are small, leading to discrete values in the total electrostatic energy of the dot. This energy can be estimated by $N(N-1)e^2/(2C)$, where C is the capacitance of the dot. Thus the addition of a single electron requires energy Ne^2/C, which is discretely spaced by the charging energy e^2/C. If this charging energy exceeds the thermal energy k_BT, the electrons cannot tunnel on and off the dot by thermal excitations alone, and transport can be blocked, which is referred to as a **Coulomb blockade**.

The two barriers define the coupling of the channel to its surroundings. The conductance of the double-barrier channel is measured as a function of the gate voltage at different temperatures.

Following Kouwenhoven and McEuen (1999), figure 3.8a schematically illustrates an electron island connected to its environment by electrostatic barriers, the so-called source and drain contacts, and a gate to which one can apply a voltage V_g as depicted in figure 3.7.

In this example, the level structure of the quantum dot connected to source and drain by tunneling barriers is sketched schematically in Figures. 3.8(a)-(c). The chemical potential inside the dot, where the discrete quantum states are filled with N electrons [i.e. the highest solid line in Figures. 3.8(a)-(c)], equals $\mu_{dot}(N) = E(N) - E(N+1)$, where $E(N)$ is the total groundstate energy (here at zero temperature).

Figure 3.8 shows the results of the experiment. We can see how the Coulomb

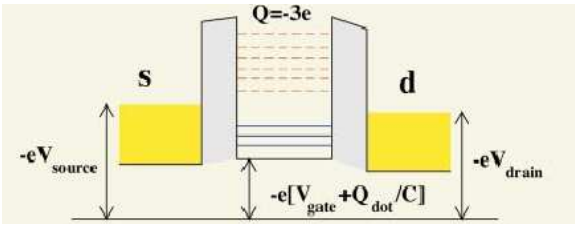

(a) Electron-transport blocked

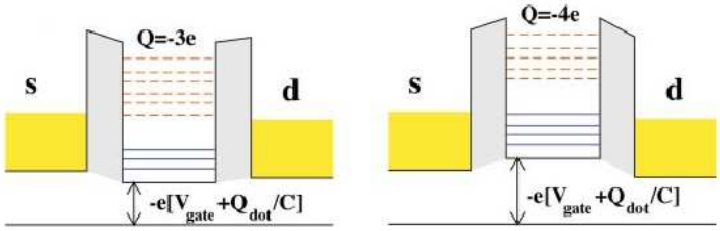

(b) Electron-transport allowed: maximum conductance

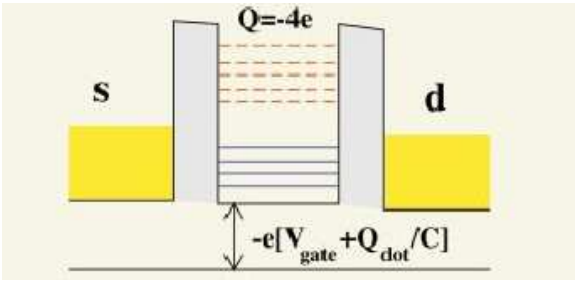

(c) Electron-transport blocked again

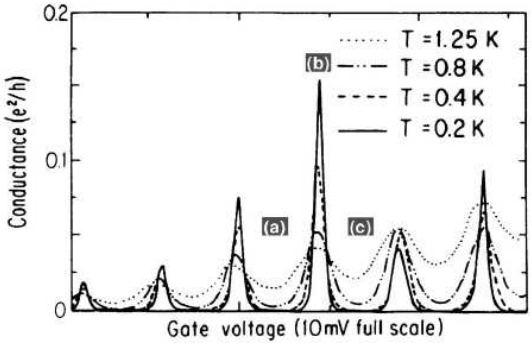

(d) Conductance of the double-barrier channel measured as a function of the gate voltage at different temperatures [41]

Figure 3.8: Single-electron transport in a quantum dot.
(a)-(c) Schematic picture of the level structures for single-electron transport (courtesy of A; Wacker). The solid lines represent the ionization potentials where the upper equals $\mu_{dot}(N)$, whereas the dashed lines refer to electron affinities, where the lowest one equals $\mu_{dot}(N+1)$. The gate bias increases from (a) to (c) [48].
(d) An example of the first measurements of Coulomb blockade as a function of the gate voltage.

blockade affects transport: clear peaks, equidistantly spaced, are separated by regions of zero conductance.

When a bias voltage is applied to the source s and the drain d, the electrochemical potentials μ_s and μ_d are different, and a transport window $\mu_s - \mu_d = -eV_{ds}$ opens up, where e is the electron charge. In the linear regime the transport window $-eV_{ds}$ is smaller than the spacing of the quantum states, and only the ground state of the dot can contribute to the conductance. By changing the voltage on the back gate, $\mu_{dot(N+1)}$ can be aligned with the transport window [Fig. 3.8b], and electrons can subsequently tunnel on and off the island at this particular gate voltage. This situation corresponds to a conductance maximum, as marked by the label (b) in Fig. 3.8d. Otherwise transport is blocked, as a finite energy is needed to overcome the charging energy. This scenario corresponds to zero conductance as marked by the labels (a) and (c) in Fig. 3.8. The mechanism of discrete charging and discharging of the dot leads to Coulomb blockade oscillations in the conductance as a function of gate voltage (as observed, for example, in Fig. 3.8d): at zero conductance, the number of electrons on the dot is fixed, whereas it is increased by one each time a conductance maximum is crossed. [48]

Spectroscopic information about the charge state and energy levels of the interacting quantum dot electrons can be obtained by analyzing the precise shape of the Coulomb oscillations and the Coulomb staircase. In this way, single electron transport can be used as a spectroscopic tool [42].

3.5 Quantum dot in a magnetic field

In many experimental situations with quantum dots, the electrons in quantum dots are manipulated using an external magnetic field. This field is usually created so that the magnetic field vector $\vec{B}$ is normal to the dot surface. For a typical quantum dot this results in a complicated spectrum of energy levels shown in figure 3.9.

The theoretical approach to the quantum dot given in the following chapter will serve as a basis to understand the spectrum of figure 3.9, even if the model used includes many approximations.

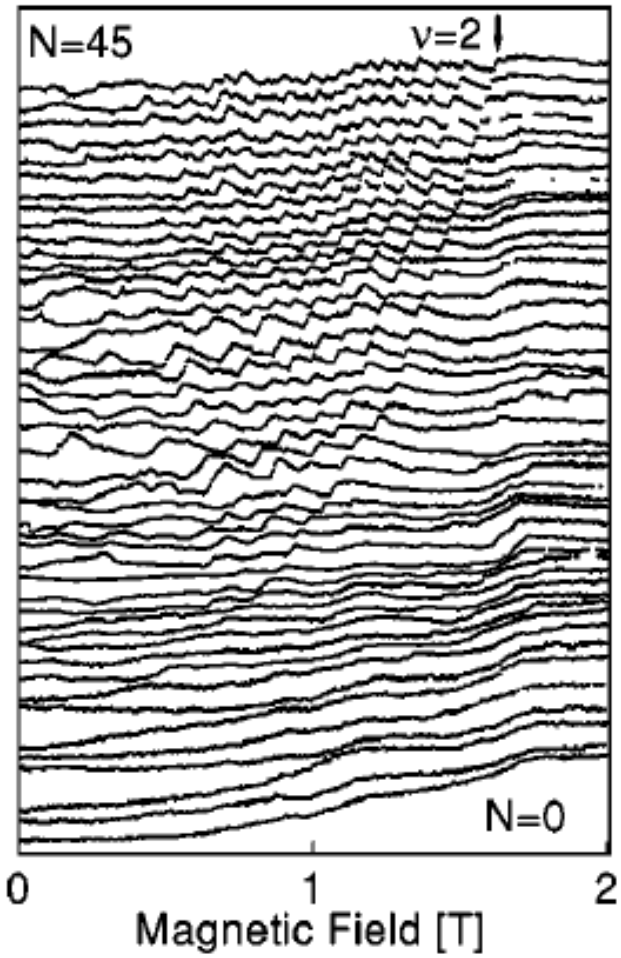

Figure 3.9: Additional energy spectrum as a function of a magnetic field. The magnetic field induces level crossings of single particle eigenstates which appear as cusps on the figure. (Image courtesy of M. Ciorga [10])

Chapter 4

Modelling of Quantum Dots

Quantum systems are governed by the Schrödinger equation (4^{th} postulate of quantum mechanics):

$$H|\psi(t)\rangle = i\hbar\frac{d}{dt}|\psi(t)\rangle \tag{4.1}$$

where H is the quantum Hamilton operator (or Hamiltonian) and $|\psi(t)\rangle$ the state vector of the system.

In particular, the solutions to the stationary form of this equation determine many physical properties of the system at hand, such as the ground state energy of the system which is the ultimate result of our simulations. As expressed in section 2.3 we need a way to validate our model and we choose the ground state energy as physical quantity that can be compared with experiments and other numerical simulations.

Solving the Schrödinger equation in the Hamiltonian formalism obviously requires a definition of this Hamiltonian which translates as well as possible our knowledge of the system into equations. We must identify the different forces/fields applied to the system in order to include their respective "potentials" into the Hamiltonian.

In the case of a quantum dot, the Hamiltionan is basically characterized by the different forces applied to its constituants. This could be done by summing over all the interactions between electrons/nuclei that constitute the quantum dot. However, if the final objective is to perform fast predictions about the system, the complexity of such a model might quickly reach the limits of the computational resources.

So we prefer a simpler model in which the system is limited to the free charge-carries, i.e. by modelling a **confining potential** that traps them into the dot as well as an **interaction potential** that characterizes the repulsion between those electrons.

In the following, a discussion is made on possible models of those potentials. The derivation of a Hamiltonian is then given for electrons that repeal each other by a Coulomb interaction and trapped in a parabolic potential and ever more confined by applying or not an external magnetic field. We show finally that rescaling the problem with proper length and energy units leads to a simple form of the Hamiltonian even when applying an external magnetic field to the quantum dot.

4.1 Theoretical approximation of the quantum dot Hamiltonian

Two-body interaction potential The interaction potential between two electrons is usually approximated proportional to the Coulomb repulsion in free space $V(\vec{r_i}, \vec{r_j}) = 1/r_{ij}$. For sake of simplicity and since it is still in use in most studies of quantum dots, we will stick to this approximation in this thesis. Nevertheless other studies have investigated other forms of potential. For example Johnson and Payne [24] assumed the interaction potential $V(\vec{r_i}, \vec{r_j})$ between particles i and j moving in the confining potential to saturate at small particle separation and to decrease quadratically with increasing separation. More recently, in order to investigate spin relaxation in quantum dots, Chaney and Maksym in [9] designed a more realistic confinement potential, electron-electron interactions, and screening where the parameters are obtained by fitting to experimental data.

The confining potential Defining the second potential that confines those electrons appears as a bigger issue while modelling a quantum dot. Some numerical [30, 38, 39, 53] and experimental [27, 21, 20] studies have shown that for a small number of electrons trapped, the harmonic oscillator potential is a good approximation, at least to first approximation. In [24], the bare (i.e. unscreened) confining potential $V(\vec{r_i})$ for the i^{th} particle is also modelled to be parabolic (i.e. the harmonic oscillator potential). It has been shown theoretically that for electrons contained in a parabolic potential there is a strong absorption of far-infrared light at the frequency corresponding to the bare parabola [6, 44, 65, 37]. This theoretical prediction is consistent with some experimental measurements on quantum dots [51]. Further evidence that the bare potential in many quantum-dot samples is close to parabolic is provided by simple electrostatic models [12].

A more complicated relation between the interactions Other studies tested different spherically symmetric confining potentials with different profiles ("soft" and "hard") on electrons in coupled QDs [35], and observed the resulting electron interaction. It shows really different behaviors of the electron interaction between the soft (Gaussian) and the hard (rectangular-like) confining potential. This means that an accurate model of the confining potential is strongly determined by the type and shape of the QD under study and produces also different type of electron interaction.

Motivation for our model Since we are focusing on the limits of the Hartree-Fock method with respect to other techniques rather than an exhaustive study of different types of quantum dots, we choose in the rest of the thesis to model the single quantum dot by a definite number of electron N_e, trapped by a pure isotropic harmonic oscillator potential and repealing each other with a two-body Coulomb interaction. Only closed shell systems are studied, meaning that the number of electrons present in the quantum dot are filling all single particle states until the Fermi level. This really simplifies the problem since all combinations of single particle states are reduced to one Slater determinant as detailled in 5.3.2.

4.2 General form of $\hat{H}$ with explicit physical interactions

In this section we derive the Hamiltonian of the quantum dot model with and without external magnetic field in order to show that the interaction with the external magnetic field will basically result in a modified harmonic oscillator frequency and a shift of the energy proportional to the strength of the field.

4.2.1 Electrons trapped in an harmonic oscillator potential

We consider a system of electrons confined in a pure isotropic harmonic oscillator potential $V(\vec{r}) = m^*\omega_0^2 r^2/2$, where m^* is the effective mass of the electrons in the host semiconductor (as defined in section 3.2), ω_0 is the oscillator frequency of the confining potential, and $\vec{r} = (x, y, z)$ denotes the position of the particle.

The Hamiltonian of a single particle trapped in this harmonic oscillator potential simply reads

$$\hat{H} = \frac{\mathbf{p}^2}{2m^*} + \frac{1}{2}m^*\omega_0^2\|\mathbf{r}\|^2 \tag{4.2}$$

where $\mathbf{p}$ is the canonical momentum of the particle.

When considering several particles trapped in the same quantum dot, the Coulomb repulsion between those electrons has to be added to the single particle Hamiltonian which gives

$$\hat{H} = \sum_{i=1}^{N_e}\left(\frac{\mathbf{p_i}^2}{2m^*} + \frac{1}{2}m^*\omega_0^2\|\mathbf{r_i}\|^2\right) + \frac{e^2}{4\pi\epsilon_0\epsilon_r}\sum_{i<j}\frac{1}{\|\mathbf{r_i} - \mathbf{r_j}\|}, \tag{4.3}$$

where N_e is the number of electrons, $-e$ ($e > 0$) is the charge of the electron, ϵ_0 and ϵ_r are respectively the free space permitivity and the relative permitivity of the host material (also called dielectric constant), and the index i labels the electrons.

4.2.2 Electrons trapped in an harmonic oscillator potential in the presence of an external magnetic field

Let's assume a static magnetic field $\overrightarrow{B}$ along the z axis.

Ignoring for now the spin-dependent terms, the Hamiltonian of those electrons in an magnetic field now reads [5]

$$\hat{H} = \sum_{i=1}^{N_e}\left(\frac{(\mathbf{p_i} + e\mathbf{A})^2}{2m^*} + \frac{1}{2}m^*\omega_0^2\|\mathbf{r_i}\|^2\right) + \frac{e^2}{4\pi\epsilon_0\epsilon_r}\sum_{i<j}\frac{1}{\|\mathbf{r_i} - \mathbf{r_j}\|}, \tag{4.4}$$

$$= \sum_{i=1}^{N_e}\left(\frac{\mathbf{p_i}^2}{2m^*} + \frac{e}{2m^*}(\mathbf{A}\cdot\mathbf{p_i} + \mathbf{p_i}\cdot\mathbf{A}) + \frac{e^2}{2m^*}\mathbf{A}^2 + \frac{1}{2}m^*\omega_0^2\|\mathbf{r_i}\|^2\right) \tag{4.5}$$

$$+\frac{e^2}{4\pi\epsilon_0\epsilon_r}\sum_{i<j}\frac{1}{\|\mathbf{r_i} - \mathbf{r_j}\|}, \tag{4.6}$$

where $\mathbf{A}$ is the vector potential defined by $\mathbf{B} = \nabla \times \mathbf{A}$.

In coordinate space, $\mathbf{p_i}$ is the operator $-i\hbar\nabla_i$ and by letting the Hamiltonian acting on the total wave function $\Psi(\mathbf{r})$ in the Schrödinger equation, we obtain the following operator acting on $\Psi(\mathbf{r})$

$$\mathbf{A}\cdot\mathbf{p_i}+\mathbf{p_i}\cdot\mathbf{A} = -i\hbar\left(\mathbf{A}\cdot\nabla_i+\nabla_i\cdot\mathbf{A}\right)\Psi \tag{4.7}$$
$$= -i\hbar\left(\mathbf{A}\cdot(\nabla_i\Psi)+\nabla_i\cdot(\mathbf{A}\Psi)\right) \tag{4.8}$$

We note that using the product rule and the Coulomb gauge $\nabla\cdot\mathbf{A}=0$ (by choosing the vector potential as $\mathbf{A}=\frac{1}{2}\mathbf{B}\times\mathbf{r}$), $\mathbf{p_i}$ and ∇_i commute and we obtain

$$\nabla_i\cdot(\mathbf{A}\Psi) = \mathbf{A}\cdot(\nabla_i\Psi)+\underbrace{(\nabla_i\cdot\mathbf{A})}_{0}\Psi = \mathbf{A}\cdot(\nabla_i\Psi) \tag{4.9}$$

This leads us to the following Hamiltonian:

$$\hat{H} = \sum_{i=1}^{N_e}\left(-\frac{\hbar^2}{2m^*}\nabla_i^2 - i\hbar\frac{e}{m^*}\mathbf{A}\cdot\nabla_i+\frac{e^2}{2m^*}\mathbf{A}^2+\frac{1}{2}m^*\omega_0^2\|\mathbf{r_i}\|^2\right) \tag{4.10}$$
$$+\frac{e^2}{4\pi\epsilon_0\epsilon_r}\sum_{i<j}\frac{1}{\|\mathbf{r_i}-\mathbf{r_j}\|}, \tag{4.11}$$

The linear term in $\mathbf{A}$ becomes, in terms of $\mathbf{B}$:

$$\frac{-i\hbar e}{m^*}\mathbf{A}\cdot\nabla_i = -\frac{i\hbar e}{2m^*}(\mathbf{B}\times\mathbf{r_i})\cdot\nabla_i \tag{4.12}$$
$$= \frac{-i\hbar e}{2m^*}\mathbf{B}\cdot(\mathbf{r_i}\times\nabla_i) \tag{4.13}$$
$$= \frac{e}{2m^*}\mathbf{B}\cdot\mathbf{L} \tag{4.14}$$

where $\mathbf{L}=-i\hbar(\mathbf{r_i}\times\nabla_i)$ is the orbital angular momentum operator of the electron i.

If assuming the electrons confined in the xy-plane, the quadratic term in $\mathbf{A}$ appearing in 4.10 can be written in the form

$$\frac{e^2}{2m^*}\mathbf{A}^2 = \frac{e^2}{8m^*}(\mathbf{B}\times\mathbf{r})^2 \tag{4.15}$$
$$= \frac{e^2}{8m^*}B^2r_i^2 \tag{4.16}$$

Until this point we have not taken into account the intrinsic magnetic moment of the electrons. These intrinsic magnetic moment, due to the electron spin in the host material, is given by

$$\mathcal{M}_s = -g_s^*\frac{e}{2m^*}\mathbf{S} \tag{4.17}$$

where $\mathbf{S}$ is the spin operator of the electron and g_s^* its effective spin gyromagnetic ratio (or efffective *g-factor* in the host material).We see that the spin magnetic moment $\mathcal{M}_s$ gives rise to an additional interaction energy [5], linear in the magnetic field,

$$\hat{H}_s = -\mathcal{M}_s\cdot\mathbf{B} = g_s^*\frac{e}{2m^*}BS_z = g_s^*\frac{\omega_c}{2}S_z \tag{4.18}$$

where $\omega_c = eB/m^*$ is known as the cyclotron frequency.

The final Hamiltonian reads

$$\hat{H} = \sum_{i=1}^{N_e} \left(\frac{-\hbar^2}{2m^*}\nabla_i^2 + \overbrace{\frac{1}{2}m^*\omega_0^2\|\mathbf{r_i}\|^2}^{\text{Harmonic ocscillator potential}} \right) + \overbrace{\frac{e^2}{4\pi\epsilon_0\epsilon_r}\sum_{i<j}\frac{1}{|\mathbf{r_i}-\mathbf{r_j}|}}^{\text{Coulomb interactions}} + \underbrace{\sum_{i=1}^{N_e}\left(\frac{1}{2}m^*\left(\frac{\omega_c}{2}\right)^2\|\mathbf{r_i}\|^2 + \frac{1}{2}\omega_c\hat{L}_z^{(i)} + \frac{1}{2}g_s^*\omega_c\hat{S}_z^{(i)}\right)}_{\substack{\text{single particle interactions} \\ \text{with the magnetic field}}}, \tag{4.19}$$

4.2.3 Scaling the problem: Dimensionless form of $\hat{H}$

In order to simplify the computation, the Hamiltonian can be rewritten on dimensionless form. For this purpose, let's introduce some constants:

- the oscillator frequency $\omega = \omega_0\sqrt{1+\omega_c^2/(4\omega_0^2)}$,
- an new energy unit $\hbar\omega$,
- and a new length unit, the oscillator length defined by $l = \sqrt{\hbar/(m^*\omega)}$, also called the characteristic length unit.

Let's rewrite the Hamiltonian in dimensionless units using:

$$\mathbf{r} \longrightarrow \frac{\mathbf{r}}{l}, \quad \nabla \longrightarrow l\,\nabla \quad \text{and} \quad \hat{L}_z \longrightarrow \hat{L}_z$$

Leading to the following Hamiltonian:

$$\hat{H} = \sum_{i=1}^{N_e}\left(-\frac{1}{2}\nabla_i^2 + \frac{1}{2}r_i^2\right) + \overbrace{\frac{e^2}{4\pi\epsilon_0\epsilon_r}\frac{1}{\hbar\omega l}}^{\substack{\text{Dimensionless} \\ \text{confinement} \\ \text{strength } (\lambda)}}\sum_{i<j}\frac{1}{r_{ij}} + \sum_{i=1}^{N_e}\left(\frac{1}{2}\frac{\omega_c}{\hbar\omega}\hat{L}_z^{(i)} + \frac{1}{2}g_s^*\frac{\omega_c}{\hbar\omega}\hat{S}_z^{(i)}\right), \tag{4.20}$$

Lengths are now measured in units of $l = \sqrt{\hbar/(m^*\omega)}$, and energies in units of $\hbar\omega$.

A new dimensionless parameter $\lambda = l/a_0^*$ (where $a_0^* = 4\pi\epsilon_0\epsilon_r\hbar^2/(e^2m^*)$ is the effective Bohr radius) describes the strength of the electron-electron interaction. Large λ implies strong interaction and/or large quantum dot [54]. Since both $\hat{L}_z$ and $\hat{S}_z$ commute with the Hamiltonian we can perform the calculations separately in subspaces of given quantum numbers L_z and S_z. Figure 4.1 displays values of the different parameters as a function of the magnetic field strength for a particular type of semiconductor: Gallium arsenide (GaAs) with know characteristics given in table 3.1.

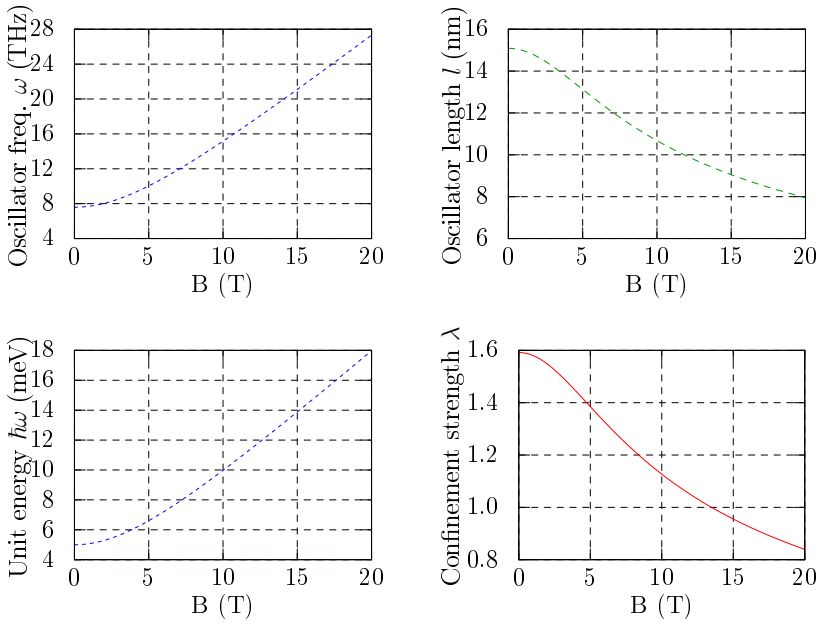

Figure 4.1: Typical values for the oscillator frequency ω, the oscillator length l, the energy unit $\hbar\omega$ and the dimensionless confinement strength λ as a function of the magnetic field strength in GaAs semiconductors assuming: $\hbar\omega_0 = 5 \times 10^{-3} eV$ [28], $\epsilon_r \simeq 12$ and $m^* = 0.067\, m_e$

The simplified dimensionless Hamiltonian becomes

$$\hat{H} = \sum_{i=1}^{N_e} \left[-\frac{1}{2}\nabla_i^2 + \frac{1}{2} r_i^2 \right] + \lambda \sum_{i<j} \frac{1}{r_{ij}} + \sum_{i=1}^{N_e} \left(\frac{1}{2} \frac{\omega_c}{\hbar\omega} L_z^{(i)} + \frac{1}{2} g_s^* \frac{\omega_c}{\hbar\omega} S_z^{(i)} \right), \tag{4.21}$$

The last term which is proportional to the magnetic field involves only the quantum numbers L_z and S_z and not the operators themselves [54]. Therefore their contributions can be added when the remaining part has been solved and the squizzing effect of the magnetic field being included simply in the parameter λ. This brings us to the simple and general form of the Hamiltonian to study:

$$\hat{H} = \sum_{i=1}^{N_e} \left(-\frac{1}{2}\nabla_i^2 + \frac{1}{2} r_i^2 \right) + \lambda \sum_{i<j} \frac{1}{r_{ij}}. \tag{4.22}$$

Chapter 5

Many-body treatment: the Hartree-Fock method

A many-body system with interactions is generally very difficult to solve exactly, except for extremely simple cases. It is the same when it comes to quantum dots that can simply be seen as a many-electron problem.

In the first section of this chapter we will detail the derivation of exact solutions for the two-electrons quantum dot for some particular parameters. Then some numerical approximations techniques are used in order to get information about the properties of the system as close as possible from their real values. In this thesis we focus on the ground state energy of quantum dots (i.e. the energy of the system at rest without external time-dependent excitations). And for this purpose, several many-body techniques can be used with of course different accuracy and efficiency.

We will of course detail the Hartree-Fock method which is a major part of this thesis and compare its results to other *Ab initio* methods such as perturbation theory, variational Monte-Carlo or large scale diagonalisation.

5.1 Analytical solutions of some particular cases

[Exact solution for 2 electrons in Simen thesis p.4 of paper 2]

5.1.1 Non-interacting particles trapped in a pure HO potential

5.1.2 Two-electrons quantum dot with/without magnetic field

In solving many-body problems (i.e.m̃any-particle problems), it common to hear in this field that "many starts at two". Analytical solution of the two-electrons QD [Taut 1993- 2D with B field + 3D without B field]

[transition for next part: there is not many exact solutions for the study of many-electron QD and for those that exist, they require particular restrictions for the model under study. So numerical methods appear as the only to implement a more general form of the QD model and to solve the many-body problem. The next section introduces the Hartree-Fock method as one possible numerical technique with

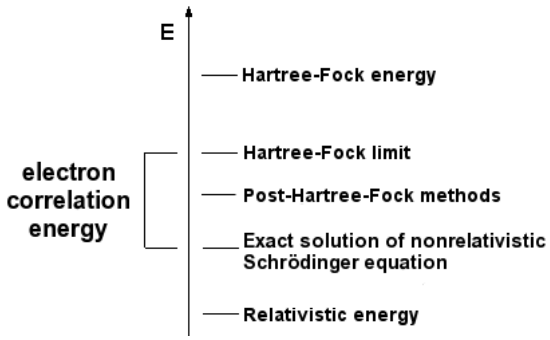

Figure 5.1: Electron correlation energy in terms of various levels of theory of solutions for the Schrödinger equation. (K. Langner, 2005)

its pros and cons wrt to other methods.]

5.2 Ab initio many-body techniques

[Introduce the Hartree-Fock method as one possible ab initio technique]

Ab-initio methods: HF, VMC, CI, PDE (pros and cons).

What other properties that the ground state energy can I expect to get from the methods? since HF is a mean-field approximation, we can't for example determine the charge localization of the system.

The term *"ab initio"* indicates that the calculation is from first principles and that no empirical data is used.

The simplest type of *ab initio* electronic structure calculation is the Hartree-Fock (HF) scheme, in which the instantaneous Coulombic electron-electron repulsion is not specifically taken into account. Only its average effect (mean field) is included in the calculation. This is a variational procedure; therefore, the obtained approximate energies, expressed in terms of the system's wave function, are always equal to or greater than the exact energy, and tend to a limiting value called the Hartree-Fock limit as the size of the basis is increased [11].

Many types of calculations begin with a Hartree-Fock calculation and subsequently correct for electron-electron repulsion, referred to also as electronic correlation. Configuration Interaction (CI) and Coupled cluster theory (CC) may be some examples of these post-Hartree-Fock methods.

Figure 5.2 presents a diagram illustrating electron correlation energy in terms of various levels of theory. As shown on the figure, HF may present the worse approximation to the exact energy of a many-body system, but its simplicity is on all fours with its computational simplicity (i.e.s̃peed) compared to other methods.

In some cases, particularly for bond breaking processes, the Hartree-Fock method is inadequate and this single-determinant reference function is not a good basis for post-Hartree-Fock methods. It is then necessary to start with a wave function that includes more than one determinant.

A method that avoids making the variational overestimation of HF in the first

place is Quantum Monte Carlo (QMC), in its variational, diffusion, and Green's function forms. These methods work with an explicitly correlated wave function and evaluate integrals numerically using a Monte Carlo integration. Such calculations can be very time-consuming, but they are probably the most accurate methods known today.

Ab initio electronic structure methods have the advantage that they can be made to converge to the exact solution, when all approximations are sufficiently small in magnitude. In particular, configuration interaction, where all possible configurations are included (called "Full CI") tends to the exact non-relativistic solution of the Schrödinger equation, and therefore to the best possible solution in principle.

However Full CI is often impossible for anything but the smallest systems. The convergence, is usually not monotonic, and sometimes the smallest calculation gives the best result for some properties.

Then the downside of ab initio methods is their computational cost. They often take enormous amounts of computer time, memory, and disk space. The HF method scales nominally as N^4 (N being the number of basis functions), i.e.ã calculation twice as big takes 16 times as long to complete. However in practice it can scale closer to N^3 as the program can identify zero and extremely small integrals and neglect them. Correlated calculations scale even less favorably - MP2 as N^5; MP4 as N^6 and coupled cluster as N^7. Density functional theory (DFT) methods scale in a similar manner to Hartree-Fock but with a larger proportionality term. Thus DFT calculations are always more expensive than an equivalent Hartree-Fock calculation [60]

[FIND BETTER SOURCE THAN WIKIPEDIA TO PROVIDE RESULTS ON THE COMPUTATIONAL COMPLEXITY]. Look at Simen's derivation for computing the error of FCI and looking at the biggest system that can be studied wrt the limit in memory of a supercomputer.

Many [4]

5.3 Time-independent Hartree-Fock Theory

say something on restricte, unrestricted HF. => descriptions in Morten's slides: FYS4410. s.386/412 $http://en.wikipedia.org/wiki/Mean_field_theory$

= derivation of HF equations. These equations will be different in the 2 simulations that will be made:

1. varying directly the wave function as in project 1 (Numerov's algo, Shooting method/Green's function/Wronskian...)

2. varying the coefficient of the HO wf which leads to solving a linear system How good is the Hartree-Fock approximation? (Moshinsky1969 p.77 [43]).

The Hartree-Fock method is a minimization method based on a mathematical technique known as the Lagrange multipliers, where the functional to minimize is the energy of the system.

Since the energy which is an expectation value of the Hamiltonian can be written explicitly as an integral, we will review an approximated method, the Variational

method and how it minimizes such a functional based on Lagrange multipliers. The *variational method* (or *variational calculus* or *calculus of variations*) is really useful in obtaining the bound state energies and wave functions of a time-independent Hamiltonian $\hat{H}$. Then the approximations applied to the wave function and the energy functional of the system are detailled when dealing with a many-body problem. The variational method and those approximations lead us to the derivation of the *Hartree-Fock method*, a mean-field variational method also categorized as a *self-consistent method*,.

[DETAILS ON MEAN-FIELD THEORY (MFT) found on wiipedia] *http* : *//en.wikipedia.org/w*
The n-body system is replaced by a 1-body problem with a chosen good external potential (i.e. field). The external field replaces the interaction of all the other particles to an arbitrary particle. The great difficulty (e.g. when computing the partition function of the system) is the treatment of combinatorics generated by the interaction terms in the Hamiltonian when summing over all states. The goal of mean field theory (MFT, also known as self-consistent field theory) is to resolve these combinatorial problems.

The main idea of MFT is to replace all interactions to any one body with an average or effective interaction. This reduces any multi-body problem into an effective one-body problem. The ease of solving MFT problems means that some insight into the behavior of the system can be obtained at a relatively low cost.

In field theory, the Hamiltonian may be expanded in terms of the magnitude of fluctuations around the mean of the field. In this context, MFT can be viewed as the "zeroth-order" expansion of the Hamiltonian in fluctuations. Physically, this means an MFT system has no fluctuations, but this coincides with the idea that one is replacing all interactions with a "mean field". Quite often, in the formalism of fluctuations, MFT provides a convenient launch-point to studying first or second order fluctuations.

In general, dimensionality plays a strong role in determining whether a mean-field approach will work for any particular problem. In MFT, many interactions are replaced by one effective interaction. Then it naturally follows that if the field or particle exhibits many interactions in the original system, MFT will be more accurate for such a system. This is true in cases of high dimensionality, or when the Hamiltonian includes long-range forces. The Ginzburg criterion is the formal expression of how fluctuations render MFT a poor approximation, depending upon the number of spatial dimensions in the system of interest.

5.3.1 Variational Calculus and Lagrange Multipliers

As we have seen in the previous part, in most cases we must resort to computers to determine the solutions of the Shrödinger equation. It is of course possible to integrate the equation using discretisation methods, but in most realistic electronic structure calculations we would need huge numbers of grid points, leading to high computer time and memory requirements. The variational method on the other hand enables us to solve the Schrödinger equation much more efficiently in many cases [55].

As for the method of Lagrange multipliers in mathematical optimization (more

details about this method in appendix **??**), the calculus of variations provides a strategy for finding the stationnary points of a function subject to some constraints. Maxima and minima can be found this way when the function is differentiable.

More specifically the calculus of variations involves problems where the quantity to be minimized or maximized (the functional) is an integral.

In the general case we have an integral of the type

$$E[\Phi] = \int_a^b f(\Phi(x), \frac{\partial \Phi}{\partial x}, x)dx,$$

where E is the quantity which is sought minimized or maximized.

The problem is that although f is a function of the variables Φ, $\partial\Phi/\partial x$ and x, the exact dependence of Φ on x is not known. This means again that even though the integral has fixed limits a and b, the path of integration is not known. In our case the unknown quantities are the single-particle wave functions and we wish to choose an integration path which makes the functional $E[\Phi]$ stationary. This means that we want to find minima, or maxima or saddle points. In physics we search normally for minima.

Our task is therefore to find the minimum of $E[\Phi]$ so that its variation δE is zero subject to specific constraints. In our case the constraints appear as the integral which expresses the orthogonality of the single-particle wave functions. The constraints can be treated via the technique of the Lagrange multipliers.

In the following, we will be more specific with the form of the functional which now reads

$$E[\Phi] = \frac{\langle \Phi | H | \Phi \rangle}{\langle \Phi | \Phi \rangle} = \frac{\int \Phi^* H \Phi d\tau}{\int \Phi^* \Phi d\tau} \tag{5.1}$$

where the integration is extended over the full range of all the coordinates of the system.

We denote by E_n the eigenvalues of the Hamiltonian and by Ψ_n the corresponding orthonormal eigenfunctions, and assume that $\hat{H}$ has at least one discrete eigenvalue. It is clear that if the function Φ is identical to one of the exact eigenfunctions Ψ_n of $\hat{H}$; then $E[\Phi]$ will be identical to the corresponding exact eigenvalue E_n.

In the following, we will show that:

1. any function Φ for which the functional $E[\Phi]$ is stationary is an eigenfunction of the discrete spectrum of $\hat{H}$.

2. using the method of the Lagrange multipliers and varying the functional $\langle \Phi | H | \Phi \rangle$ subject to the normalisation condition $\langle \Phi | \Phi \rangle = 1$, the Lagrange multiplier itself has the significance of an energy eigenvalue.

3. the functional $E[\Phi]$ gives an upper bound for the ground state energy, also known as the *variational principle*.

4. it is possible to solve the Schrödinger equation using the variational method.

Any function Φ *for which the functional* $E[\Phi]$ *is stationary is an eigenfunction of* $\hat{H}$
If Φ and an exact eigenfunction Ψ_n differ by an arbitrary infinitesimal variation $\delta\Phi$,

$$\Phi = \Psi_n + \delta\Phi,$$

then the corresponding first-order variation of $E[\Phi]$ vanishes:

$$\delta E = 0, \tag{5.2}$$

and the eigenfunctions of $\hat{H}$ are solutions of the variational equation 5.2.

To prove this statement, we note re-writting the functional as

$$E[\Phi] \int \Phi^* \Phi d\tau = \int \Phi^* H \Phi d\tau,$$

and varying it gives:

$$\delta E \int \Phi^* \Phi d\tau + E \int \delta\Phi^* \Phi d\tau + E \int \Phi^* \delta\Phi d\tau = \int \delta\Phi^* H \Phi d\tau + \int \Phi^* H \delta\Phi d\tau.$$

Since $\Phi|\Phi$ is assumed to be finite and non-vanishing, we see that the variational equation 5.2 is equivalent to

$$\int \delta\Phi^* (H - E)\Phi d\tau + \int \Phi^* (H - E)\delta\Phi d\tau = 0. \tag{5.3}$$

Although the variations $\delta\Phi$ and $\delta\Phi^*$ are not independent, they may in fact be treated as such, so that the individual terms in 5.3 can be set equal to zero. TO see how this comes about, we replace the arbitrary variation $\delta\Phi$ by $i\delta\Phi$ in 5.3 so tht we obtain

$$-i \int \delta\Phi^* (H - E)\Phi d\tau + i \int \Phi^* (H - E)\delta\Phi d\tau = 0. \tag{5.4}$$

By combining 5.3 with 5.4 we then obtain the two equations

$$\begin{cases} \delta\Phi^* (H - E)\Phi d\tau = 0 \\ \Phi^* (H - E)\delta\Phi d\tau = 0 \end{cases} \tag{5.5}$$

which is the desired result. Using the fact that $\hat{H}$ is Hermitian, we see that the two equation 5.5 are equivalent to the Schödinger equation $(H - E[\Phi])\Phi = 0$.

Thus any function $\Phi = \Psi_n$ for which the functional 5.1 is stationary is an eigenvalue of $\hat{H}$ corresponding to the eigenvalue $E_n = E[\Psi_n]$. It is worth stressing that if Φ and Ψ_n differ by $\delta\Phi$, the variational equation 5.2 implies that the leading term of the difference $E[\Phi] - E_n$ is quadratic in $\delta\Phi$. As a result, errors in the approximate energy are of second order in $\delta\Phi$ when the energy is calculated from the functional 5.1.

the Lagrange multiplier has the significance of an energy eigenvalue We also remark that the functional 5.1 is independent of the normalisation and of the phase of Φ. In particular, it is often convenient to impose the condition $\langle\Phi|\Phi\rangle = 1$. The above results may then be retrieved by varying the functional $\langle\Phi|H|\Phi\rangle = 1$ subject to the condition $\langle\Phi|\Phi\rangle = 1$, namely

$$\delta \int \Phi^* H \Phi d\tau = 0, \quad \int \Phi^* \Phi d\tau = 1.$$

The constraint $\langle\Phi|\Phi\rangle = 1$ may be taken care of by introducing a Lagrange multiplier (as described in appendix **??**) which we denote by Σ.

We define the Lagrangian Λ as

$$\Lambda(\Phi, \Sigma) = \int \Phi^* H \Phi d\tau - \Sigma \left(\int \Phi^* \Phi d\tau - 1 \right),$$

so that the variational equation reads

$$\delta\Lambda(\Phi, \Sigma) = 0 \tag{5.6}$$

$$\delta \left[\int \Phi^* H \Phi d\tau - \Sigma \int \Phi^* \Phi d\tau \right] = 0, \tag{5.7}$$

or

$$\int \delta\Phi^* (H - \Sigma)\Phi d\tau + \int \Phi^* (H - \Sigma)\delta\Phi d\tau = 0,$$

This equation is identical to 5.3, and we see that the Lagrange multiplier $\Sigma = E$ has the significance of an energy eigenvalue.

the variational principle An important additional property of the functional 5.1 is that it provides an upper bound to the exact ground state E_0. To prove this result, we expand the arbitrary, normalisable function Φ in the complete set of orthonormal eigenfunctions Ψ_n of $\hat{H}$. This reads

$$\Phi = \sum_n a_n \Psi_n. \tag{5.8}$$

Substituing the expansion 5.8 into the functional 5.1, we find that

$$E[\Phi] = \frac{\sum_n |a_n|^2 E_n}{\sum_n |\ a_n\ |^2}, \tag{5.9}$$

where we have used the fact that $H\Psi_n = E_n\Psi_n$ and $\langle\Phi|\Phi\rangle = \sum_n |a_n|^2$. If we now subtract E_0, the lowest energy eigenvalue, from both sides of the functional 5.9 we have

$$E[\Phi] - E_0 = \frac{\sum_n |a_n|^2 (E_n - E_0)}{\sum_n |a_n|^2}. \tag{5.10}$$

Since $E_n \geq E_0$, the right-hand side of 5.10 is non-negative, so that

$$E_0 \leq E[\Phi] \tag{5.11}$$

and the functional $E[\Phi]$ gives an upper-bound, or in order words a *minimum principle* for the ground state energy [5].

Solving the Schrödinger equation using the variational method In the variational method, the possible solutions (i.e.the stationary states of the energy functional) are restricted to a subspace of the Hilbert space, and in this subspace we seek the "best possible" solution. An important example is linear variational calculus, in which the subspace is spanned by a set of basis vectors χ_i for $i = 1, \ldots, P$ where P is the size of the basis set. We take these to be orthonormal at first, that is,

$$\langle \chi_i | \chi_j \rangle = \delta_{ij}.$$

For an arbitrary state $|\Psi\rangle = \sum_i C_i |\chi_j\rangle$, the energy functional is given by

$$E = \frac{\langle \Psi | H | \Psi \rangle}{\langle \Psi | \Psi \rangle} = \frac{\sum_{i,j=1}^{R} C_i^* C_j H_{ij}}{\sum_{i,j=1}^{R} C_i^* C_j \delta_{ij}},$$

where $H_{ij} = \langle \chi_i | H | \chi_j \rangle$ is assumed to be known.

The stationary states follow from the condition that the derivative of this functional with respect to the C_i vanishes, which leads to

$$\sum_{j=1}^{R} (H_{ij} - E\delta_{ij}) C_j = 0, \qquad for \quad i = 1, \ldots, R. \tag{5.12}$$

Equation 5.12 is then an eigenvalue problem which can be written in matrix notation as

$$\mathbf{HC} = \mathbf{EC}. \tag{5.13}$$

This is the Schrödinger equation, formulated for a finite, orthonormal basis.

The lowest eigenvalue of eq. 5.13 is always higher that or equal to the ground state energy, as we proved that the ground state is the minimal value assumed by the energy-functional in the full Hilbert space. If we restrict ourselves to a part of this space, then the minimum value of the energy functional must always be higher than or equal to the ground state of the full Hilbert space. Including more basis functions into our setm the subspace becomes larger and consequently the minimum of the energy functional will decrease (or stay the same). The behaviour of the spectrum found by solving 5.13 with increasing size of the basis set R is depicted in figure 5.2.

Then variational approach discussed here provides a powerful method for obtaining approximate solutions of the wave function. But this might not be sufficient when dealing with a system made of many interacting particles, where more approximations have to be done about the wave function of the system in order to lead again to a simple eigenvalue problem.

5.3.2 Approximated wave function of the many-body system

The Schrodinger equation for a system of N electron reads:

$$\hat{H}(\mathbf{r_1}, \mathbf{r_2}, \ldots, \mathbf{r_N}) \Psi_\eta(\mathbf{r_1}, \mathbf{r_2}, \ldots, \mathbf{r_N}) = E_\eta \Psi_\eta(\mathbf{r_1}, \mathbf{r_2}, \ldots, \mathbf{r_N}) \tag{5.14}$$

where the vector $\mathbf{r}_i$ represents the coordinates (spatial and spin) of a particle i, η stands for all the quantum numbers needed to classify a given N-particle state and Ψ_η is the corresponding eigenfunction.

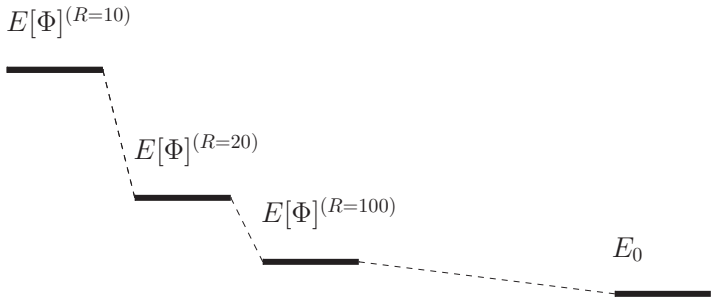

Figure 5.2: The behaviour of the ground state energy of eq. 5.12 with increasing basis set size R in linear variational calculus. The upper index is the number of states in the basis set.

The Hamiltonian can be written in the form

$$\hat{H} = \hat{T} + \hat{V}$$

where $\hat{T}$ represents the kinetic energy of the system

$$\hat{T} = \sum_{i=1}^{N} \frac{\mathbf{p_i^2}}{2m_i} = \sum_{i=1}^{N} \left(-\frac{\hbar^2}{2m_i} \nabla_i^2 \right) = \sum_{i=1}^{N} t(\mathbf{r_i})$$

while the operator $\hat{V}$ represents the potential energy given by

$$\hat{V} = \underbrace{\sum_{i=1}^{N} u(\mathbf{r_i})}_{\substack{\text{one-particle} \\ \text{interaction}}} + \underbrace{\sum_{i<j}^{N} v(\mathbf{r_i}, \mathbf{r_j})}_{\substack{\text{two-particles} \\ \text{interaction}}} = \underbrace{\sum_{i=1}^{N} \frac{1}{2} m\omega^2 r_i^2}_{\substack{\text{confining} \\ \text{potential}}} + \underbrace{\lambda^* \sum_{i<j}^{N} \frac{1}{\| \vec{r_i} - \vec{r_j} \|}}_{\substack{\text{Coulomb} \\ \text{repulsion}}} \tag{5.15}$$

where ω is the frequency of the harmonic oscillator potential and λ^* is the dimensionless parameter characterizing the interaction strength as defined in eq. (**??**).

Hereafter we use atomic units, viz. $\hbar$=c=e=1 with e the elementary charge and c the speed of light. This means that momenta and masses have dimension energy. In the last equation we have singled out an external one-body potential term u which is meant to represent an effective one-body field in which our particles move (i.e.the harmonic oscillator potential in our first approximation for the confining potential of the QD model) .

We have therefore assumed that a picture consisting of individual electrons is a viable starting point for wave function approximations. We can rewrite the Hamiltonian for N electrons as

$$\hat{H} = \hat{H}_0 + \hat{H}_1 = \sum_{i=1}^{N} \hat{h}_i + \lambda^* \sum_{i<j}^{N} \frac{1}{r_{ij}}, \tag{5.16}$$

where we have defined $r_{ij} = \| \vec{r_i} - \vec{r_j} \|$ and $\hat{h}_i = t(\mathbf{r_i}) + u(\mathbf{r_i})$.

The first term of the eq.(5.16), $\hat{H}_0$, is the sum of the N one-body Hamiltonians $\hat{h}_i$. Each individual Hamiltonian $\hat{h}_i$ contains the kinetic energy operator of an electron

and its potential energy due to the confining potential. The potential energy term due to the harmonic oscillator potential defines the one-body field $u_i = u(\mathbf{r_i})$ of eq.(5.15). We have moved this term into the $\hat{H}_0$ part of the Hamiltonian, instead of keeping it in $\hat{V}$ as in eq.(5.15). The reason is that we will hereafter treat $\hat{H}_0$ as our non-interacting Hamiltonian. For a many-body wavefunction Ψ_η defined by an appropriate single-particle basis, we may solve exactly the non-interacting eigenvalue problem

$$\hat{H}_0\Psi_\eta = E_\eta\Psi_\eta,$$

with E_η being the non-interacting energy. This energy is defined by the sum over single-particle energies. In our model of the quantum dot, the single-particle energies are the harmonic oscillator single-particle energies in 2D or 3D respectively.

The second term of the eq.(5.16), $\hat{H}_1$, is the sum of the $N(N-1)/2$ two-body interactions between each pair of electrons. Note that the double sum carries a restriction $i < j$.

Irrespective of these approximations, there is a wealth of experimental evidence that these interactions have to obey specific symmetries. The total Hamiltonian should be translationally invariant. If angular momentum is conserved, the Hamiltonian is invariant under rotations. Furthermore, it is invariant under the permutation (interchange) of two particles. Since we deal with fermions, the total wave function is antisymmetric.

Let $\hat{P}$ be an operator which interchanges two particles. Due to the symmetries we have ascribed to our Hamiltonian, this operator commutes with the total Hamiltonian,

$$[\hat{H}, \hat{P}] = 0,$$

meaning that $\Psi_\eta(\mathbf{r_1}, \mathbf{r_2}, \ldots, \mathbf{r_N})$ is an eigenfunction of $\hat{P}$ as well, that is

$$\hat{P}_{ij}\Psi_\eta(\mathbf{r_1}, \mathbf{r_2}, \ldots, \mathbf{r_i}, \ldots, \mathbf{r_j}, \ldots, \mathbf{r_N}) = \beta\Psi_\eta(\mathbf{r_1}, \mathbf{r_2}, \ldots, \mathbf{r_j}, \ldots, \mathbf{r_i}, \ldots, \mathbf{r_N}),$$

where β is the eigenvalue of $\hat{P}$. We have introduce the suffix ij in order to indicate that we permute particles i and j. The Pauli principle tell us that the total wave function for a system of fermions has to be antisymmetric, resulting in the eigenvalue β=-1 [reference:Morten book??? chap.2 citemortenBook].

We approximate our many-body wave function with the product of single-particle wave functions. Since we assume that our Hamiltonian is time-independent, these single-particle wave functions are normally the eigenfunctions of a selected one-body Hamiltonian $\hat{h}_i$ acting on particle i.

In Hartree-Fock we approximate the exact eigenfunction[1] Ψ_λ by a trial wave

[1] We reserve Ψ as labelling for our exact wave function (eigen function, since there is no time-dependence). The Slater determinant is only an approximation of the exact solution.

function Φ built as a Slater determinant

$$\Phi(\mathbf{r_1}, \mathbf{r_2}, \ldots, \mathbf{r_N}, \alpha, \beta, \ldots, \sigma) = \frac{1}{\sqrt{N!}} \begin{vmatrix} \psi_\alpha(\mathbf{r}_1) & \psi_\beta(\mathbf{r}_2) & \ldots & \psi_\sigma(\mathbf{r}_N) \\ \psi_\alpha(\mathbf{r}_1) & \psi_\beta(\mathbf{r}_2) & \ldots & \psi_\sigma(\mathbf{r}_N) \\ \vdots & \vdots & \ddots & \vdots \\ \psi_\alpha(\mathbf{r}_1) & \psi_\beta(\mathbf{r}_2) & \ldots & \psi_\sigma(\mathbf{r}_N) \end{vmatrix}, \tag{5.17}$$

where the variables $\mathbf{r_i}$ include the coordinates of spin and space of particle i, and $\alpha, \beta, \ldots, \sigma$ encompass all possible quantum numbers needed to specify a particular system. The single-particle function $\psi_\alpha(\mathbf{r_i})$ are eigenfunctions of the onebody Hamiltonian $\hat{h}_i$, that is

$$\hat{h}_i = h(\mathbf{r_i}) = t(\mathbf{r_i}) + u(\mathbf{r_i}),$$

with eigenvalues

$$\hat{h}_i \psi_\alpha(\mathbf{r_i}) = \left[t(\mathbf{r_i}) + u(\mathbf{r_i})\right] \psi_\alpha(\mathbf{r_i}) = \epsilon_\alpha \psi_\alpha(\mathbf{r_i}).$$

As defined previously, for modelling a quantum dot we will equate $\hat{h}_i$ with the single-particle Hamiltonian of the harmonic oscillator. Then the energies ϵ_α are the so-called non-interacting single-particle energies, or unperturbed energies. The total energy is in this case the sum over all single-particle energies, if no two-body or more complicated many-body interactions are present.

We note again that the wave-function is antisymmetric with respect to an interchange of any two particles, as required by the Pauli principle. For an N-body Slater determinant we have thus (omitting the quantum numbers α, ...,σ)

$$\Phi(\mathbf{r_1}, \mathbf{r_2}, \ldots, \mathbf{r_i}, \ldots, \mathbf{r_j}, \ldots, \mathbf{r_N}) = -\Phi(\mathbf{r_1}, \mathbf{r_2}, \ldots, \mathbf{r_j}, \ldots, \mathbf{r_i}, \ldots, \mathbf{r_N}).$$

5.3.3 Approximated energy of the system

Assume E_0 to be the ground state energy. According to the variational principle (given in eq. 5.11) we have

$$E_0 \leq E[\Phi_T] = \int \Phi_T^* \hat{H} \Phi_T d\tau$$

where we have used the shorthand $d\tau = d\mathbf{r_1}, d\mathbf{r_2}, \ldots, d\mathbf{r_N}$, and where Φ_T is a trial function which we assume to be normalized

$$\int \Phi_T^* \Phi_T d\tau = 1.$$

In the Hartree-Fock method, correlations between electrons are not taken into account and the trial function is just the Slater determinant of eq. (5.17) which can be rewritten as

$$\Phi_T(\mathbf{r_1}, \mathbf{r_2}, \ldots, \mathbf{r_N}, \alpha, \beta, \ldots, \sigma) = \frac{1}{\sqrt{N!}} \sum_p (-)^p P \Psi_\alpha(\mathbf{r_1}) \Psi_\beta(\mathbf{r_2}) \ldots \Psi_\sigma(\mathbf{r_N}) = \sqrt{N!}\, \mathcal{A} \Phi_H \tag{5.18}$$

where we have introduced the antisymmetrization operator $\mathcal{A}$ defined by the summation over all possible permutations of 2 nucleons. It is defined as

$$\mathcal{A} = \frac{1}{N!}\sum_{P}(-)^{p}\hat{P}, \tag{5.19}$$

with p standing for the number of permutations. We have introduced here the so-called Hartree function, defined by the simple product of all possible single-particle functions

$$\Phi_H(\mathbf{r_1}, \mathbf{r_2}, \ldots, \mathbf{r_N}, \alpha, \beta, \ldots, \sigma) = \Psi_\alpha(\mathbf{r_1})\Psi_\beta(\mathbf{r_2})\ldots\Psi_\sigma(\mathbf{r_N}). \tag{5.20}$$

Both $\hat{H}_0$ and $\hat{H}_1$ are invariant under all possible permutations of any two electrons and hence commute with $\mathcal{A}$

$$[\hat{H}_0, \hat{\mathcal{A}}] = [\hat{H}_1, \hat{\mathcal{A}}] = 0. \tag{5.21}$$

Furthermore, $\mathcal{A}$ satisfies

$$\mathcal{A}^2 = \mathcal{A} \tag{5.22}$$

since every permutation of the Slater determinant reproduces it.

The expectation value of $\hat{H}_0$

$$\begin{aligned}\langle\Phi_T|\hat{H}_0|\Phi_T\rangle = \int \Phi_T^*\hat{H}_0\Phi_T d\tau &= N!\int \mathcal{A}\Phi_H^*\hat{H}_0\mathcal{A}\Phi_H d\tau \\ &= N!\int \Phi_H^*\hat{H}_0\mathcal{A}^2\Phi_H d\tau \\ &= N!\int \Phi_H^*\hat{H}_0\mathcal{A}\Phi_H d\tau\end{aligned}$$

where we have used eq. (5.21) and (5.22). The next step is to replace the antisymmetrization operator by its definition in eq.(5.19) and to replace $\hat{H}_0$ with the sum of one-body operators as in eq.(5.16)

$$\int \Phi_T^*\hat{H}_0\Phi_T d\tau = \sum_{i=1}^{N}\sum_{P}(-)^{p}\int \Phi_H^*\hat{h}_i\hat{P}\Phi_H d\tau.$$

The integral vanishes if two or more electrons are permuted in only one of the Hartree functions Φ_H because the individual single-particle wave functions are assumed orthogonal ($\langle\Psi_\alpha|\Psi_\beta\rangle = \delta_{\alpha\beta}$).

We obtain then

$$\int \Phi_T^*\hat{H}_0\Phi_T d\tau = \sum_{i=1}^{N}\int \Phi_H^*\hat{h}_i\Phi_H d\tau.$$

The orthogonality of the single-particle functions allows us to further simplify the integral, and we arrive at the following expression for the expectation values of

the sum of one-body Hamiltonians (i.e.the expectation value of the non-interacting single particle energies)

$$\int \Phi_T^* \hat{H}_0 \Phi_T d\tau = \sum_{\mu=1}^{N} \int \Psi_\mu^*(\mathbf{r}) \hat{h} \Psi_\mu(\mathbf{r}) d\mathbf{r} = \sum_{\mu=1}^{N} \langle \mu | h | \mu \rangle \tag{5.23}$$

Regarding the interaction part, the expectation value of the two-body Hamiltonian is obtained in a similar manner. We have

$$\langle \Phi_T | \hat{H}_1 | \Phi_T \rangle = \int \Phi_T^* \hat{H}_1 \Phi_T d\tau = N! \int \mathcal{A} \Phi_H^* \hat{H}_1 \mathcal{A} \Phi_H d\tau,$$

which reduces to

$$\int \Phi_T^* \hat{H}_1 \Phi_T d\tau = \sum_{i<j=2}^{N} \sum_P (-)^p \int \Phi_H^* V(r_{ij}) \hat{P} \Phi_H d\tau,$$

by following the same arguments as for the one-body Hamiltonian. Because of the dependence on the inter-electron distance r_{ij}, permutations of any two electrons no longer vanish.

$$\begin{aligned} \int \Phi_T^* \hat{H}_1 \Phi_T d\tau &= \sum_{i<j=2}^{N} \int \Phi_H^* V(r_{ij}) \Phi_H d\tau - \int \Phi_H^* V(r_{ij}) P_{ij} \Phi_H d\tau \\ &= \sum_{i<j=2}^{N} \int \Phi_H^* V(r_{ij}) (1 - P_{ij}) \Phi_H d\tau, \end{aligned}$$

where P_{ij} is the permutation operator that interchanges electron i and electron j. Again we use the assumption that the single-particle wave functions are orthogonal (as eigenvectors of an hermitian operator, the Hamiltonian), and we get

$$\int \Phi^* \hat{H}_1 \Phi d\tau = \frac{1}{2} \sum_{\mu=1}^{N} \sum_{\nu=1}^{N} \left[\int \Psi_\mu^*(\mathbf{r_i}) \Psi_\nu^*(\mathbf{r_j}) V(r_{ij}) \Psi_\mu(\mathbf{r_i}) \Psi_\nu(\mathbf{r_j}) d\mathbf{r_i} d\mathbf{r_j} \right] \tag{5.24}$$

$$- \frac{1}{2} \sum_{\mu=1}^{N} \sum_{\nu=1}^{N} \left[\int \Psi_\mu^*(\mathbf{r_i}) \Psi_\nu^*(\mathbf{r_j}) V(r_{ij}) \Psi_\mu(\mathbf{r_j}) \Psi_\nu(\mathbf{r_i}) d\mathbf{r_i} d\mathbf{r_j} \right] \tag{5.25}$$

The first term is the so-called direct term. It is frequently also called the Hartree term, while the second is due to the Pauli exclusion principle and is called the exchange term or just the Fock term. The factor 1/2 is introduced because we now run over all pairs twice.

The last equation allows us to introduce soe further definitions. The single-particle wave functions $\Psi_\mu(\mathbf{r})$, defined by the quantum number μ and $\mathbf{r}$ (recall that $\mathbf{r}$ also includes spin degree) are defined as

$$\Psi_\alpha(\mathbf{r}) = \langle \mathbf{r} | \alpha \rangle$$

Since we will work in what is called the occupation number representation (or just second quantization) of quantum mechanical states and operators, we will not show the coordinate space dependence of various quantum mechanical objects.

We introduce the following shorthands for the above two integrals

$$\langle\mu\nu|V|\mu\nu\rangle = \int \Psi^*_\mu(\mathbf{r_i})\Psi^*_\nu(\mathbf{r_j})V(r_{ij})\Psi_\mu(\mathbf{r_i})\Psi_\nu(\mathbf{r_j})d\mathbf{r_i}d\mathbf{r_j}$$

and

$$\langle\mu\nu|V|\nu\mu\rangle = \int \Psi^*_\mu(\mathbf{r_i})\Psi^*_\nu(\mathbf{r_j})V(r_{ij})\Psi_\nu(\mathbf{r_i})\Psi_\mu(\mathbf{r_j})d\mathbf{r_i}d\mathbf{r_j}$$

Since the interaction is invariant under the interchange of two particles it means for example that we have

$$\langle\mu\nu|V|\mu\nu\rangle = \langle\nu\mu|V|\nu\mu\rangle,$$

or in the more general case

$$\langle\mu\nu|V|\sigma\tau\rangle = \langle\nu\mu|V|\tau\sigma\rangle.$$

The direct and exchange matrix elements can be brought together if we define the antisymmetrized matrix element

$$\langle\mu\nu|V|\mu\nu\rangle_{AS} = \langle\mu\nu|V|\mu\nu\rangle - \langle\mu\nu|V|\nu\mu\rangle,$$

or for a general matrix element

$$\langle\mu\nu|V|\sigma\tau\rangle_{AS} = \langle\mu\nu|V|\sigma\tau\rangle - \langle\mu\nu|V|\tau\sigma\rangle.$$

It has the symmetry property

$$\langle\mu\nu|V|\sigma\tau\rangle_{AS} = -\langle\mu\nu|V|\tau\sigma\rangle_{AS} = \langle\nu\mu|V|\sigma\tau\rangle_{AS}.$$

The antisymmetric matrix element is also hermitian, implying

$$\langle\mu\nu|V|\sigma\tau\rangle_{AS} = \langle\sigma\tau|V|\mu\nu\rangle_{AS}.$$

With these notations we write eq.(5.24) as

$$\langle\Phi_T|\hat{H}_1|\Phi_T\rangle = \int \Phi^*_T\hat{H}_1\Phi_T d\tau = \frac{1}{2}\lambda^* \sum_{\mu=1}^{N}\sum_{\nu=1}^{N}\langle\mu\nu|V|\mu\nu\rangle_{AS}. \tag{5.26}$$

Combining eqs.(5.23) and (5.26) we obtain the energy functional

$$E[\Phi_T] = \sum_{\mu=1}^{N}\langle\mu|h|\mu\rangle + \frac{1}{2}\lambda^* \sum_{\mu=1}^{N}\sum_{\nu=1}^{N}\langle\mu\nu|V|\mu\nu\rangle_{AS}. \tag{5.27}$$

which we will use as our starting point for the Hartree-Fock calculations.

5.3.4 The restricted Hartree-Fock equations and their self-consistent solutions

Since it is based on a variational method and Lagrange multipliers (discussed in section 5.3.1), the Hartree-Fock technique also aims at minimizing the energy functional given in eq. 5.27. Nevertheless obtaining an eigenvalue problem to solve the eigenvalue problem is not straight forward when dealing with many interacting particles (as shown in 5.3.1) until we do a second approximation about the interacting potential.

Indeed the Coulomb repulsion induces a two-body interaction. As we show in the following, this leads to a system of coupled single-particle equations. A way to decouple those equations is to define an *effective potential*, which is an average of the Coulomb repulsion over all the electrons of the system. That is why the Hartree-Fock method is categorized as a *mean-field approximation* or also a *self-consistent field approximation* when refering to the iterative process of the method.

The following discussion only details the Restricted Hartree-Fock (RHF) method, where the quantum dot is modelled as a closed-shell system with all orbitals doubly occupied (electrons spin up and down). Open-shell systems, where some of the electrons are not paired, are not treated in this thesis, but can be handled by one of these other Hartree-Fock methods:

- Restricted open-shell Hartree-Fock (ROHF)
- Unrestricted Hartree-Fock (UHF)

[SAY SOMETHING about ROOTHAN equations]

The Roothaan equations are a representation of the Hartree-Fock equation in a non-orthonormal basis set which can be of Gaussian-type or Slater-type. It applies to closed-shell systems where all orbitals are doubly occupied. This is generally called Restricted Hartree-Fock theory. The method was developed independently by Clemens C. J. Roothaan and George G. Hall in 1951, and is thus sometimes called the Roothaan-Hall equations. The Roothaan equations can be written in a form resembling generalized eigenvalue problem, although they are not a standard eigenvalue problem because they are nonlinear:

$$\mathbf{FC} = \mathbf{SC}\epsilon$$

where F is the so-called Fock matrix (which depends on the coefficients C due to electron-electron interactions), C is a matrix of coefficients, S is the overlap matrix of the basis functions, and ϵ is the (diagonal, by convention) matrix of orbital energies. In the case of an orthonormalised basis set the overlap matrix, S, reduces to the identity matrix.

[DIFFERENT IMPLEMENTATION OF THE HARTREE-FOCK METHOD: 2 techniques to do that (cf.Morten slides in FYS4410): either vary the spatial part of the single particle wave functions, or expand each single particle wave functions in a given basis (i.e. the HO basis set) and vary the coefficients of those single particle wf. In the following, we use the latter technique, which is the more common (industrial) way to apply Hartree-Fock.]

One technique for solving this problem starts by expanding each single-particle eigenvector Ψ_i in terms of any convenient complete set of single-particle states $|\alpha\rangle$:

$$\Psi_i = |i\rangle = \sum_\alpha c_i^\alpha |\alpha\rangle. \tag{5.28}$$

In our case, the complete set of single-particle states $|\alpha\rangle$ corresponds to the harmonic oscillator states. While the expansion (5.28) in general involves an infinite number of terms, we always truncate it in approximation procedures, so that we shall assume here that (5.28) is a finite sum [43] in the subspace of dimension K.

$$\Psi_i = |i\rangle = \sum_\alpha^K c_i^\alpha |\alpha\rangle. \tag{5.29}$$

Introducing the expansion (5.29) in the expectation value of $\hat{H}$ (eq. 5.27), we can write

$$E[\Phi] = \langle\Phi|\hat{H}_0|\Phi\rangle + \langle\Phi|\hat{H}_1|\Phi\rangle \tag{5.30}$$

$$= \sum_{i=1}^N \langle i|h|i\rangle + \frac{1}{2}\lambda^* \sum_{i=1}^N \sum_{j=1}^N \langle ij|V|ij\rangle_{AS} \tag{5.31}$$

$$= \sum_{i=1}^N \sum_{\alpha\gamma}^K C_i^{\alpha*} C_i^\gamma \langle\alpha|h|\gamma\rangle + \frac{1}{2}\lambda^* \sum_{i,j=1}^N \sum_{\alpha\beta\gamma\delta}^K C_i^{\alpha*} C_j^{\beta*} C_i^\gamma C_j^\delta \langle\alpha\beta|V|\gamma\delta\rangle_{AS}. \tag{5.32}$$

the objective is of course to minimize the energy functional in eq. 5.30 with respect to some constraints that insure the orthonormality of the single-particle eigenvectors. For that purpose we introduce the ϵ_i as Lagrange multipliers to insure the constraints of orthonormality, meaning for any particle i and j

$$\langle i|j\rangle = \delta_{ij}$$

$$\sum_{\alpha\beta}^K C_i^{\alpha*} C_j^\beta \underbrace{\langle\alpha|\beta\rangle}_{\delta_{\alpha\beta}} = \delta_{ij} \tag{5.33}$$

$$\sum_\alpha^K C_i^{\alpha*} C_j^\alpha = \delta_{ij} \tag{5.34}$$

Then a variatonal analysis implies minimizing the Lagrangian Λ

$$\Lambda = \Lambda(C_1^\alpha, C_2^\alpha, \ldots, C_N^\alpha, \epsilon_1, \epsilon_2, \ldots, \epsilon_N), \tag{5.35}$$

$$= E[\Phi] - \sum_{i=1}^N \epsilon_i \left(\sum_\alpha^K C_i^{\alpha*} C_i^\alpha \right), \tag{5.36}$$

with respect to the coefficient $C_i^{\alpha*}$ (or C_i^α).

The variational equation as defined in 5.6 leads to take the derivative of (5.35) with respect to $C_i^{\alpha *}$ and to set it to zero

$$\frac{d}{dC_i^{\alpha *}} \left[\Lambda(C_1^\alpha, C_2^\alpha, \ldots, C_N^\alpha, \epsilon_1, \epsilon_2, \ldots, \epsilon_N)\right] = 0 \quad \forall\, i \in \mathbb{N}^*$$

$$\frac{d}{dC_i^{\alpha *}} \left[E[\Phi] - \sum_{i=1}^{N} \epsilon_i \sum_{\alpha}^{K} C_i^{\alpha *} C_i^\alpha\right] = 0 \quad \forall\, i \in \mathbb{N}^*.$$

Remembering that C_i^α and $C_i^{\alpha *}$ can be treated as independent, we arrive at the Hartree-Fock equations (one equation for each particle i in its state $|\alpha\rangle$)

$$\sum_{\gamma}^{K} \langle \alpha|h|\gamma\rangle \; C_i^\gamma + \lambda^* \sum_{j=1}^{N} \sum_{\beta\gamma\delta}^{K} C_j^{\beta *} \langle \alpha\beta|V|\gamma\delta\rangle_{AS} \; C_i^\gamma \; C_j^\delta = \epsilon_i \; C_i^\alpha \quad \forall\, i \in \mathbb{N}^* \tag{5.37}$$

The Hartree-Fock equations in (5.37) may be rewritten as

$$\sum_{\gamma}^{K} \langle \alpha|h|\gamma\rangle \; C_i^\gamma + \lambda^* \sum_{\gamma}^{K} \left[\sum_{j=1}^{N} \sum_{\beta\delta}^{K} C_j^{\beta *} \langle \alpha\beta|V|\gamma\delta\rangle_{AS} \; C_j^\delta\right] C_i^\gamma = \epsilon_i \; C_i^\alpha \quad \forall\, i \in \mathbb{N}^*$$

$$\sum_{\gamma}^{K} \mathcal{O}_{\alpha\gamma} \; C_i^\gamma = \epsilon_i \; C_i^\alpha \quad \forall\, i \in \mathbb{N}^* \tag{5.38}$$

from where we notice that eq.(5.37) is a system of non-linear equations in the C_i^α, $C_i^{\alpha *}$, since $\mathcal{O}_{\alpha\gamma}$ depends itself on the unknowns, which may be solved by an iterative procedure.

The iterative (self-consistant) procedure may be derived as follows. Let us define an *effective Coulomb interaction potential* U as

$$\langle \alpha|U|\gamma\rangle \equiv \lambda^* \sum_{j=1}^{N} \sum_{\beta\delta}^{K} C_j^{\beta *} \langle \alpha\beta|V|\gamma\delta\rangle_{AS} \; C_j^\delta \tag{5.39}$$

and calculate these matrix elements with initial values for C_i^α, say δ_i^α. When we substitute the result in eq.(5.37), we get a system of linear equations in the C_i^α; this we can now solve in the standard way. If we started with a set of K states $|\alpha\rangle$, the vectors C_i^α are K-dimensional and orthogonal, and so obey

$$\sum_{\alpha}^{K} C_i^{\alpha *} C_j^\alpha = \delta_{ij}.$$

There are thus K independent vector solutions of the linearised version of eq.(5.37),

$$\sum_{\gamma}^{K} \left[\langle \alpha|h|\gamma\rangle + \langle \alpha|U|\gamma\rangle\right] C_i^\gamma = \epsilon_i \; C_i^\alpha.$$

Among those solutions we select those for the n lowest eigenvalues ϵ_i and substitute them back into (5.39); this provides the starting point for the next iteration. The process is continued until self-consistency is reached, or in other words until the C_i^α converge within a certain approximation [43].

The Hartree-Fock equations in (5.37) may again be rewritten as

$$\begin{aligned}\sum_{\gamma}^{K}\langle\alpha|h|\gamma\rangle\, C_i^\gamma + \lambda^* \sum_{\gamma}^{K}\left[\sum_{j=1}^{N}\sum_{\beta\delta}^{K} C_j^{\beta*}\langle\alpha\beta|V|\gamma\delta\rangle_{AS}\, C_j^\gamma\, C_j^\delta\right] C_i^\gamma = \epsilon_i\, C_i^\alpha \quad \forall\, i \in \mathbb{N}^* \\ \sum_{\gamma}^{K}\left[t_{\alpha\gamma} + \lambda^* \sum_{j=1}^{N}\sum_{\gamma,\delta=1}^{K} V_{\alpha\beta\gamma\delta}\, C_j^{\beta*}\, C_j^\delta\right] C_i^\gamma = \epsilon_i\, C_i^\alpha \quad \forall\, i \in \mathbb{N}^*\end{aligned} \tag{5.40}$$

where the two-body interaction matrix element $V_{\alpha\beta\gamma\delta}$ can be computed in advance

$$V_{\alpha\beta\gamma\delta}(ij) = \langle\alpha\beta|V(ij)|\gamma\delta\rangle_{AS}$$

as well as the one-body piece $t_{\alpha\gamma}(i)$

$$\sum_{\gamma}^{K} t_{\alpha\gamma}(i) = \sum_{\gamma}^{K}\langle\alpha|h(i)|\gamma\rangle = \epsilon_{HO}^\alpha$$

where ϵ_{HO}^α are the energy eigenvalues of the one-body harmonic oscillator in state $|\alpha\rangle$ (then solution of the eigenproblem: $h_{HO}|\alpha\rangle = \epsilon_{HO}^\alpha|\alpha\rangle$).

5.3.5 Computational efficiency of the Hartree-Fock method

"Time complexity" and "space complexity" (memory requirements)

try to reproduce Simen's derivation when looking at the accuracy of the method [PhD p.25 [33]].

5.4 Corrections to the HF energy: perturbation theory

5.4.1 2^{nd} and 3^{rd} order time-independent degenerate perturbation theory corrections

detailled in [18,47] about second order and third order expressions.

5.4.2 Occupation number formalism

detailled in [47], Hamiltonian formalism in [OpenFCI paper of Simen] and [chap.2 from Morten lectures] and [http://www.iue.tuwien.ac.at/phd/pourfath/node109.html]

When we start developing the expression of an excited state of the unperturbed Hamiltonian as given from the perturbation theory, it becomes really complicated to write the combinations of Slater determinants in terms of permutations of occupied and unoccupied single particle orbitals.

Historically, quantum physics first dealt only with the quantization of the motion of particles, leaving the electromagnetic field classical (Schrödinger, Heisenberg and Dirac, 1925-26). Later also the electromagnetic field was quantized (Dirac, 1927), and even the particles themselves got represented by quantized fields (Jordan and Wigner, 1927), resulting in the development of quantum electrodynamics and quantum field theory in general. By convention, the original form of quantum mechanics is denoted first quantization, while quantum field theory is formulated in the language of occupation number formalism, also known as second quantization.

As we will show, second quantization greatly simplifies the discussion of many interacting particles. This approach merely reformulates the original Schrödinger equation. Nevertheless, it has the advantage that in second quantization operators incorporate the statistics, which contrasts with the more cumbersome approach of using symmetrized or anti-symmetrized products of single-particle wave functions. In the second quantization formalism a quantum mechanical basis is used that describes the number of particles occupying each state in a complete set of single-particle states. For this purpose the time-independent abstract state vectors for an N-particle system are introduced

$$|n_1, n_2, \ldots\rangle, \quad where \quad \sum_j n_j = N. \tag{5.41}$$

The notation means that there are n_1 particles in the state 1, n_2 particles in the state 2, and so forth. It is therefore natural to define occupation number operators $\hat{n}_j$ which have the basis states $|n_j\rangle$ as eigenstates, and have the number n_j of particles occupying the state j as eigenvalues $\hat{n}_j|n_j\rangle = n_j|n_j\rangle$. For fermions (such as the electrons of our quantum dot) n_j can be 0 or 1, while for Bosons it can be any non-negative number.

5.5 Variational Monte-Carlo method

see vmx.tex given by Morten [email 28/05/2009]

5.6 Full Configuration Interaction (Exact or Large Scale Diagonalization) method

A configuration interaction wave function is a multiple-determinant wave function. This can be constructed by starting with the HF wave function and making new determinants by promoting electrons from the occupied to unoccupied orbitals. Configuration interaction calculations can be very accurate, but the cost in CPU time is very high (N^8 time complexity or worse).

Configuration interaction calculations are classified by the number of excitations used to make each determinnat. If only one electron has been moved for each determinant, it is called a configuration interaction single-excitation (CIS) calculation.

CIS calculations give an approximation to the excited states of a molecule, but do not change the ground-state energy. Single and double excitation (CISD) calculations yield a ground state energy that has been corrected for correlation. Triple-excitation (CISDT) and quadruple-excitation (CISDTQ) calculations are done only when very-high-accuracy resuts are desired.

The configuration interaction calculation with all possible excitations is called a full CI. The full CI calculation using an infinitely large basis set will give an exact quantum mechanical result. However, full CI calculations are very rarely done due to the immense amount of computer power required.

[Some more info about the reference used (HF or Gaussian) in input in Google book on computational chemistry.]

[also in Simen thesis: CI+effective interaction in paper 1]

5.6.1 Effective Interaction

5.7 Corrections to the HF energy: perturbation theory

5.8 Time-dependent Hartree-Fock Theory

paper from Moan on How to solve a Time-dependent Schro. eq. using "Splitting methods" (weekly meeting 10/09/2008)

5.9 Comparison with Variational Monte Carlo???

info about that in the thesis from Rontani

may include a comparison as done last semester between DFT and HF!!!!

Chapter 6

Implementation and Results

TEST to cite a class: class `CoulombMatrix`

```
% Place nodes
\node [block] (init) {Initialize:\\
Set $\mathbb{R}$, $\alpha$ and $\Psi_{T-\alpha}(\mathbb{R})$};
\node [block, below of=init] (suggestMove) {Suggest a move};%:\\ $\mathbb{x}^{trial}_p = \ma
\node [block, below of=suggestMove] (evaluateAcceptance) {Compute acceptance ratio};%: $R =
```

[use code here to generate DECISION TREES, same guy who made timer.hpp: http://oldmill.uchicago.edu/ wilder/Code/pst/]

Give a list of states, non-ordered, then ordered an explain why.

Detail constraint on momentum/spin conservation on the implementation

6.1 Code Implementation in the energy basis

[DESCRIBES THE IMPLEMENTATION AS A LOGICAL REPRESENTATION OF THE BLACK BOX OF THE HF METHOD]

The main program processes a textual configuration file (*parameters.inp*) with problem parameters (size of the closed shell system, dimension of the problem, interaction strength,...) before proceeding with the Hartree-Fock algorithm. While running the executable, the Hartree-Fock approximation of the total energy is computed in a self-consistent way and finally printed out to screen.

The code is organized in different classes to allow generalization of the problem, and more particularly the possibilities to compute the Hartree-Fock approximation of the total energy using different methods (analytical expression of the Coulomb interaction or numerical integration in different basis set using the Numerov's algorithm instead of solving an eigenvalue problem) and for different forms of the confining potential, in two and three dimensions.

; ;

Figure [6.1] tries to summarize the code implementation in a diagram.

The current version only consider closed-shell systems where particles are trapped within an isotropic harmonic oscillator potential. Given the maximum energy level R, the class *singleParticelOrbitals* generates all single particle states and build a

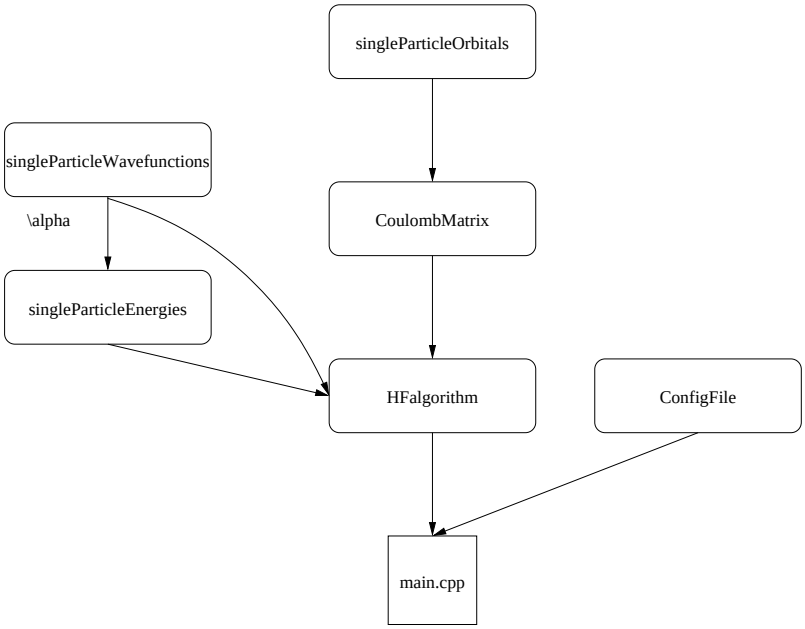

Figure 6.1: Diagram of the code implementation

table of states with their respective quantum numbers ($|\alpha\rangle \rightarrow |n, ml, ms\rangle$) in both 2D and 3D. The class $CoulombMatrix$ generates and stores a matrix of the 2-body Coulomb interaction computing its analytical expression [54] [49] in two dimension only.

$$V_{\alpha\beta\gamma\delta} = \langle\alpha\beta|V_{ij}|\gamma\delta\rangle_{as}.$$

The classes $singleParticleWavefunctions$ and $singleParticleEnergies$ are assumed to provide respectively multiple choices of basis set ($|\alpha\rangle \rightarrow \varphi_\alpha(r, \theta, \phi)$) and their corresponding single particle energies ($|\alpha\rangle \rightarrow \epsilon_\alpha = \langle\alpha|\hat{h}|\alpha\rangle$). Since the Coulomb matrix elements are computed in 2D from an analytical expression obtained in the harmonic oscillator basis set, no numerical integration are required in the current version of the code. This is the reason why no explicit basis, neither numerical integration methods have been implemented yet. The single particle energies for non-interacting particles have also simple analytical forms in the harmonic oscillator basis ($\epsilon_\alpha^{HO} = 2n + |m_l|$ in 2D). Then the classes $singleParticleWavefunctions$ and $singleParticleEnergies$ are really simple now, but have been created for future generalization of the code.

The class $HFalgorithm$ solves the Hartree-Fock equations by solving an eigenvalue problem. This eigenvalue problem comes from the expansion of the single particle wave functions in the harmonic oscillator basis set and from the initialization of an effective potential initially computed thanks to a guess of the single particle wave functions and the pre-computed Coulomb matrix elements. This class also implements an iterative procedure, where the solution of the eigenvalue problem are injected back into the computation of the effective potential. This new effective potential is then used to solve a new eigenvalue problem, giving rise to a new set of single particle wavefunctions and a lower energy of the system. The process is

continued until self-consistency is reached.

The main file reads the paramters of the problem from file and simply build the objects of the classes described earlier one after the other in order to define, to initialize and to solve the problem. An example of the basic configuration file is shown below.

As an example, table 6.1 shows a different ground state Hartree-Fock energies (in units of $\hbar\omega_0$) when varying the parameters *dimension*, R, *lambda* and running the executable each time.

	$2D$			$3D$		
R	$\# e^-$	$\lambda = 1$	$\lambda = 2$	$\# e^-$	$\lambda = 1$	$\lambda = 2$
0	2	3.25331	4.50663	2		
1	6	22.21981	34.43963	8		
2	12	73.76555	119.53110	20		
3	20	177.96330	295.92660	40		
4	30	357.54370	605.08739	70		
5	42	637.55964	1093.11930	112		

Table 6.1: Hartree-Fock approximations of the ground state energy of the quantum dot obtained for different sets of input parameters in two and three dimensions.

Table **??** compares the ground state energies reported in [???] with my Hartree-fock approximation. [NOT FOUND A REFERENCE YET !!]

The code does not support parallel computation yet. This could be useful when solving the eigenvalue problem or computing numerical integrations, but the code is already fast enough to produce results in a few second or minutes for reasonnably large systems ($R \leq 4$).

6.1.1 The Hilbert space

In this part, description of the way the basis set is build. Recall this is done on a closed shell system. Describe the tables of states in the basis set with their respective quantum numbers (in 2D and 3D), as wel las the table of "hole" states for the states occupied by a particle. Describe the table of states-couple, which is used in the generation of the Coulomb interaction.

Also describe the function that re-order the basis set within blocks of common angular momentum and spin. the reason for it is given later in the Hartree-Fock algo with consideration of parity invariance and when it comes to solve the eigenvalue problem, this re-ordering leads to a block diagonal matrix to diagonalize, which can then be split to several smaller matrices. This is much more efficient when it comes to solve the eigenvalue problem.

6.1.2 The Coulomb interaction

describe what we are building here and how (Analytical expression described in [49, 3, 15]).

6.1.3 The energy basis

analytical energies of the "single-states" in the Hibert space. Explain that this class simply computes the HO energies for each states of the basis set analytically. In the perspective of a more general problem with a confining potential different from the HO potential, these energies would be computed using numerical integration. That's why it is linked to a class of wave functions in their explicit form (including Laguerre polynomials for example in the case of the HO basis set).

6.1.4 The Hartree-fock algorithm

- Don't forget to mention **parity**:consider it liek one more quantum number, since ml should be conserved by the hamiltonian, if matrix organized by groups of states with identical ml, we should observe that his matrix is block diagonal, then reducing the eigenvalue problem to several (much smaller) eigenvalue problems.

- **Householder method** for tridiagonalization the Ãÿatrix and **tqli()** to diagonalise the tridiagonal matrix obtained

details the link between this class, the algorithm described in 5.3.4 and how it calls oher part of the code described previoulsy (call to the basis set, the quantum numbers of each state in the set, the "hole" states, call to the Coulomb matrix elements).

explains that this class just performs the job done in one iteration of the iterative procedure, and that it can also check if the self-consistency is achieved or not.

Explain finally that the loop over iterations is done in the "main" class. This class is really simple, just

- defining the objects one after the others: the basis set, the Coulomb matrix, the Hartree-fock equations

- performing the loop over iteration calling for functions of the Hartree-Fock class to solve the eigenvalue problem and update the effective potential

- write to log the input/output data

- compute the duration of each part of the simulation

6.2 Numerical Analysis

6.2.1 Comparison with analytical results (TAUT, Espen with B fiedl, Simen)

2-electrons QD with interactions solved anaytically by TAUT. Write a subchapter in the theoretical background on QD!!!!

6.2.2 Comparison with other numerical calculations (VMC, DFT, Large Scale diag from Simen exact for 2 electrons)

References: Rune, Simen Kvaal, ... Fidn reference for Hartree-Fock Calculation of QD too !!!!!!! IMPORTANT !!! (VMC, DFT, Large Scale diag from Simen exact for 2 electrons)

6.2.3 Study of the convergence behaviour

speed (stability) and accuracy with respect to the arbitrary size of the basis of HO wf (discussion with Simen Kvaal 05/09/2008)

vendredi 5 septembre 2008 Discussion with Simen Kvaal: Reliability of my simulator??? 1. TO CHECK IF MY SIMULATOR OBTAINS GOOD RESULTS = compare to references

* check with Morten if any analytical solution of Hartree-Fock method for QD exists?? * Checks my results with references of numerical calculations

2. TO CHECK IF THE HF CODE WORKS

* test this interaction V(r12)=const/r12, there is an analytical solution of that. * test V(r12)=const=K, then V(rij)=KâĞŠ Îč V(rij) = N (N-1) K (trivial example, maybe too trivial since it may not show some error in the HF code) * finally check V(r12)=a.r12Âš+b

3. TO CHECK IF MY SIMULATOR IS CONVERGING PROPERLY (fast enough, with a sufficiently big basis of HO wave functions) Necessaire MAIS PAS SUFFISANT !!!!!

* basis made of HO wave functions=$\Phi_{nlm}|2n+|l|R$ for 3D case * R reprensents a given energy level composed of a lot of degenerate states * calculate the probability to be at a given energy level, probability: ĬĽ(R) o at a given energy level, a given R, and the set of wf at this level is: $\Phi_{nlm}|2n+|l|=R$ o then $(R)=\sum|\Phi_{nlm}|\Psi_j|^2$ with j such that $2n+|l|=R$ o plot log[ĬĽ(R)] as a function of log[R] o should observe ecponential convergence with Hartree-Fock (as Simen has seen during his summer course in august 2008) o if you see noise ($log[(R)]=10^(-16)$), then you achieved the numerical precision of the machine o you can also plot: ÎŤE(R)=E(R)-E(RâĹđ)

6.3 Toward a more realistic model of a colloidal QD

6.3.1 Impact of some defect on the surface of the quantum dot

Some defect might obviously change the potential energy from a spherical HO potentialto something else: ???

Will this lead to a Quantum chaos = some really strange/no symmetric eigenvalues???

This could be shown by studying the distribution of $\Delta E = E_{n+1} - E_n$ and see if we get the nice decreasing exponential (eigenstate not varying much from eachother) or a pseudo-gaussian characteristic from the chaotic behaviour???

Discussion at the Weekly Journal on the 11/09/08 by Simen Kvaal.

Might consider looking at the Green's function to solve such chaotic system, or at least approximation of the Green's function.

6.3.2 Impact of the environment on the system

New model for the external field applied: will a dipole or quadrupole field be a better approximation for the IR/UV radiations?

Is the coating and the acquous environment having any effect on the potential energy? What could be a better model of the potential?

Chapter 7

Computational Results and Analysis

This simulator allows the computation of the Hartree-Fock approximation to the ground-state energy of a quantum dot, a many-body perturbation theory approximation up to third order in the harmonic oscillator basis, and a second and third order perturbation theory correction to the Hartree-Fock energy.

The accuracy and the stability of the simulator will depend on the arbitrary set of input parameters associated to the Hartree-Fock technique (size of the basis set, precision required in the self-consistent process), and also the parameters modelling the quantum dot (the number of electrons trapped into the dot, the strength of its parabolic potential, the strength of the external magnetic field). As derived in chapter 4.2 its possible to rescale and to simplify the Hamiltonian leading to the following set of simulation parameters:

The Fermi level R^f $(R^f \in \mathbb{N}\ R^f \geq 0)$ which characterizes the number of charge-carriers trapped into the dot, since our closed-shell system "fills" the shells with electrons up to the Fermi level (i.e. in the harmonic oscillator basis: $R^f = 0 \Rightarrow 2$ electrons in the dot, $R^f = 1 \Rightarrow 6$ electrons in the dot, $R^f = 2 \Rightarrow 12$ electrons, $\cdots$).

The size of the basis set characterized by R^b $(R^b \in \mathbb{N}\ R^b \geq R^f)$ which defines the maximum shell number in the model space (i.e. the shell-truncated Hilbert space) for our Hartree-Fock computation. It implies the number of single orbital in which each single particle wavefunction will be expanded. So the bigger the basis set, the more accurate the single particle wavefunction is expected. In mathematical notation, R^b and the size of the basis set $\mathcal{B}$ are defined by

$$\mathcal{B} = \mathcal{B}(R^b) = \left\{ |\phi_{nm_l}(\mathbf{r})\rangle \quad : 2n + |m_l| \leq R^b \right\} \tag{7.1}$$

where $|\phi_{nm_l}(\mathbf{r})\rangle$ are the single orbital in the Harmonic oscillator basis with quantum numbers n, m_l such that the single orbital energy reads: $\epsilon_{nm_l} = 2n + |m_l| + 1$ in two dimension.

The confinement strength λ $(\lambda \in \mathbb{R}^+)$ which characterises both the type and size of the material and also incorporate the change in confinement strength due to an external magnetic field as described in section 4.2.3.

The precision of the self-consistent Hartree-Fock process ϵ^{HF} $(\epsilon^{HF} \in \mathbb{R}^+)$ has default value set to 10^{-12} which is a good approximation with respect to the accuracy of other constants of the system (i.e. e, m_e, a_0^*, $\hbar$, $\cdots$ whose accuracy doesn't undergo 10^{-12} [62]). This arbitrary parameter may have important consequences for the convergence of Hartree-Fock when the electron interaction becomes too high if a maximum number of iterations was not set.

7.1 Validation of the simulator

The objectives of those tests is to show if some part of the code have been implemented correctly. Unfortunately those are not sufficient to assume that our simulator gives correct results. At least they help to believe it.

7.1.1 Reproducing the non-interacting ground state energy

A first simple test consists in checking if the simulator reproduces easily the exact ground state energy for a QD with non-interacting particles. It is done by switching off the interaction piece (possible by setting `includeCoulombInteractions = false` in the input parameter file), or by zeroing the confinement strength λ (also accessible from the `parameters.inp`). The expected energy is the sum over each occupied single harmonic oscillator orbital with the definite energy $\epsilon_{nm_l} = 2n + |m_l| + 1$ as derived in section ???. This test has been done and summarized in table 7.1 and correspond exactly to the ground state energy of particles trapped in a harmonic oscillator when neglecting the electron interaction.

Basis	Particles in the Quantum dot			
Size	2	6	12	20
R^b	$(R^f = 0)$	$(R^f = 1)$	$(R^f = 2)$	$(R^f = 3)$
0	2 $\hbar\omega$	10 $\hbar\omega$	28 $\hbar\omega$	60 $\hbar\omega$
1	2 $\hbar\omega$	10 $\hbar\omega$	28 $\hbar\omega$	60 $\hbar\omega$
2	2 $\hbar\omega$	10 $\hbar\omega$	28 $\hbar\omega$	60 $\hbar\omega$
$\vdots$	$\vdots$	$\vdots$	$\vdots$	$\vdots$
12	2 $\hbar\omega$	10 $\hbar\omega$	28 $\hbar\omega$	60 $\hbar\omega$

Table 7.1: Ground state energy of quantum dots with non-interacting particles.

7.1.2 Checking the two-body interaction matrix with *OpenFCI* results

Another test consists in comparing the Coulomb interaction matrix computed analytically in our simulator (the analytical expression is detailled in appendix **??**) to the numerical computation developed by S. Kvaal in his Configuration interaction simulator called "**OpenFCI**" [32].

As described in section ????, the two-body interaction $V_{\alpha\beta\gamma\delta}$ is stored as a matrix and act on two couples of single orbitals ($|\alpha\rangle$, $|\beta\rangle$), ($|\gamma\rangle$, $|\delta\rangle$):

$$\begin{aligned} V_{\alpha\beta\gamma\delta} &= \langle\alpha(r_i)\beta(r_j)|V(r_{ij})|\gamma(r_i)\delta(r_j)\rangle_{as} \\ &= \underbrace{\langle\alpha(r_i)\beta(r_j)|V(r_{ij})|\gamma(r_i)\delta(r_j)\rangle}_{\text{Direct term}} - \underbrace{\langle\alpha(r_i)\beta(r_j)|V(r_{ij})|\gamma(r_j)\delta(r_i)\rangle}_{\text{Exchange term}} \end{aligned}$$

where $V(r_{ij}) = 1/r_{ij}$ is the Coulomb interaction operator acting on particle i and j.

It is actually possible to compare the direct term of each simulator by comparing the results of the functions that generate them: `anisimovas()` in our simulator and `singleElement()` in **OpenFCI**.

```
double anisimovas (const int n1, const int m1, const int n2, const int m2,
                   const int n3, const int m3, const int n4, const int m4);

double QdotInteraction::singleElement(int N1, int m1, int N2, int m2,
                                      int N1pr, int m1pr, int N2pr, int m2pr);
```

It should be noted that the quantum numbers called in both functions do not exactly correspond. Indeed if state $|\alpha\rangle$ correspond to both states $|n_1\, m_1\rangle$ from `anisimovas()` and $|N_1\, m_1\rangle$ from `singleElement()`, the quantum number N is here defined by $N = 2n + |m|$. Therefore it is possible to call the **OpenFCI** function using the quantum numbers of our simulator by the following

```
singleElement(2*n1+abs(m1), m1, 2*n2+abs(m2), m2,
              2*n3+abs(m3), m3, 2*n4+abs(m4), m4);
```

A few outputs of the functions have been computed and listed in table 7.2. The difference between the results of the functions are on the orde of 10^{-15} or lower, showing a clear agreement. The computation of those direct terms based on numerical integrations in **OpenFCI** being much faster than using our analytical expression, a modification of the code has been made in order to build the Coulomb matrix of interactions by reading the values from file, previously obtained by running the `tabulate()` function of **OpenFCI** (see [34] for more information).

7.1.3 Comparison of HF and MBPT results with a similar numerical experiment

In a similar study of quantum dots by Waltersson [57], many-body perturbation theory (MBPT) and many-body perturbation correction to the Hartree-Fock energy are performed on an open-shell system. Whereas closed-shell and open-shell might not produce the exact same results, we try here to compare and observe our results with it. Therefore we aim at reproduce a study of the convergence of the second order perturbation correction to the Hartree-Fock energy as a function of the basis size. In his open-shell model, Waltersson represents the basis size either by $max(n)$ or $max(|m_l|)$, whereas in our closed-shell model both $max(n)$ and $max(|m_l|)$ depend on the value of the maximum shell number R^b which are here

$$max(n) = floor(R^{/}2) \tag{7.2}$$

$$max(|m_l|) = R^b \tag{7.3}$$

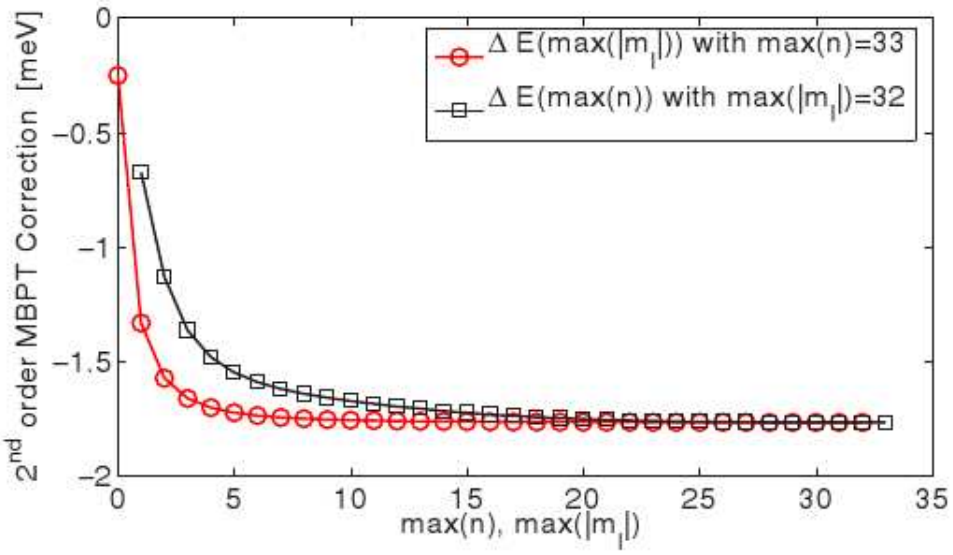

Figure 7.1: Second-order perturbation theory correction to the energy as function of $max(n)$ (squares) and $max(|m_l|)$ (circles) for the two electron dot with the confinement strength $\hbar\omega = 6\,meV$. [57]

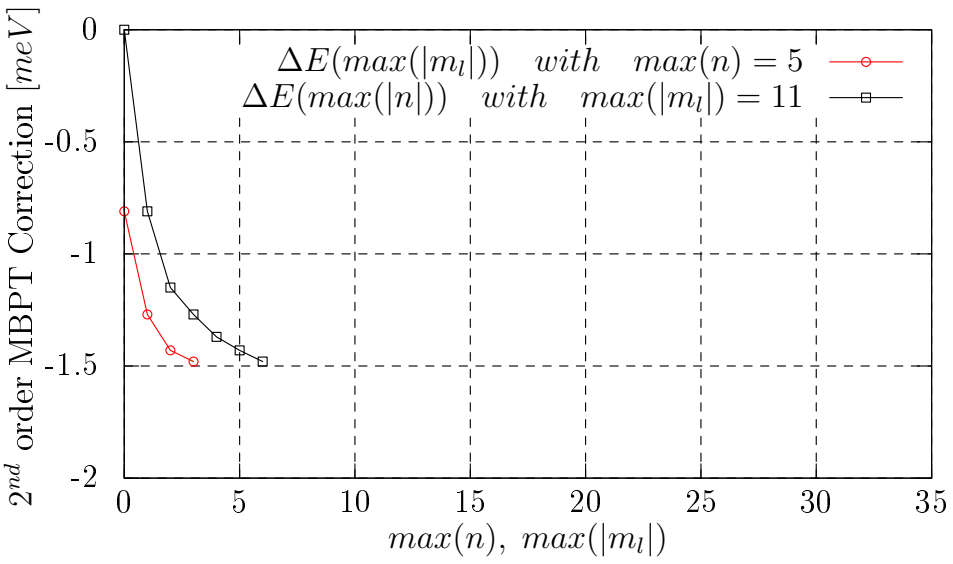

Figure 7.2: Second-order perturbation theory correction to the energy as function of $max(n)$ (squares) and $max(|m_l|)$ (circles) for the two electron dot with the confinement strength $\hbar\omega = 6\,meV$ which translates into a dimensionless confinement strength of $\lambda = 1.406$ using the same material characteristics of GaAs than Waltersson.

Quantum numbers								Direct terms		Difference
n1	m1	n2	m2	n3	m3	n4	m4	singleElement()	anisimovas()	
0	-2	0	-2	0	-2	0	-2	+0.71600465852496875	+0.716004658524967640	1.11e-15
0	-2	0	-1	0	-2	0	-1	+0.75394678572885431	+0.753946785728855317	9.99e-16
0	-2	0	-1	0	-1	0	-2	+0.30353701763109730	+0.303537017631097860	5.55e-16
0	-2	0	0	0	-2	0	0	+0.74415526903108020	+0.744155269031077759	2.44e-15
0	-2	0	0	0	-1	0	-1	+0.27694591420398728	+0.276945914203986898	3.89e-16
0	-2	0	0	0	0	0	-2	+0.11749820037332800	+0.117498200373328198	1.94e-16
0	-2	0	1	0	-2	0	1	+0.75394678572885809	+0.753946785728855317	2.78e-15
0	-2	0	1	0	-1	0	0	+0.27694591420398728	+0.276945914203986898	3.89e-16
0	-2	0	1	0	0	0	-1	+0.16616754852239221	+0.166167548522392211	0.00e+00
0	-2	0	1	0	1	0	-2	+0.14687275046666059	+0.146872750466660123	4.72e-16
0	-2	0	2	0	-2	0	2	+0.71600465852497219	+0.716004658524967640	4.55e-15
0	-2	0	2	0	-1	0	1	+0.30353701763109858	+0.303537017631097860	7.22e-16
0	-2	0	2	0	0	0	0	+0.11749820037332819	+0.117498200373328198	0.00e+00
0	-2	0	2	0	1	0	-1	+0.14687275046666051	+0.146872750466660123	3.89e-16
0	-2	0	2	0	2	0	-2	+0.12851365665832831	+0.128513656658326258	2.05e-15
0	-1	0	-2	0	-2	0	-1	+0.30353701763109730	+0.303537017631097749	4.44e-16
0	-1	0	-2	0	-1	0	-2	+0.75394678572885442	+0.753946785728855317	8.88e-16
0	-1	0	-1	0	-2	0	0	+0.27694591420398728	+0.276945914203986842	4.44e-16
0	-1	0	-1	0	-1	0	-1	+0.86165346940440823	+0.861653469404406013	2.22e-15
0	-1	0	-1	0	0	0	-2	+0.27694591420398728	+0.276945914203986898	3.89e-16
0	-1	0	0	0	-2	0	1	+0.27694591420398728	+0.276945914203986842	4.44e-16
0	-1	0	0	0	-1	0	0	+0.93998560298662536	+0.939985602986624479	8.88e-16
0	-1	0	0	0	0	0	-1	+0.31332853432887497	+0.313328534328874808	1.67e-16
0	-1	0	0	0	1	0	-2	+0.16616754852239229	+0.166167548522392211	8.33e-17
0	-1	0	1	0	-2	0	2	+0.30353701763109858	+0.303537017631097749	8.33e-16
0	-1	0	1	0	-1	0	1	+0.86165346940440690	+0.861653469404406013	8.88e-16
0	-1	0	1	0	0	0	0	+0.31332853432887491	+0.313328534328874808	1.11e-16
0	-1	0	1	0	1	0	-1	+0.23499640074665628	+0.234996400746656397	1.11e-16
0	-1	0	1	0	2	0	-2	+0.14687275046666051	+0.146872750466660123	3.89e-16
0	-1	0	2	0	-1	0	2	+0.75394678572885776	+0.753946785728855317	2.44e-15
0	-1	0	2	0	0	0	1	+0.27694591420398717	+0.276945914203986898	2.78e-16
0	-1	0	2	0	1	0	0	+0.16616754852239229	+0.166167548522392211	8.33e-17
0	-1	0	2	0	2	0	-1	+0.14687275046666059	+0.146872750466660123	4.72e-16

Table 7.2: Comparison of a few Direct terms $\langle n_1\, m_1, n_2\, m_2|V(r_{ij})|n_3\, m_3, n_4\, m_4\rangle$ computed either using numerical integration within **OpenFCI** (`singleElement()`), or computed from an analytical expression within our simulator (`anisimovas()`).

The convergence of the second order many-body perturbation correction as a function of the basis size by Waltersson is given in figure 7.1 while our reproduction of the experiment is given in figure 7.2. Those two figures look similar in shape and values. However the results from Waltersson are slightly shifted to lower values which could represent a better correction to the positive Hartree-Fock energy, and this shift probably results from the different shell models.

7.2 Restrictions to the closed-shell model

7.2.1 Limits of the model through a theoretical approximation

In this section we would like to show the theoretical limit of our closed-shell model within a magnetic field. This is supposed to provide a theoretical upper bound to the external magnetic field, above which the electronic structure is not anymore correctly reprensented by the particles filling all the shells up to the Fermi level, but possibly by a new structure where the total spin or total angular momentum might differ

from zero.

When neglecting the repulsions between the particles, the eigenenergies $\epsilon_{n\,m_l}$ as a function of the magnetic field B can be solved analytically for a parabolic confining potential $V(r) = 1/(2m^*\omega_0^2 r^2)$ leading to a spectrum known as the Fock-Darwin states [13, 31]

$$\epsilon_{n\,m_l} = (2n + |m_l| + 1)\,\hbar\omega - \frac{1}{2}\hbar\omega_c\, m_l \tag{7.4}$$

$$= (2n + |m_l| + 1)\,\hbar\omega_0\sqrt{1 + \frac{\omega_c^2}{4\omega_0^2}} - \frac{1}{2}\hbar\omega_c\, m_l \tag{7.5}$$

where $\hbar\omega_0$ is the electrostatic confinement strength, and $\omega_c = e\,B/m^*$ is the cyclotron frequency. Each state $|n, m_l\rangle$ is spin-degenerate.

Rewriting the eigenenergies in unit of $\hbar\omega_0$, $\epsilon_{n\,m_l}$ become dimensionless and we obtain

$$\epsilon_{n\,m_l} = (2n + |m_l| + 1)\sqrt{1 + \frac{(\omega_c/\omega_0)^2}{4}} - \frac{1}{2}(\omega_c/\omega_0)\, m_l \tag{7.6}$$

$$= (2n + |m_l| + 1)\sqrt{1 + (\frac{eB}{2m^*\omega_0})^2} - \frac{eB}{2m^*\omega_0}\, m_l \tag{7.7}$$

Those eigenenergies are plotted in figure 7.3 as a function of the magnetic field. The orbital degeneracies at $B = 0$ are lifted in a magnetic field. As B increases, a single-particle state with a positive or negative angular momentum (m_l) shifts to lower or higher energy respectively. The lowest energy state $|n, m_l\rangle = |0, 0\rangle$ is a two-fold spin degenerate (The Zeeman spin-splitting in a magnetic field is neglected). The next state has a double orbital degeneracy, $\epsilon_{0,1} = \epsilon_{0,-1}$. This degeneracy forms the second shell, which can contain up to four electrons when we include the two-fold spin degeneracy. It will be filled for $N = 6$. The third shell has a triple-orbital degeneracy formed by $|1, 0\rangle$, $|0, 2\rangle$ and $|0, -2\rangle$ so that it can hold up to six electrons. This shell leads to the magic number $N = 12$.

When the magnetic field is increased, the electron occupying the highest energy state is forced into different orbitals states. As an example, consider a seven non-interacting electrons system. The transitions for the state of the 7^{th} electron is indicated in figure 7.3 by a thicker line. At low B, the highest occupied state is $|0, 2\rangle$, which decreases in energy with B. At some point it crosses the increasing energy state $|0, -1\rangle$. With a slightly higher magnetic field, $|0, 2\rangle$ has now a lower energy than $|0, -1\rangle$. This forces the electrons to switch states and it ends up with two electrons in state $|0, 2\rangle$ and only one in state $|0, -1\rangle$. For $\hbar\omega_0 = 3meV$ this occurs at $B \simeq 2.1\,T$. The seventh electron makes a second transition into the state $|0, 3\rangle$ at $2\,T$. Similar transitions are also seen for different numbers of particles and with an increasing number of crossings for larger systems. After the last crossing the electrons occupy states forming the so-called, lowest orbital Landau level. These states are characterized by the quantum numbers $(0, m_l)$ with $m_l \geq 0$.

Considering such transitions, we see that increasing the magnetic field will change the shell structure of our system and we may wonder what happen to the closed-shell

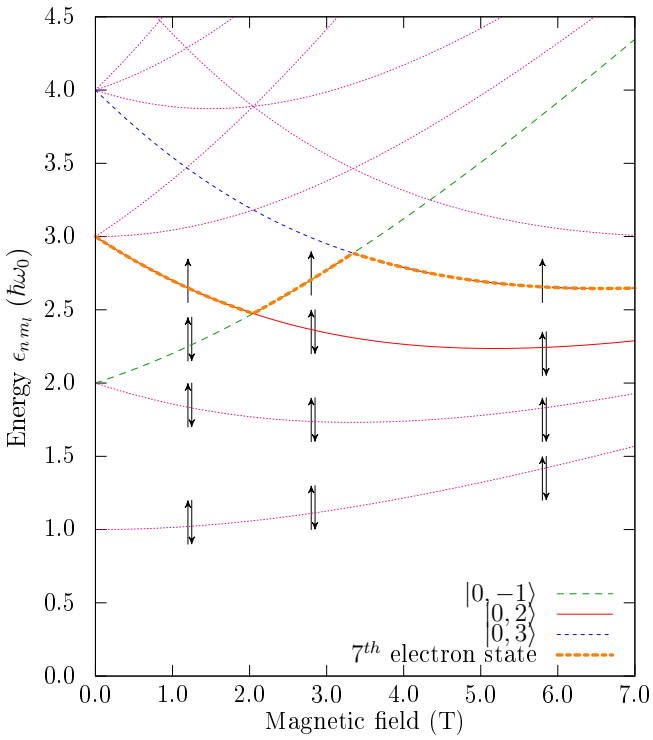

Figure 7.3: Spectrum of Fock-Darwin orbitals for a system of seven non-interacting particles with typical values for GaAs: confinement energy $\hbar\omega_0 = 5meV$, relative permittivity $\epsilon_r = 12$, effective mass $m^* = 0.067m_e$.

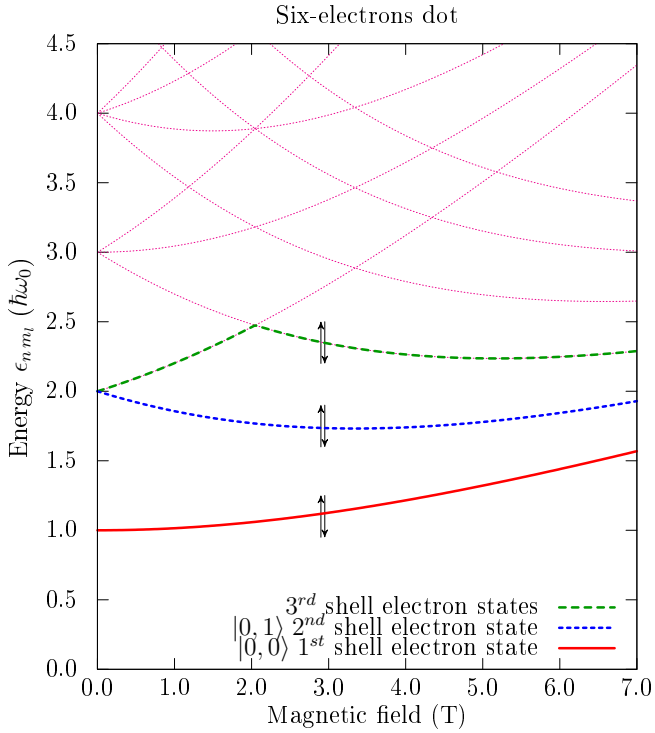

Figure 7.4: Spectrum of Fock-Darwin orbitals for a system with six non-interacting particles and using typical values for GaAs: confinement energy $\hbar\omega_0 = 5meV$, relative permittivity $\epsilon_r = 12$.

model. The closed shell system is described by a single Slater determinant. Therefore any new configuration implying the occupation of a state with an energy higher than the Fermi level would break it. Since our simulator is based on a single Slater determinant, our shell structure is initialized and kept with particles occupying the lowest states identical to those with a zero magnetic field. Therefore any transition from an occupied state to an "excited" state (non-occupied state when B was low or null) will mark the end of the model. In this case the total angular momentum M or total spin S may change from zero to a positive value, the single particle energies associated to the new occupied states will switch to a higher value, and our complete computation of the ground state with constant non-interacting eigenenergies, zero total angular momentum and zero total spin fails.

Figures 7.4 and 7.5 display with thick lines the different transitions of states when the magnetic field is increased respectively for a six- and twelve-particle quantum dot. For the six-particle dot we see for example that the two electrons in the 3^{rd} shell (figure (7.4)) are in the state $|0,-1\rangle$ without magnetic field, but switch to the state $|0,3\rangle$ when the magnetic field exceed $2.1\,T$, whereas electrons in the first and second shell stay respectively in the states $|0,0\rangle$ and$|0,1\rangle$, even under a high magnetic field.

Therefore a theoretical study of the Fock-Darwin orbitals may predict that our model should be restricted to a maximum B field of $2.1\,T$ for a six-particle dot, and $1.2\,T$ for a twelve-particle dot. In order to compare those values of the magnetic field to the inversely proportional (dimensionless) parameter λ, according to section 4.2.3

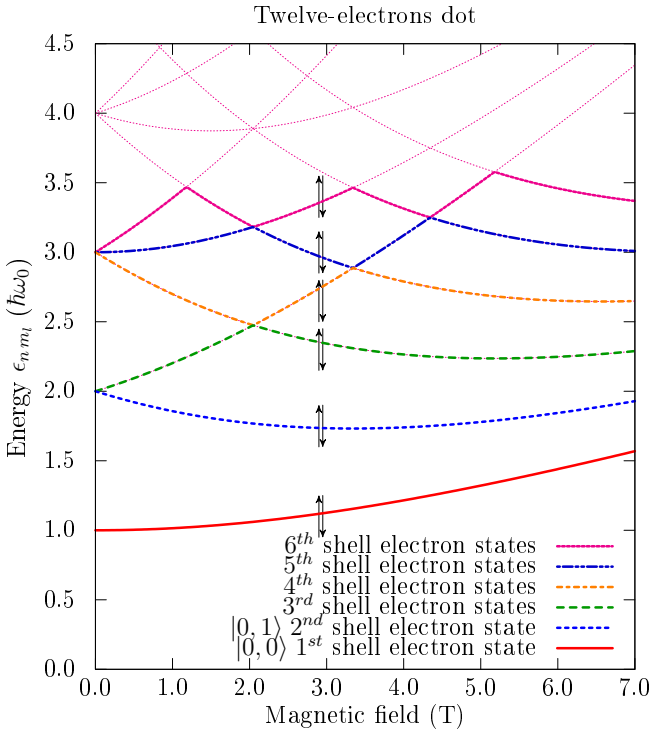

Figure 7.5: Spectrum of Fock-Darwin orbitals for a system with twelve non-interacting particles and using typical values for GaAs: confinement energy $\hbar\omega_0 = 5meV$, relative permittivity $\epsilon_r = 12$.

the confinement strength is related to B by the following expression

$$\lambda(B) = \frac{1}{a_0^*}\left(\frac{4\hbar^2}{4\omega_0^2 m^* + e^2 B}\right)^{1/4} \tag{7.8}$$

Considering GaAs material (with typical values $\hbar\omega_0 = 5meV$, $m^* = 0.067m_e$ and $\epsilon_r = 12 \;\Rightarrow\; a_0^* = 9.47 \times 10^{-9}m$), this gives $\lambda \geq 1.543$ for a six-particle dot, and $\lambda \geq 1.575$ for a twelve-particle dot, and no lower bound for λ (i.e. no upper bound for B) in the case of a two-particle dot as summarized in table 7.3. For information, note

Nb. of electrons	Maximum B field	Minimum confinement strenght λ
2	∞	0
6	2.1 T	1.543
12	1.2 T	1.575
20	0.85 T	1.583

Table 7.3: Restriction on λ and B for a valid closed-shell model

that a refrigirator magnet has a magnetic field of about 5 mT, magnetic resonance imaging (MRI) field strengths ranges from 1.5 T to 3 T, while a NMR spectrometer works with a field strength of 11.7 T. Higher strength can be achieved: for example

16 T are necessary to levitate a frog and the strongest continuous magnetic field yet produced in a laboratory is about 45 T [61]. This gives a rough idea of the domain of application of the closed shell model for the simulation of laboratory experiments.

However this theoretical study should not be taken with too much care since it does not take into account the repulsion between the electrons, which will change the shell structure and obivously the limitations on B and λ we previously mentionned. As derived in section 4.2.3 we saw that the characteristic length l decreases with an increase of the magnetic field, indicating that the confinement becomes stronger for larger B. This is also observed as a shrinking of the wavefunctions [28]. The effect is that when B is increased, two electrons occupying the same state will be pushed closer together. The decreasing distance between the electrons will increase the Coulomb interactions which may change the electron configuration which results in a break of the closed-shell model and evetually may prevent our Hartree-Fock technique to converge. Numerical calculations which include the electron interactions are then necessary to build an accurate shell structure as a function of the magnetic field. This is done in the next section using full configuration interaction.

7.2.2 Limits of the closed-shell model better approximated with full configuration interaction

To check the reliability of the closed-shell model, it is a rough approximation to neglect the Coulomb interaction as we did through the study of the Fock-Darwin orbitals. With a two-electrons quantum dot, it is likely that the ground state remains characterized by the two electrons lying in the first shell $(n, m_l) = (0, 0)$ when increasing the magnetic field up to the maximum values achievable in laboratory.

For 6 electrons, the closed shell model with the six electrons occupying the first levels $(n, m_l) = \{(0, 0), (0, 1), (0, -1)\}$ might not always be the optimal electron configuration as a function of the magnetic field. This is what we tried to show by using the **OpenFCI** (full configuration interaction) simulator and running it for different electron configurations. Taking as minimum input parameters: the number of particles N, the total angular momentum M, the total spin S and the confinement strength λ, this simulator computes the first minimum eigenenergies (the lowest one being the ground state energy of the system) using large scale diagonalisation.

Figures 7.6 and 7.7 resume the ground state energies of a six-particle quantum dot for various combinations of M and S, each plot corresponding to different confinement strength $\lambda = \{0.1, 0.5, 1, 2\}$ in figure 7.6 and $\lambda = \{5, 10, 20, 50\}$ in figure 7.7 respectively from top to bottom. Despite the trend of the ground state energy as a function of M and S, it might not be easy to observe which combination gives the lowest energy. Tables 7.4 and 7.5 list the energies corresponding to each combination and the lowest energy for each value of the confinement strength λ is highlighted in bold face.

The tables clearly show that the closed-shell model looks valid for a confinement strength in the range $\lambda = 0.1 \rightarrow 10$. These values can be either translated into a possible range of the applied external magnetic field, or into the size of the quantum dot itself, or even into a combination of both the Qdot size and the magnetic

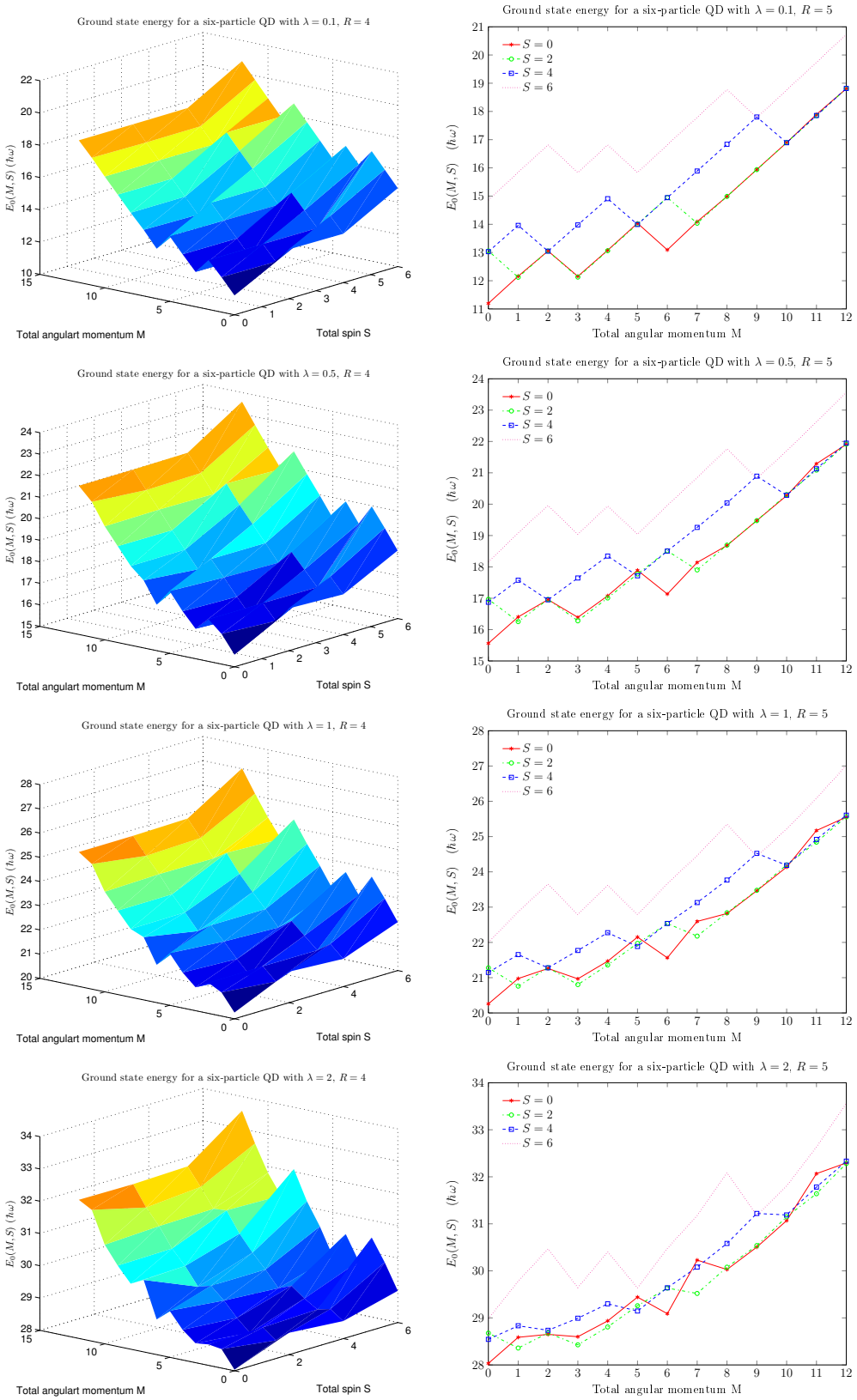

Figure 7.6: Ground state energies for a six-particle QD computed using **OpenFCI** as a function of the total spin S ans total angular momentum M. Each plot corresponds to a given value of the confinement strength $\lambda = 0.1$, 0.5, 1 and 2. One can observe that the lowest energy is not always obtained for $(M, S) = (0, 0)$ as the confinement strength increases.

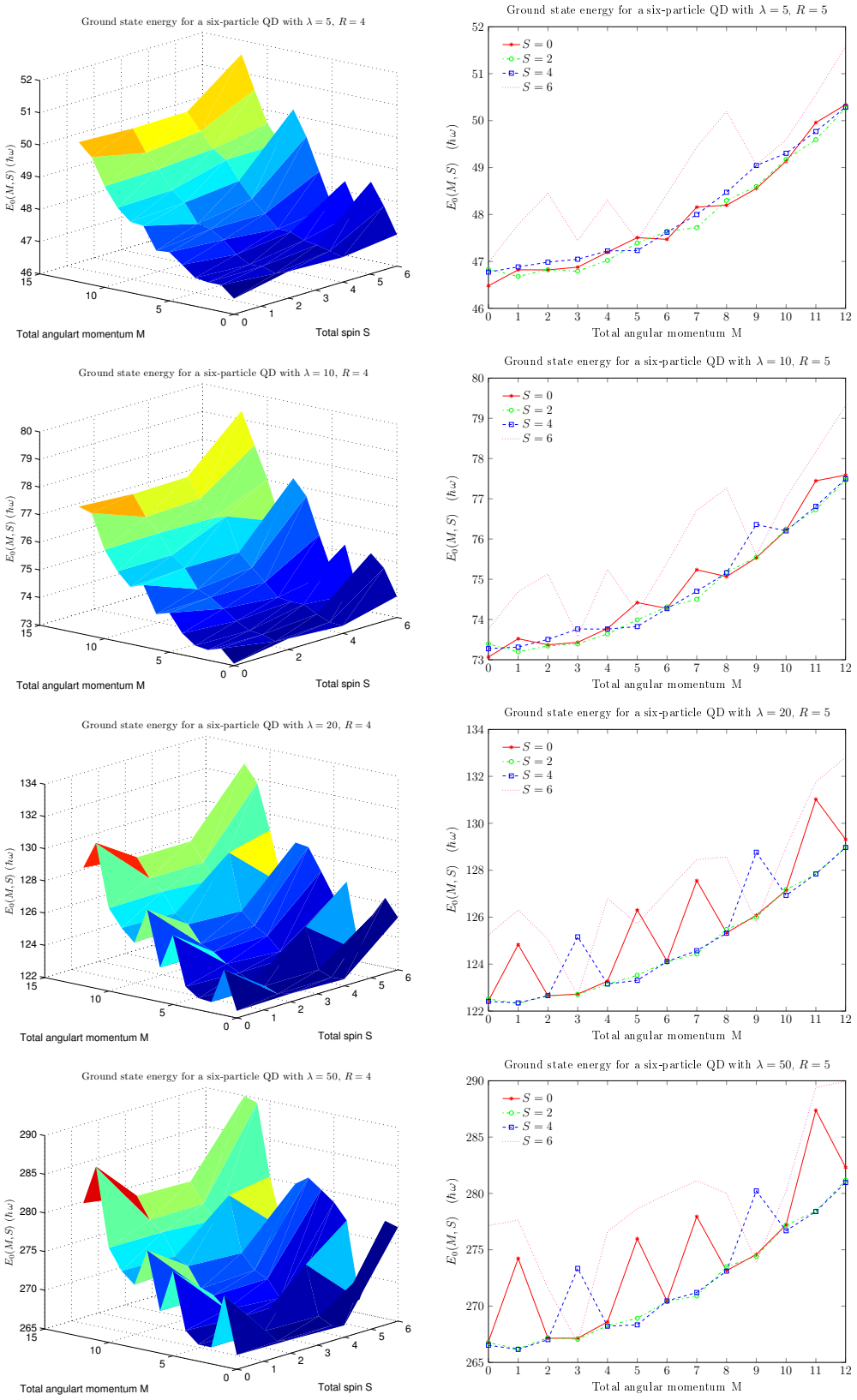

Figure 7.7: Ground state energies for a six-particle QD computed using **OpenFCI** as a function of the total spin S ans total angular momentum M. Each plot corresponds to a given value of the confinement strength $\lambda = 5$, 10, 20 and 50. One can observe that the lowest energy is not always obtained for $(M, S) = (0, 0)$ as the confinement strength increases.

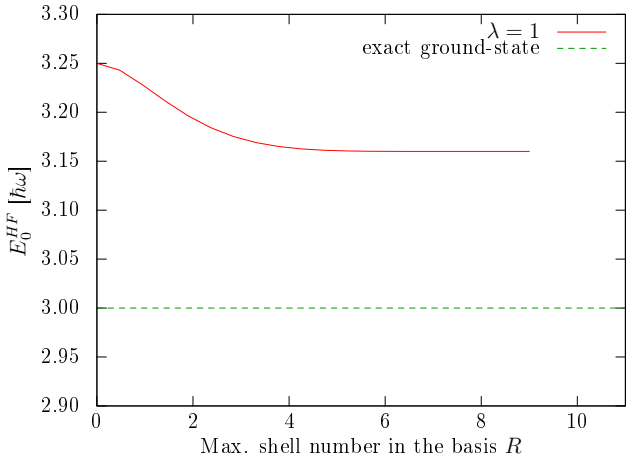

Figure 7.8: Hartree-Fock approximation to the ground state energy of a two-particle quantum dot, with a confinement strength $\lambda = 1$

field. These results obviously predominate the ones obtained in section 7.2.1 which neglected the electron interactions.

7.3 Convergence, stability and accuracy of the Hartree-Fock Algorithm

7.3.1 Importance of the model space

Hartree-Fock approximation to the ground state energies E_0^{HF} as a function of the size of the basis set R^b, for 3 differentes values of the confinement strenght $\lambda = 0.5, 1$ or 2.

Figure (7.8) presents the results of the simulator, providing the Hartree-Fock approximation to the ground state energy of a two-particle quantum dot where the charge carriers are confined with a dimensionless confinement strength $\lambda = 1$. In two-dimension, the exact ground state energy of such a system is known to be equal to $E_0 = 3$ in units of $\hbar\omega$ as shown in chapter 4. Therefore we see easily that Hartree-Fock provides a rough approximation to the exact energy with a difference of 5.33%.

Figure (7.9) presents the convergence plots (left plots) of the Hartree-Fock approximation to the ground state energy of different quantum dot size (2, 6, 12 and 20-particles QD) as a function of the maximum shell number in the basis set (R^b) and for different values of the confinement strength λ. Its shows that Hartree-Fock converges to its best approximation with a basis set of a few shells above the Fermi level. With the case of a 2-electron quantum dot (top of figure (7.9)), we see that Hartree-Fock has achieved its convergence limit with a basis set up to the 4^{th} shell. For a 6-particles QD, the limit seems to be achieved from the 5^{th} shell and from the 7^{th} shell for a 12-particles QD.

When increasing the size of the quantum dot one shell at a time, the convergence limit $E^{HF}(R^b_{max})$ doesn't seem to be achieved with a linear increase in the size of

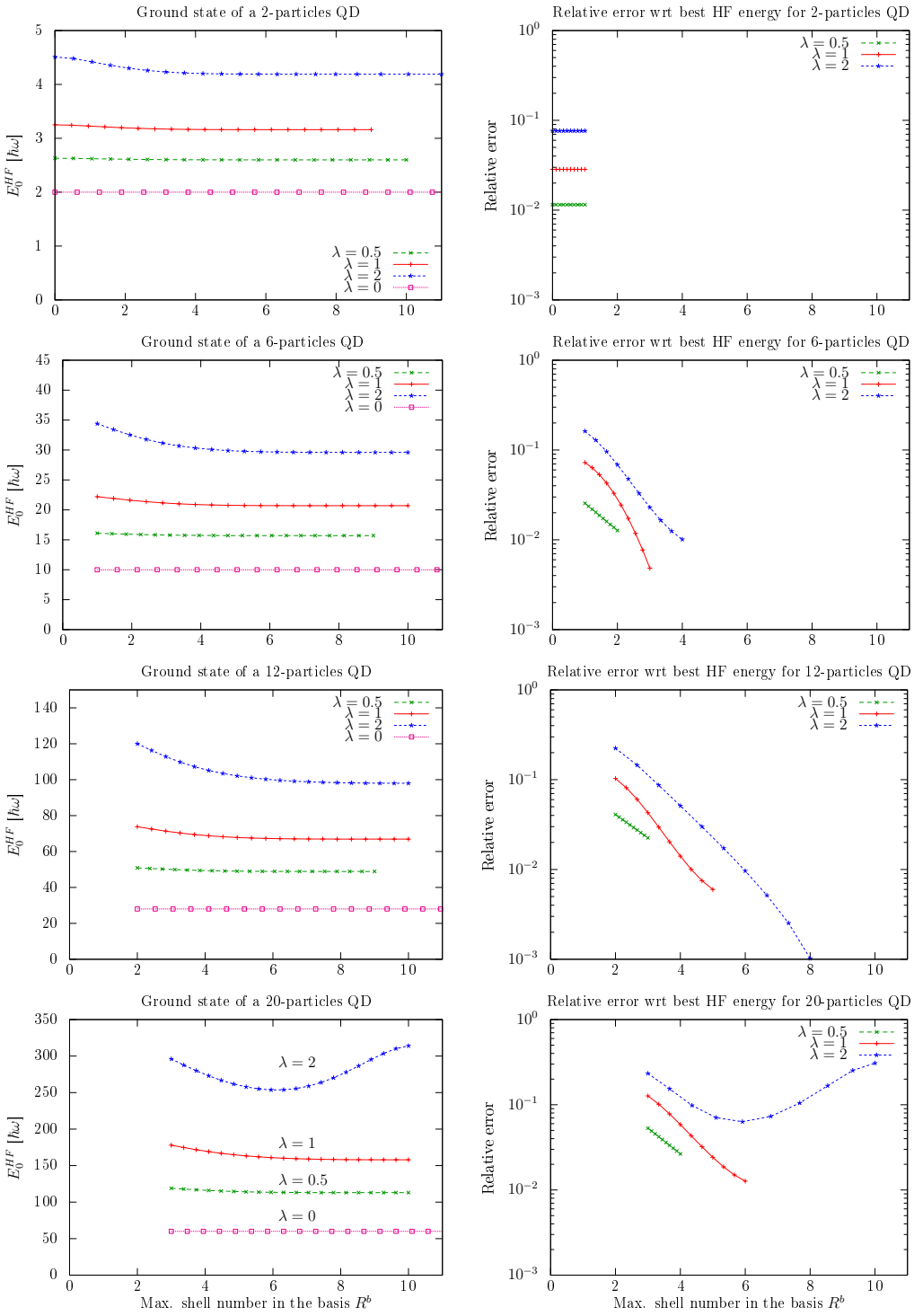

Figure 7.9: (Left) Hartree-Fock approximation to the ground state energy of quantum dots with 2, 6, 12 and 20 trapped particles as a function of the size of the basis set, and for different values of the confinement strength $\lambda = 0, 0.5, 1$ or 2. As the number of particles in the dot increases, the minimum model space includes all the shells occupied by particles. This explains for example why for 20 particles, the first energies are obtained only from $R^b = 3$.
(Right) Hartree-Fock relative error $(E^{HF}(R^b) - E^{HF}_{min})/E^{HF}_{min}$ as a function of the size of the basis set for the same quantum dots. Exponential dependence in R^b can be observed in the cases where the relative error is not exactly zero.

the basis set. Then another interesting plot should show how the Hartree-Fock limit is scaled with the size of the basis set. This is displayed on right plots of figure (7.9)), where the relative error $\left(E^{HF}(R^b) - E^{HF}_{min}\right)/E^{HF}_{min}$ is given as a function of the maximum shell number in the basis set (R^b). The plots display amost linear curves, implying an quasi exponential dependence in R^b.

We also remark in the case of the 20-particles QD (bottom of figure (**??**)) that Hartree-Fock stops improving its limit when increasing the basis set in the case of the "high" confinement strength $\lambda = 2$. This is our first observation of Hartree-Fock breaking for a high number of particles within a strong confinement strength (i.e. for a GaAs QD, $\lambda = 2$ would correspond to $\hbar\omega_0 =$).

7.3.2 Importance of the (confinement) interaction strength

We discussed the ranges of the confinement strength λ that would make sense physically through a theoretical approximation of a dot with non-interacting particles in section 7.2.1. However we saw that this study was an approximation since neglecting any electron-electron interactions, but also on a computational point of view, it is interesting to study the convergence of the Hartree-Fock algorithm for a wider range of λ.

Here we study how fast the iteration process of hartree-Fock is converging. To do so we look at the "convergence history" of a simulation, meaning that we look at the improvement in energy over iterations. This could be done by plotting the relative energy difference expressed by

$$\delta(iter) = \frac{|E^{HF}(iter) - E^{HF}(\infty)|}{E^{HF}(\infty)}$$

But since the self-consistency in our simulator is decided upon the convergence of the eigenenergies and not upon the total energy, it seems more natural to plot the following relative energy difference

$$\delta(iter) = \frac{\sum_{n\,m_l} |\epsilon_{n\,m_l}(iter) - \epsilon_{n\,m_l}(\infty)|}{\sum_{n\,m_l} \epsilon_{n\,m_l}(\infty)}$$

where $\epsilon_{n\,m_l}$ is the eigenenergy of the system of the single orbital $|n\,m_l\rangle$.

For a higher resolution than the machine resolution (e.g. $\epsilon = \times 10^{-17}$), we know that the simulator will never converge and then be stopped at the maximum number of iterations (here fixed to 1000). The interesting point is to observe how fast Hartree-Fock converges over the iterations. So the relative energy difference over iterations is plotted in figure **??**.

HERE INTRODUCE AND PLOT $\delta(iter)$ as a function of iter.

Another way to look at this "convergence history", maybe more intuitive, would be to write:

$$\delta(iter) \simeq 10^{-\beta\, iter}$$

where β is a constant depending on the parameters (R^b, R^f and λ). In this case we can interpret the plot saying that, at this iteration, you improve the precision on the relative energy difference with β digits compared to the previous iteration.

show how λ can affect the iterative process/procedure and how it changes the accuracy of the problem ($\simeq$ decreasing the machine precision), making the choice of the "precision" parameter important in order to get convergence of HF.

7.4 Comparison: Hartree-Fock, Perturbation theory, VMC, FCI

shows breaking of perturbation theory much before Hartree-Fock when increasing the confinement strength.

shows breaking of HF compared to VMC and FCI as λ increases.

table of accuracy between the *ab-initio* methods for different values of λ. When $\lambda = 1$, can also compare to exact solution for two particles.

table with duration/complexity/model size achievable (nb.electrons) of the simulations for VMC/HF/PT/FCI and produce Spider chart to visually compare the methods.

λ	M	Energy in unit of $\hbar\omega$ of a six-particle dot obtained for each combination of (M,S and λ)						
		$S=0$	$S=1$	$S=2$	$S=3$	$S=4$	$S=5$	$S=6$
	0	**11.1978891344**	–	13.0565458509	–	13.0306198232	–	14.8617426362
	1	12.161788636	–	12.1228998086	–	13.9619523669	–	15.8438291847
	2	13.0541409412	–	13.0543696462	–	13.0479092548	–	16.8150801525
	3	12.1565732709	–	12.1286041835	–	13.9783634734	–	15.8336957766
	4	13.0808492317	–	13.0642360558	–	14.9084543531	–	16.8102750026
	5	14.0377732477	–	14.0097760564	–	13.9937294856	–	15.8342807494
0.1	6	13.0936355988	–	14.9480199174	–	14.944795351	–	16.8159076585
	7	14.0939135823	–	14.0386678117	–	15.8883056992	–	17.7896003155
	8	14.9868752972	–	14.9897402773	–	16.8362996072	–	18.7685556996
	9	15.941652286	–	15.9381674099	–	17.8024364205	–	17.7820000116
	10	16.8929103322	–	16.8993329996	–	16.8911751901	–	18.7560481367
	11	17.8934864395	–	17.8470437348	–	17.8557578353	–	19.7384254286
	12	18.8059869671	–	18.8084023637	–	18.8153875945	–	20.7254199174
	0	**15.5617751019**	–	16.966166432	–	16.871772355	–	18.1622424979
	1	16.4044292865	–	16.2537138896	–	17.5752283136	–	19.0834975974
	2	16.9555562338	–	16.9636785505	–	16.9488349783	–	19.9589980355
	3	16.3909605917	–	16.279069572	–	17.6459810924	–	19.0380846039
	4	17.077692629	–	17.0081494281	–	18.345626646	–	19.9390056216
	5	17.8923198765	–	17.7746900892	–	17.7147205056	–	19.0403232195
0.5	6	17.1345648299	–	18.5115121013	–	18.5052825396	–	19.9636653826
	7	18.1412125077	–	17.9027034622	–	19.2596187485	–	20.8466577601
	8	18.6823740646	–	18.6940902667	–	20.0384606413	–	21.765094962
	9	19.4781018652	–	19.4754973684	–	20.8935077402	–	20.8207439572
	10	20.272873974	–	20.3068987984	–	20.2841911217	–	21.6997487647
	11	21.2895239718	–	21.0858286183	–	21.1290221438	–	22.623042277
	12	21.9075379553	–	21.9160281905	–	21.9475742808	–	23.5741455919
	0	**20.2571791113**	–	21.2789981289	–	21.1483419586	–	22.0022205941
	1	20.9749296631	–	20.7598331889	–	21.6538800561	–	22.8661695662
	2	21.2599579854	–	21.2821095699	–	21.2792687299	–	23.6550135103
	3	20.9671026881	–	20.8035334518	–	21.7707471281	–	22.7866733195
	4	21.4667705078	–	21.359594087	–	22.2749375665	–	23.6214565309
	5	22.150155073	–	21.9721573278	–	21.884399932	–	22.7881516577
1	6	21.5630576706	–	22.5351676942	–	22.5364737402	–	23.663506028
	7	22.5942511253	–	22.1780128424	–	23.1282803854	–	24.4604431194
	8	22.8188269396	–	22.8406352537	–	23.7672441229	–	25.3487993204
	9	23.4647807574	–	23.4774102878	–	24.5237438226	–	24.437111507
	10	24.1348663101	–	24.1974193667	–	24.1850198476	–	25.2140293553
	11	25.1712359394	–	24.8418490148	–	24.9187878288	–	26.0851798722
	12	25.5513885819	–	25.5581213564	–	25.6071999655	–	27.0164861198
	0	**28.0329550231**	–	28.6765243777	–	28.5433569395	–	28.9829490384
	1	28.5875104818	–	28.3590590553	–	28.8329004272	–	29.7800781342
	2	28.6493239207	–	28.6775309794	–	28.7364010594	–	30.4662810353
	3	28.5996827157	–	28.4274289424	–	28.9932495629	–	29.644371783
	4	28.9358749584	–	28.8071713271	–	29.2994140078	–	30.4045371792
	5	29.4418369302	–	29.2587757025	–	29.1463913256	–	29.6368235281
2	6	29.0891272881	–	29.6336201736	–	29.6403711077	–	30.4767147494
	7	30.2288380451	–	29.5200135448	–	30.0805742171	–	31.1766133172
	8	30.0290919414	–	30.0780756092	–	30.5833574696	–	32.0854456593
	9	30.5051303098	–	30.5382881767	–	31.2206550065	–	31.1827194217
	10	31.0686354739	–	31.149558625	–	31.1891682104	–	31.804014365
	11	32.0668783868	–	31.6399906569	–	31.7814747312	–	32.6329816775
	12	32.2950020122	–	32.2812570977	–	32.3335540202	–	33.5602013595

Table 7.4: Ground state energies in units of $\hbar\omega$ obtained with **OpenFCI** which implements the full configuration interaction method (with the maximum shell number $R = 5$). The ground state energy for each value of the confinement strength $\lambda = \{0.1, 0.5, 1, 2\}$ is highlighted in bold face, showing the lowest energy configuration with respect to the total angular momentum M and total spin S.

λ	M	Energy in unit of $\hbar\omega$ of a six-particle dot obtained for each combination of (M,S and λ)						
		$S=0$	$S=1$	$S=2$	$S=3$	$S=4$	$S=5$	$S=6$
5	0	**46.4816466894**	–	46.8289419415	–	46.7729495876	–	46.9796295496
	1	46.821461584	–	46.6822362309	–	46.8843337823	–	47.7848726408
	2	46.8201453068	–	46.8249059264	–	46.9848775309	–	48.4486722898
	3	46.8779563634	–	46.7912636224	–	47.0478259205	–	47.4454818065
	4	47.1987202116	–	47.0226098251	–	47.2249177042	–	48.3011580081
	5	47.5068819564	–	47.3915579062	–	47.2320124154	–	47.4490465265
	6	47.4707134722	–	47.6406084941	–	47.6225860534	–	48.4409476451
	7	48.1568096159	–	47.7204807904	–	47.9994772522	–	49.4379811615
	8	48.1984357789	–	48.2999644817	–	48.4746160616	–	50.1957421823
	9	48.5541561686	–	48.59619815	–	49.0445852679	–	49.0600386679
	10	49.1359494783	–	49.1738310071	–	49.3040250889	–	49.5922406417
	11	49.9574758125	–	49.5945573352	–	49.7675922721	–	50.5562628698
	12	50.3406681585	–	50.2685117969	–	50.2883288438	–	51.5769349731
10	0	**73.0673544574**	–	73.3937354921	–	73.2756230049	–	73.7604409912
	1	73.5223189729	–	73.1969130995	–	73.314432723	–	74.6926730698
	2	73.369959718	–	73.3430190975	–	73.505676967	–	75.1294284718
	3	73.4328685759	–	73.3935786445	–	73.7640234958	–	73.5827509737
	4	73.7779468448	–	73.6422706745	–	73.7622908159	–	75.2480804704
	5	74.4201391726	–	73.9923135684	–	73.8249480462	–	74.1676534336
	6	74.275657278	–	74.3145190656	–	74.2719444082	–	75.4031376911
	7	75.2365149728	–	74.5014772184	–	74.7022012351	–	76.7150715151
	8	75.065712931	–	75.1754875658	–	75.1587445552	–	77.2589383227
	9	75.5338734086	–	75.5425839372	–	76.3604025086	–	75.5927771225
	10	76.2182975427	–	76.2458499788	–	76.2016020677	–	77.0332670376
	11	77.446936995	–	76.7277275927	–	76.8120478435	–	78.1695584306
	12	77.5889257943	–	77.4613580659	–	77.4947139477	–	79.31688644
20	0	122.433260001	–	122.513927462	–	122.412603516	–	125.245351666
	1	124.83102857	–	**122.325695478**	–	122.349574793	–	126.305882321
	2	122.651699164	–	122.652094474	–	122.656796984	–	125.06124293
	3	122.724689893	–	122.704445685	–	125.162233987	–	122.655970732
	4	123.274569702	–	123.144311312	–	123.155865954	–	126.791966535
	5	126.304835917	–	123.524537031	–	123.307211571	–	125.717615043
	6	124.131186017	–	124.096504504	–	124.112622923	–	127.11380913
	7	127.556372534	–	124.437366492	–	124.571606214	–	128.454779116
	8	125.334635172	–	125.480351924	–	125.316900883	–	128.563403526
	9	126.083358337	–	126.001938857	–	128.767780557	–	125.791509155
	10	127.141726105	–	127.175867638	–	126.930157706	–	128.98634957
	11	131.023783431	–	127.831188112	–	127.842559193	–	131.765377421
	12	129.313935266	–	128.962957408	–	128.970840663	–	132.806412758
50	0	266.841126092	–	266.750910329	–	266.526734173	–	277.147035697
	1	274.228755187	–	266.208423455	–	**266.157018073**	–	277.62841964
	2	267.147031866	–	267.194265882	–	267.023748867	–	271.5724201
	3	267.147365528	–	267.057824922	–	273.347485885	–	266.753856556
	4	268.599530467	–	268.252383419	–	268.218253995	–	276.629703425
	5	275.976226157	–	268.916913575	–	268.334355515	–	278.64440077
	6	270.45288965	–	270.396270638	–	270.458488948	–	279.926665828
	7	277.94909902	–	270.902043113	–	271.210761746	–	281.122638855
	8	273.150436294	–	273.492671773	–	273.101699304	–	280.003137843
	9	274.583720663	–	274.417711384	–	280.223263543	–	273.854144798
	10	277.220770836	–	277.175271179	–	276.687664537	–	280.205053778
	11	287.375386311	–	278.435414894	–	278.391012402	–	289.407892825
	12	282.30352042	–	281.17733536	–	280.970785713	–	289.947408632

Table 7.5: Ground state energies in units of $\hbar\omega$ obtained with **OpenFCI** which implements the full configuration interaction method (with the maximum shell number $R = 5$). The ground state energy for each value of the confinement strength $\lambda = \{5, 10, 20, 50\}$ is highlighted in bold face, showing the lowest energy configuration with respect to the total angular momentum M and total spin S.

Chapter 8

Conclusion

[critical discussion should lead to reflections, and reflections should lead to perspectives]

8.0.1 Findings + critical discussion of the results

Summary of subject, methods, results Be critical !!!!

- Explain what is more restrictive in this Hartree-Fock simulation: the break of the closed-shell model (obtained thanks to OpenFCI) or the limit of convergence of Hartree-Fock as the number of electron, *lambda*, the size of the basis increases.
- what are the limitations of HF according to the strength of the confinement wrt other methods? Compare all methods to some theoretical/reference results.
  - accuracy wrt other methods for different the size of the system?
  - simulation duration (compare the limits of each method for a given system, and compare the size of the biggest system achievable by each method-> other method like **DFT** might be of interest to study huge system in a reasonnable amount of time)?
  - Are HF results accurate enough for the confinement (B field) in use today in laboratories for confining electrons in a quantum dot?
- what are the improvements when using the HF basis set as input of VMC or CI? Does it really help (accuracy and duration improvements)?
- I did it both in 2D and 3D (Waltersson 2007 [[57]] just in 2D), but not easy to compare since he didnt' include results for closed shell systems

8.0.2 Perspectives for future works

- Open Shell HF, to be able to increase the limit of the simulator to higher B field. An set an option to find the most probable occupied state, for example to see if a 6-electrons dot use the first and second shell, or the first, and third shell when the magnetic field increases, even if the total M and total S are zero.

- Rontani p.85 wrote a paper on the range of validity of different theoretical scheme and show a strong **impact of the dimensionality** of the QD. Shows that 3D scheme are more adequate to describe real QD. [could lead to a study VMC from Rune, my Hf, CI from Espen to see how dimensionality affect the results for the different methods]

- not done in 3D yet since the Coulomb matrix expression was based on an analytical formula in 2D only, could improve it by doing numerical computation of the Coulomb Matrix elements and that will also allow to generalize to other confining potential than just the HO potential, maybe closer to more realistic systems (ex.: how to simulate the environment when we want to model colloidal QD)

- How the complexity increases with the size of the system (= with the nb. of electrons)? = DIMENSIONALITY (binomial M N en bas, avec M nb of state possible, N the nb. of particle) Cf: ComphPhys course + Simen ("curse of Dimensionality")

- HOW fast HF converges wrt other ab initio methods? It is possible to explicitely give the convergence rate?

- in order to make some visualization of the QD, plot density probability, BUT, since HF is based on effective potential, sphericcaly symm., we are not able to see much (I though I could see the point like electron by fixing one), but it might be possible to see some quantum effect if some regions are prohibited (we might see some rings)

Appendix A

Appendix

A.1 The Quantum Mechanical Harmonic Oscillator

One of the very useful models in quantum mechanics is the harmonic oscillator. This model provides the basis for discussing any system fluctuating by small amounts near a configuration of stable equilibrium [Shankar]. It is the basis for extremely diverse many-body calculations in nuclear physics, quantum chemistry and quantum dot calculations in solid state physics. For completness, let's begin with a review of of the harmonic oscillator in 1D.

A.1.1 Single Harmonic Oscillator without spin in 1D

[J.E. HOUSE] In one-dimension, a spinless particle trapped in a harmonic oscillator potential well written as $\frac{1}{2}m\omega^2x^2$ has Hamiltonian:

$$H_{\text{HO}} = -\frac{\hbar^2}{2m}\frac{\partial^2}{\partial x^2} + \frac{1}{2}m\omega^2x^2, \tag{A.1}$$

The Schrodinger equation reads $\hat{H}\psi = E\psi$ where E stands for the eigenenergy and ψ its corresponding eigenvector. With the hamiltonian above, the Schrodinger equation becomes:

$$\begin{aligned} H_{\text{HO}}\psi(x) =& E\psi(x) \\ \left(-\frac{\hbar^2}{2m}\frac{\partial^2}{\partial x^2} + \frac{1}{2}m\omega^2x^2\right)\psi(x) =& E\psi(x) \end{aligned}$$

and can be simplified to the following non-linear differential equation:

$$\frac{\partial^2\psi(x)}{\partial x^2} = -\left(\frac{2mE}{\hbar^2} - \frac{m^2\omega^2}{\hbar^2}x^2\right)\psi(x) \tag{A.2}$$

To solve such an equation, let's assume a solution on the form: $\psi(x) = ce^{-bx^2}$ where $b, c \in \mathbb{R}$. Then the 1^{st} and 2^{nd} derivatives of the wave function reads:

$$\begin{aligned} \frac{\partial\psi(x)}{\partial x} =& -2bcxe^{-bx^2} = -2bx\psi(x) \\ \frac{\partial^2\psi(x)}{\partial x^2} =& -(2b - 4b^2x^2)\psi(x) \end{aligned} \tag{A.3}$$

By comparing eqn.(refeq:nonlinearEqDiff) and (A.3), it comes that $b = \frac{m\omega}{2\hbar}$ and $E = \frac{\hbar\omega}{2}$. Thus $\psi(x) = cexp(\frac{-m\omega}{2\hbar}x^2)$ is a solution of the Schrodinger equation.

In order to find a general solution of the harmonic oscillator, eqn. (A.2) can be re-written to the following:

$$\frac{\partial^2\psi(x)}{\partial x^2} + \left(\alpha - \beta^2x^2\right)\psi(x) = 0 \tag{A.4}$$

with $\alpha = \frac{2mE}{\hbar^2}$ and $\beta = \frac{m\omega}{\hbar}$

a new variable is introduced: $z = \sqrt{\beta}x$, then eqn.(A.4) reads:

$$\frac{\partial^2\psi(z)}{\partial z^2} + \left(\frac{\alpha}{\beta} - z^2\right)\psi(z) = 0 \tag{A.5}$$

In order to solve this new non-linear differential equation, let's assume the solution on the form: $\psi(z) = u(z)e^{\frac{-z^2}{2}}$. Again computing the 1^{st} and 2^{nd} derivatives of the wave function reads:

$$\begin{aligned}\frac{\partial\psi(z)}{\partial z} &= (u' - uz)e^{\frac{-z^2}{2}} \\ \frac{\partial^2\psi(z)}{\partial z^2} &= (u'' - 2u'z - u + uz^2)e^{\frac{-z^2}{2}}\end{aligned} \tag{A.6}$$

Inserting the expression of the 2^{nd} derivative given by (A.6) back into eqn. (A.5), a new non-linear differential equation arises as a function of $u(z)$:

$$\frac{\partial^2u(z)}{\partial z^2} - 2z\frac{\partial u}{\partial z} + \left(\frac{\alpha}{\beta} - 1\right)u(z) = 0 \tag{A.7}$$

Equation (A.7) has well known solutions for specific values of α and β when compared to the Hermite equation:

$$u''(z) - 2zu'(z) + 2nu(z) = 0, n \in \mathbb{N} \tag{A.8}$$

Thus the quantization arises from the restrictions on the nature of Hermite's equation:

$$\frac{\alpha}{\beta} = \frac{8\pi mE}{2\hbar\omega} = 2n + 1, n \in \mathbb{N}$$

The eigenvalues (i.e. eigenenergies) of H_{HO} are:

$$E = E_n = \hbar\omega(n + \frac{1}{2}), n \in \mathbb{N}$$

In order to solve the Hermite's equation (A.8), let's assume $u(z)$ on the form:

$$u(z) = H(z) = a_0 + a_1z + a_2z^2 + \cdots = \sum_{p=0}^{\infty} a_pz^p$$

Then computing the 1^{st} and 2^{nd} derivatives of $H(z)$ reads:

$$H'(z) = a_1 + 2a_2z + 3a_3z^2 + \cdots = \sum_{p=0}^{\infty} pa_pz^{p-1}$$

$$H''(z) = 2a_2 + 3 * 2a_3z + 4 * 3a_4z^2 + \cdots = \sum_{p=0}^{\infty} p(p+1)a_pz^{p-2} = \sum_{p=0}^{\infty}(p+2)(p+1)a_{p+2}z^p$$

Back into eqn.(A.8), it gives the following relation between the coefficients:

$$a_{p+2} = \frac{-(2n-2p)}{(p+1)(p+2)} a_p$$

Note that a_0 and a_1 are not obtained from the recursion, but from the differential equation itself.

The next step in the solution is to show that the series can be written in terms of $exp(-z^2)$ and that appropriate values can be assigned to the constants a_0 and a_1 to result in a well-behaved wave function. However the process to show it is rather tedious and can be found in advanced text books [23].

The Hermite polynomials $H_n(z)$ can be written as:

$$H_n(z) = (-1)^n e^{z^2} \frac{d^n}{dz^n}(e^{-z^2})$$

leading to those first polynomials: $\left\| \begin{array}{ll} H_0(z) = & 1 \\ H_1(z) = & 2z \\ H_2(z) = & 2(2z-1) \\ H_3(z) = & 4(2z^3-3z) \\ \cdots & \end{array} \right.$

Therefore, the eigenvectors of H_{HO} are:

$$\psi(z) = \psi_k(z) = N_k H_k(z) e^{\frac{-z^2}{2}}, k \in \mathbb{N}$$

with N_k a normalisation constant and $H_k(z)$ the Hermite polynomial.

As a summary, eigenvalues and eigenfunction of H_{HO} are given by

$$\left\{ \begin{array}{lll} E_n = & \hbar\omega(n+\frac{1}{2}) & \\ \psi_n(z) = & N_n H_n(z) e^{\frac{-z^2}{2}} & , n \in \mathbb{N} \quad , z = x\sqrt{\frac{m\omega}{\hbar}} \end{array} \right.$$

A.1.2 N-Harmonic Oscillators with spin

A spinless particle of mass m in an isotropic harmonic potential has Hamiltonian:

$$H_{\text{HO}} = -\frac{\hbar^2}{2m}\nabla^2 + \frac{1}{2}m\omega^2\|\vec{r}\|^2, \tag{A.9}$$

Scaling with proper energy and length units, i.e., $\hbar\omega$ $\sqrt{\hbar/m\omega}$ respectively [Simen Kvaal]. New hamiltonian

A.2 Single electron Quantum Dot (i.e. isotropic Quantum Harmonic Oscillator)

A.2.1 3D solution

A.2.2 2D solution

A.3 N-electrons Quantum Dots without e-e interactions = N particles HO

A.4 Exact solution of a 2-electrons Quantum Dots WITH e-e interactions (TAUT)

also detailled in a paper of Simen: "Harmonic oscillator eigenfunction expansions, quantum dots, and effective interactions" (august 2008)

Bibliography

[1] *Electron transport in quantum dots*, Proceedings of the Advanced Study Institute, 1997.

[2] R. Albrigtsen. Computational environment for many-electron systems. Master's thesis, University of Oslo, March 2009.

[3] E. Anisimovas and A. Matulis. Energy spectra of few-electron quantum dots. *J. Phys.: Condens. Matter*, 10(3):601–615, January 1998.

[4] R. J. Bartlett. Many-body perturbation theory and coupled cluster theory for electron correlation in molecules. *Ann. Rev. Phys. Chem*, 32:359–401, 1981.

[5] B. H. Bransden and C. J. Joachain. *Physics of Atoms and Molecules; 2nd ed.* Prentice-Hall, Harlow, 2003.

[6] L. Brey, N. F. Johnson, and B. I. Halperin. Optical and magneto-optical absorption in parabolic quantum wells. *Phys. Rev. B*, 40(15):10647–10649, Nov 1989.

[7] M. Bruchez, M. Moronne, P. Gin, S. Weiss, and P. A. Alivisatos. Semiconductor nanocrystals as fluorescent biological labels. *Science*, 281(5385):2013–2016, September 1998.

[8] W. C. W. Chan and S. Nie. Quantum dot bioconjugates for ultrasensitive nonisotopic detection. *Science*, 281(5385):2016–2018, September 1998.

[9] D. Chaney and P. A. Maksym. Size-dependent suppression of spin relaxation in electrostatic quantum dots. *Physical Review B (Condensed Matter and Materials Physics)*, 75(3):035323, 2007.

[10] M. Ciorga, A. S. Sachrajda, P. Hawrylak, C. Gould, P. Zawadzki, S. Jullian, Y. Feng, and Z. Wasilewski. Addition spectrum of a lateral dot from coulomb and spin-blockade spectroscopy. *Phys. Rev. B*, 61(24):R16315–R16318, Jun 2000.

[11] C. J. Cramer. *Essentials of computational chemistry : theories and models*. John Wiley & Sons, 2008.

[12] J. Dempsey, N. F. Johnson, L. Brey, and B. I. Halperin. Collective modes in quantum-dot arrays in magnetic fields. *Phys. Rev. B*, 42(18):11708–11713, Dec 1990.

[13] V. Fock. Bemerkung zur quantelung des harmonischen oszillators im magnetfeld. *Zeitschrift für Physik A Hadrons and Nuclei*, 47(5):446–448, May 1928.

[14] X. Gao, Y. Cui, R. M. Levenson, L. W. Chung, and S. Nie. In vivo cancer targeting and imaging with semiconductor quantum dots. *Nat Biotech*, 22(8):969–976, 2004.

[15] S. M. Girvin and T. Jach. Interacting electrons in two-dimensional landau levels: Results for small clusters. *Phys. Rev. B*, 28(8):4506–4509, October 1983.

[16] M. B. Haider, J. L. Pitters, G. A. DiLabio, L. Livadaru, J. Y. Mutus, and R. A. Wolkow. Controlled coupling and occupation of silicon atomic quantum dots at room temperature. *Physical Review Letters*, 102(4):046805, 2009.

[17] W. A. Harrison. *Electronic Structure and the Properties of Solids: The Physics of the Chemical Bond*. Dover Publications, July 1989.

[18] O. Heinonen, E. Gross, and E. Runge. *Many-Particle Theory*. Hilger, 1991.

[19] T. Heinzel. *Mesoscopic Electronics in Solid State Nanostructures*. Wiley-VCH, Weinheim, 2003.

[20] D. Heitmann. Far infrared spectroscopy of quantum-dots and antidot arrays. *Physica B: Condensed Matter*, 212(3):201 – 206, 1995. Proceedings of the Workshop on Novel Physics in Low-Dimensional Electron Systems.

[21] D. Heitmann and J. P. Kotthaus. The spectroscopy of quantum dot arrays. *Physics Today*, 46(6):56–63, 1993.

[22] A. Hoshino, K. ichi Hanaki, K. Suzuki, and K. Yamamoto. Applications of t-lymphoma labeled with fluorescent quantum dots to cell tracing markers in mouse body. *Biochemical and Biophysical Research Communications*, 314(1):46 – 53, 2004.

[23] J. E. House. *Fundamentals of Quantum Mechanics*. Academic Press, 1998.

[24] N. Johnson and M. Payne. Exactly solvable model of interacting particles in a quantum dot. *Phys. Rev. Lett.*, 67:1157, 1991.

[25] N. Johnson and M. Reina. The accuracy of the hartree-fock approximation for quantum dots. *Journal of Physics: Condensed Matter*, 4:623–628, September 1992.

[26] K. Kalyanasundaram. Cleavage of water by visible-light irradiation of colloidal cds solutions; inhibition of photocorrosion by ruo_2. *Angewandte Chemie International Edition in English*, 20(11):987–988, 2003.

[27] W. Kohn. Cyclotron resonance and de haas-van alphen oscillations of an interacting electron gas. *Phys. Rev.*, 123(4):1242–1244, Aug 1961.

[28] L. P. Kouwenhoven, D. G. Austing, and S. Tarucha. Few-electron quantum dots. *Reports on Progress in Physics*, 64(6):701–736, 2001.

[29] M. Kralj and K. Pavelic. Medicine on a small scale. *EMBO reports*, 4(11):1008âĂŞ1012, 2003.

[30] S. F. Kumar A, Laux SE. Electron states in a gaas quantum dot in a magnetic field. *Physical Review B (Condensed Matter and Materials Physics)*, 42:5166–5175, Sept. 1990.

[31] W. Kutzelnigg. Diamagnetism in relativistic theory. *Physical Review A*, 67(3):032109+, Mar 2003.

[32] S. Kvaal. Open source fci code for quantum dots and effective interactions. *arXiv.org*, 1:1, Oct 2008.

[33] S. Kvaal. *Analysis of many-body methods for quantum dots.* PhD thesis, University of Oslo, January 2009.

[34] S. Kvaal. Openfci home page, 08 2009.

[35] A. Kwasniowski and J. Adamowski. Effect of confinement potential shape on exchange interaction in coupled quantum dots. *Journal of Physics: Condensed Matter*, 20(21):215208 (8pp), 2008.

[36] C. S. Lent, P. D. Tougaw, W. Porod, and G. H. Bernstein. Quantum cellular automata. *Nanotechnology*, 4(1):49–57, 1993.

[37] Q. P. Li, K. Karraï, S. K. Yip, S. Das Sarma, and H. D. Drew. Electrodynamic response of a harmonic atom in an external magnetic field. *Phys. Rev. B*, 43(6):5151–5154, Feb 1991.

[38] M. Macucci, K. Hess, and G. J. Iafrate. Electronic energy spectrum and the concept of capacitance in quantum dots. *Phys. Rev. B*, 48(23):17354–17363, Dec 1993.

[39] M. Macucci, K. Hess, and G. J. Iafrate. Numerical simulation of shell-filling effects in circular quantum dots. *Phys. Rev. B*, 55(8):R4879–R4882, Feb 1997.

[40] I. L. Medintz, T. H. Uyeda, E. R. Goldman, and H. Mattoussi. Quantum dot bioconjugates for imaging, labelling and sensing. *Nat Mater*, 4(6):435–446, June 2005.

[41] Y. Meir, N. S. Wingreen, and P. A. Lee. Transport through a strongly interacting electron system: Theory of periodic conductance oscillations. *Phys. Rev. Lett.*, 66(23):3048–3051, Jun 1991.

[42] H. Mizuta, H.-O. Muller, K. Tsukagoshi, D. Williams, Z. Durrani, A. Irvine, G. Evans, S. Amakawa, K. Nakazato, and H. Ahmed. Nanoscale coulomb blockade memory and logic devices. *Nanotechnology*, 12(2):155–159, 2001.

[43] M. Moshinsky and Y. F. Smirnov. *The Harmonic Oscillator in Modern Physics: From Atoms to Quarks*. Taylor & Francis, 1996.

[44] F. M. Peeters. Magneto-optics in parabolic quantum dots. *Phys. Rev. B*, 42(2):1486–1487, Jul 1990.

[45] D. Pfannkuche, V. Gudmundsson, and P. A. Maksym. Comparison of a hartree, a hartree-fock, and an exact treatment of quantum-dot helium. *Physical Review B*, 47(4):2244–2250, January 1993.

[46] S. Rahman. Applications of quantum dots in the biological sciences. Simula Research Laboratory, Lysaker, Norway, January 2008.

[47] S. Raimes. *Many-electron Theory*. North-Holland Publishing, 1972.

[48] S. M. Reimann and M. Manninen. Electronic structure of quantum dots. *Rev. Mod. Phys.*, 74(1):1283–1342, November 2002.

[49] M. Rontani. *Electronic States in Semiconductor Quantum Dots*. PhD thesis, Universita degli Studi di MODENA e REGGIO EMILIA, October 1999.

[50] R. Rossetti, S. Nakahara, and L. E. Brus. Quantum size effects in the redox potentials, resonance raman spectra, and electronic spectra of cds crystallites in aqueous solution. *The Journal of Chemical Physics*, 79(2):1086–1088, 1983.

[51] C. Sikorski and U. Merkt. Spectroscopy of electronic states in insb quantum dots. *Phys. Rev. Lett.*, 62(18):2164–2167, May 1989.

[52] H. Soo Choi, W. Liu, P. Misra, E. Tanaka, J. P. Zimmer, B. Itty Ipe, M. G. Bawendi, and J. V. Frangioni. Renal clearance of quantum dots. *Nat Biotech*, 25(10):1165–1170, Oct. 2007.

[53] M. Stopa. Quantum dot self-consistent electronic structure and the coulomb blockade. *Phys. Rev. B*, 54(19):13767–13783, Nov 1996.

[54] M. B. Tavernier, E. Anisimovas, F. M. Peeters, B. Szafran, J. Adamowski, and S. Bednarek. Four-electron quantum dot in a magnetic field. *Phys. Rev. B*, 68(20):205305, Nov 2003.

[55] J. Thijssen. *Computational Physics*. Cambridge University Press, Cambridge, UK, 2007.

[56] E. B. Voura1, J. K Jaiswal1, H. Mattoussi, and S. M. Simon. Tracking metastatic tumor cell extravasation with quantum dot nanocrystals and fluorescence emission-scanning microscopy. *Nature Medicine*, 10:993 – 998, 2004.

[57] E. Waltersson and E. Lindroth. Many-body perturbation theory calculations on circular quantum dots. *Phys. Rev. B*, 76(045314):045314, July 2007.

[58] C. Weisbuch, H. Benisty, and R. Houdrï£¡. Overview of fundamentals and applications of electrons, excitons and photons in confined structures. *Journal of Luminescence*, 85(4):271 – 293, 2000.

[59] H. Weller, H. M. Schmidt, U. Koch, and A. FojtikCorresponding. Photochemistry of colloidal semiconductors. onset of light absorption as a function of size of extremely small cds particles. *Chem. Phys. Lett.*, 124(6):557–560, 1986.

[60] Wikipedia. Ab initio quantum chemistry methods — Wikipedia, the free encyclopedia, 04 2009. [Online; accessed 9-April-2009].

[61] Wikipedia. Orders of magnitude (magnetic field) — wikipedia, the free encyclopedia, 2009. [Online; accessed 2-August-2009].

[62] Wikipedia. Physical constants — Wikipedia, the free encyclopedia, 2009. [Online; accessed 13-August-2009].

[63] R. K. Willardson and A. C. Beer. *Semiconductors and semimetals.* Academic Press, 1971.

[64] J. O. Winter. *Development and optimization of quantum dot-neuron interfaces.* PhD thesis, The University of Texas at Austin, 2004.

[65] S. K. Yip. Magneto-optical absorption by electrons in the presence of parabolic confinement potentials. *Phys. Rev. B*, 43(2):1707–1718, Jan 1991.